GEM TN-91-00010

GEM Electronics/Triggering/DAQ Meeting at SSCL

September 4, 1991

Abstract:

Transparencies and contributions from the Electronics/Triggering/Data Acquistion Meeting held at the SSCL on September 4, 1991

GEM Trigger Meeting

Name	Inst.	Phone	EMAIL
Dan Marlow	Princeton	609-258-4383	PUPHEP::MARLOW
Mikhail Leltchouk	Columbia Univ. Nevis. Labs	(914) 591-8100 ext 221	NEVIS::LELTCHOUK
Michel Seman	Columbia Univ	(914)-591-8100 ext 232	NEVIS :: SEMAN
Mark Lowry	LLNL	415-423-2924	MLowry@LLNL.GOV
Steve Kettell	Temple Univ.	(516) 282-3977	BULDAG :: KETTELL
Richard Sumner	LeCroy	914 425 2000 X3317	SUMNER::SSCVX1
Jack Ritchie	U. Texas, Austin	(512) 471-4488	RITCHIE@UTAPHY.bitu
Cas Milner	SSCL	(214) 956-7506	Milner@sscvx1.ssc.Gov
Jheroen Dorenbosch	SSCL	(214) 708 6118	Dorenbosch@SSCVX1
Maris ABOLINS	Michigan State U/Fnal	(708) 840-4257	FNALDØ::ABOLINS
IRWIN A. PLESS	MIT	(617) 253-2367	MITLNS::PLESS
Mike Shaevitz	Columbia	914-591-8100	SHAEVITZ@NEVIS NEVIS::SHAEVITZ
Chuck Lane	Drexel	215-895-1545	lane@duphy4.drexel.edu
Craig Wuest	LLNL	(510)423-2909	WUEST@LLNL.GOV

Electronics / Triggering / DAQ Group

Wed. Sept. 4, 1991

Time	Speaker	Topic
8:30	Shaevitz	Overview of Trigger Architecture etc.
9:00	Marlow	Front End Specifications, rack placement, et
9:30	Lowry	Update on Electro-optic modulators
10:00	Coffee	
10:20	Seman	TRD Muon Trigger
10:50	Pless	RPC Muon Trigger
11:20	Texas Instr.	High-Speed GaAs ADC's
12:00	Lunch	
1:00	Crosetto	A Programmable System for Missing E_T Trigge: Cluster Finding, and DAQ/Compaction
1:40	Botlo	DAQ Schemes

Next three talks to be held in joint session with Computing Group . . .

2:30	t.b.a	Intel Touchstone Level 2/Level 3 Processor Farm
3:00	Coffee	
3:20	Wang	Missing E_T Triggers (to be confirmed)
4:00	McFarlane	Status of GEM MC Package

Return to Trigger Group Only . . .

4:20	Discussion	Plans for LoI etc.

Shaevitz

Work in Progress for Letter of Intent

- Outline of General Trigger/DAQ Architecture
- Generic Triggers and Rates — e, γ, μ, jets, $\not{E}_T$
- Level 1, Level 2 Trigger Strategies/Rates
- Estimate of Level 1 Trigger time
- Estimate of Event Size
- Cost Estimate
- Data flow into Microfarm
  - → Show that [illegible] OK
- Data flow in general
  - Inner Tracker into L2 Trigger (Electron ID)

Electronics Working Group Activity

- Members: Bauer, Denes (CERN), O'Connor, Paffrath, Radeka, Sippach, Sumner, Wadsworth (Marlow & Shaevitz *ex officio*)

- Activities

  — System Architecture

  — Strobe Timing Distribution

  — Analog Sampling

  — Calibration

  — Rack Placement

Calorimeter Readout Performance Specifications

- 16 ns sample rate. $\sim$ 2-5 samples per hit
- Dynamic Range $\geq 2^{16}$
- Resolution $\geq$ 8 bits
- Total Conversion time $\leq$ 10 μs (for $\simeq$ 5 samples)
- Packaging
  - — $\sim$ 25 channels per FASTBUS-sized board
  - — $\Longrightarrow$ < 3 W/channel

3. Sippach

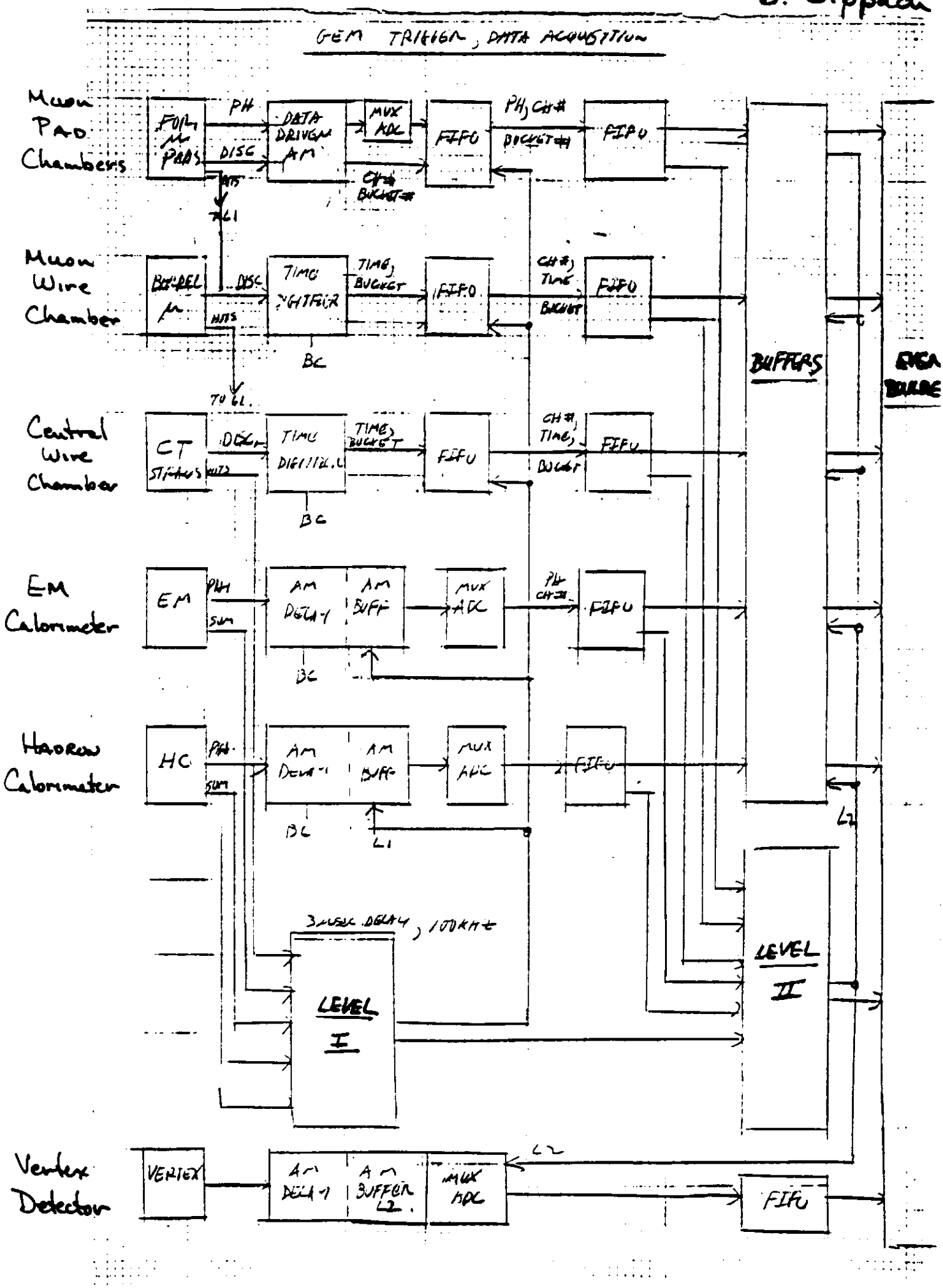
GEM TRIGGER, DATA ACQUISITION
Muon Pad Chambers
PH
DISC
HITS
DATA DRIVEN AM
MUX ADC
FIFO
PH, CH#
BUCKET#
CH#
BUCKET#
TO L1
Muon Wire Chamber
DISC
HITS
TIME DIGITIZER
TIME, BUCKET
CH#, TIME
BUCKET
BC
TO L1
Central Wire Chamber
CT
DISC
HITS
TIME DIGITIZER
TIME, BUCKET
CH#, TIME, BUCKET
BC
EM Calorimeter
EM
PH
SUM
AM DELAY
AM BUFF
MUX ADC
PH CH#
BC
Hadron Calorimeter
HC
PH
SUM
AM DELAY
AM BUFF
MUX ADC
BC
L1
3 μsec DELAY, 100 KHz
LEVEL I
BUFFERS
LEVEL II
L2
Vertex Detector
VERTEX
AM DELAY
AM BUFFER
MUX ADC
FIFO
L2

GaAs HETEROJUNCTION BIPOLAR ADC TECHNOLOGY

KEY PARAMETERS

f_T	25 GHz
FEATURE SIZE	5x5 µm EMITTER
METAL PITCH	5 µm
ΔV_{BE}	±1mV
V_A	>100V

NPN HBT CROSS SECTION

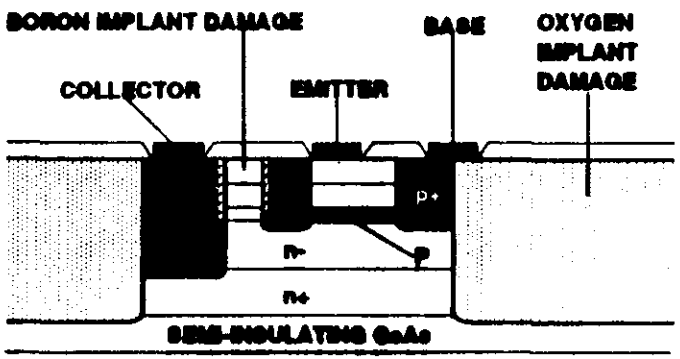

5 BIT, 1.2 Gsps FLASH ADC

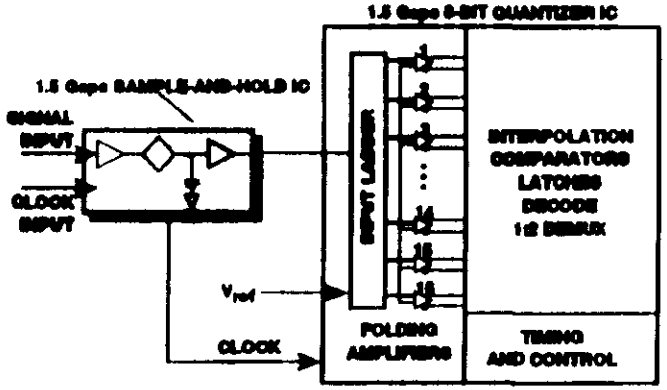

1.5 Gsps 8-BIT A-D CONVERTER

Placement Options

OE: On Element ⇔ No cable
ID: In Detector, e.g. in gap between EM and HCAL.
OD: On Detector, e.g. bolted to return yoke.
ND: Near Detector, e.g. lower counting room.
OS: On Surface, e.g. headhouse.

Location Summary				
		Cable Path	Radiation	
Loc.	Access Time	meters	Rad/Year	Comments
OE	Weeks	~ 0	500 – 150K	Access difficult
ID	Weeks	2 – 5	< 10	Limited Space
OD	Hours	20 – 30	—	Beam Off
ND	Minutes	60 – 80	—	Beam On
SD	Constant	100 – 130	—	

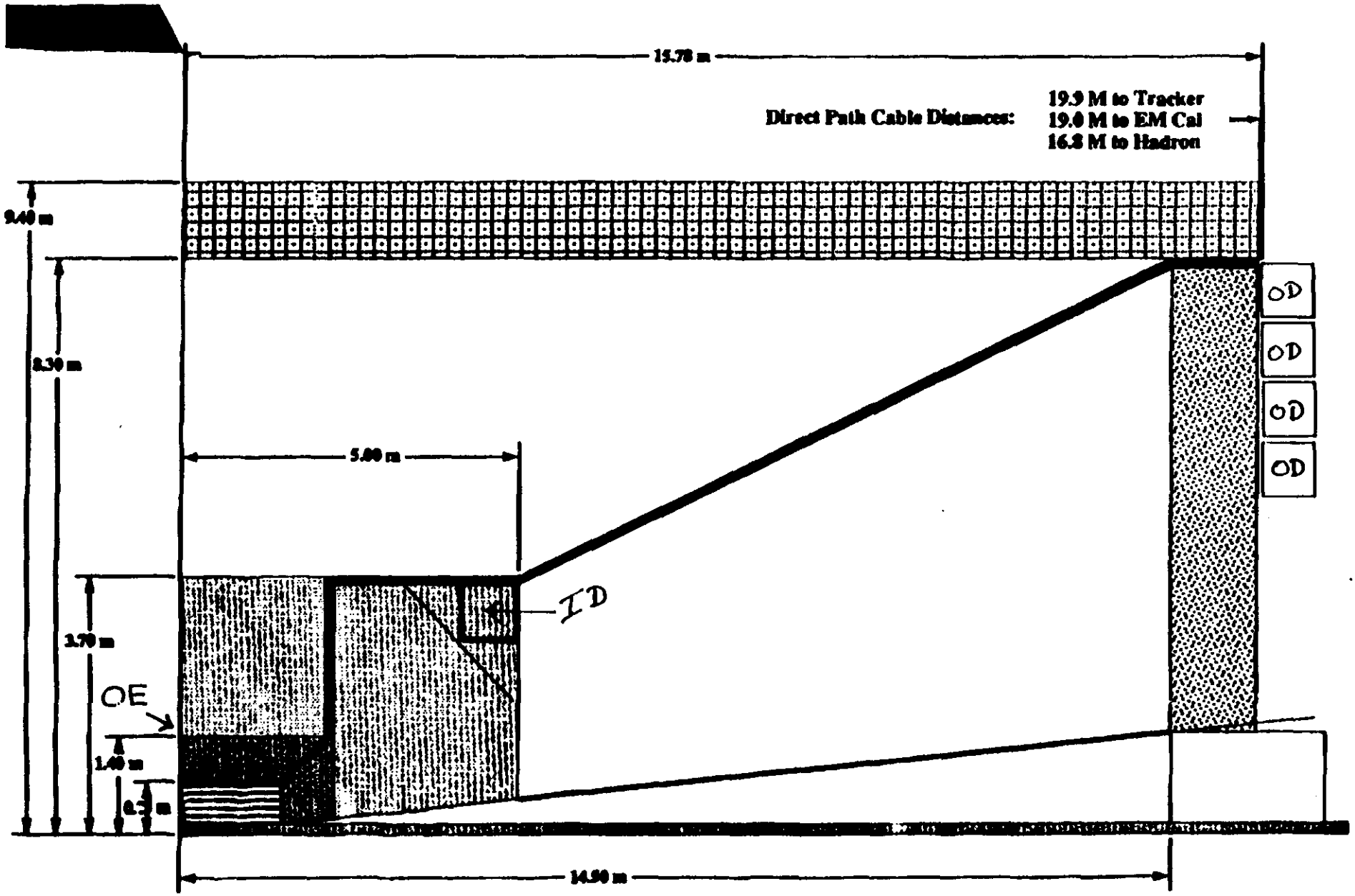

GEM DETECTOR CABLE ROUTING

OE = "On Element"
ID = "In Detector"
OD = "On Detector"

GEM.03.GN.00010

RENNICH

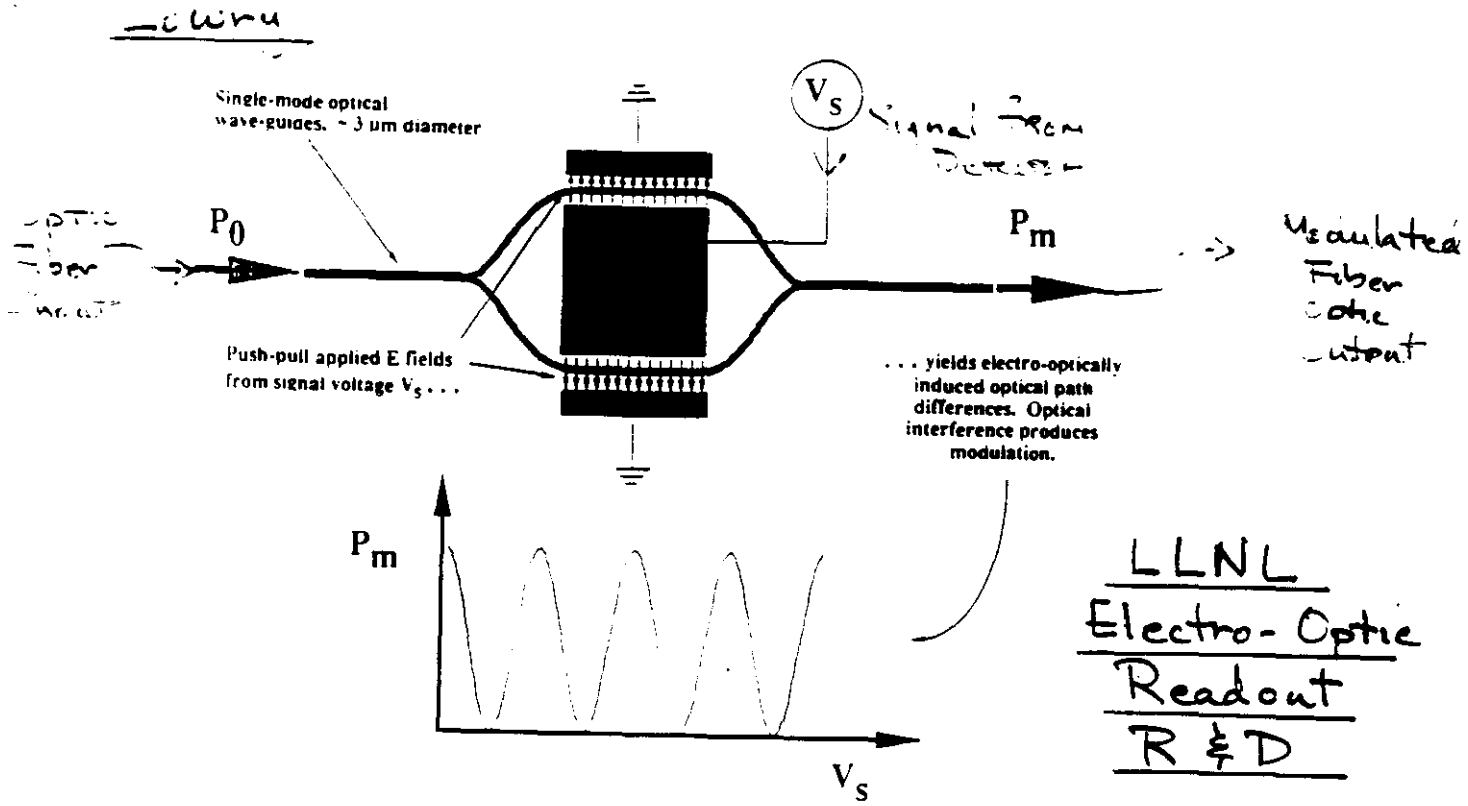

Figure 3. Simplified diagram of the operation of the Mach-Zehnder integrated optical modulator.

of the modulator response function. This setting is denoted as the half-power point. For the small signal levels typically read off the drift chamber sense wire, the modulator transfer curve was linear about the half-power operating point. If

tions of the Nd:YAG laser source. This resultant signal was sent to an oscilloscope for observation and recording. Figure 4 shows a picture of the output of the modulator/receiver system. The pulses are clearly discernable over the noise.

Our experimental demonstrations of LLNL E/O technology in the HEP environmen have been very successful, and well received

.....concentrating on goals that would bolster credibility and quickly demonstrate institutional effectiveness.

- Sensitivity demonstration with 800 and 1300 nm systems
  dynamic range of 5 decades reasonable target, ref. 1
- First observation of muon chamber charge signals with E/O modulator without electron
  ... achieved with LLNL muon chamber, ref. 2
- Collaboration with MIT (Ulrich Becker, et. al. from Ting's group)
  - -- demonstrated direct charge readout of drift tube--- no preamp !!
  - -- measured Fe 55 decay spectrum
  - -- demonstrated direct readout in B-field environment expected within the SSC detec
    ... at 0.8 Tesla no effect
  - -- measured muon track resolution with modulator readout system
  - -- familiarized key members of HEP community with technology
  - -- ref. 3
- Radiation hardness demonstrated in collaborative experiment at LAMPF
  - -- ref. 4

~ 10 SSC year dose → Only slight effects

Typical problems of Digital triggers & Data acquisition/compaction in Calorimetry of High Energy Physics.

For any number of channels:

1. Calculate the total energy and the transverse energy

2. Calculate the geographical address of clusters (local maxima).

3. Apply a threshold to the combined energy of a local maxima and of its neighbors.

4. Isolate from the empty calorimeter channels:
   - the clusters found along with their regions of interest and
   - calculate their cluster shape-factors (e.g. to separate pions/electrons).

⇒ Programmable System for Calorimetry DAQ Using Commercial Components
(Example of Level 2 Architecture)

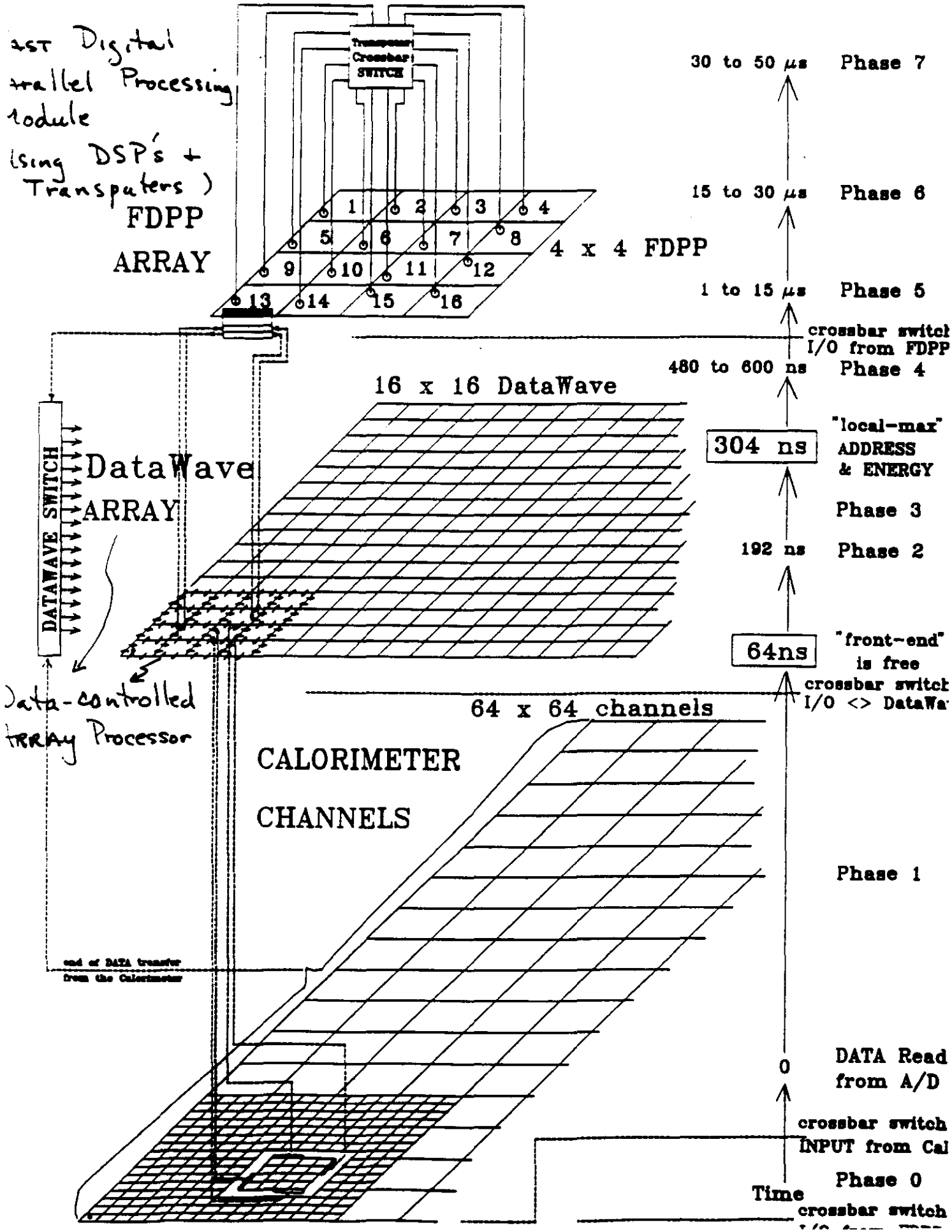
ast Digital
rallel Processing
odule
(sing DSP's +
Transputers)
FDPP
ARRAY
Transputer
Crossbar
SWITCH
1
2
3
4
5
6
7
8
9
10
11
12
13
14
15
16
4 x 4 FDPP
30 to 50 μs
Phase 7
15 to 30 μs
Phase 6
1 to 15 μs
Phase 5
crossbar switch
I/O from FDPP
480 to 600 ns
Phase 4
16 x 16 DataWave
DATAWAVE SWITCH
DataWave
ARRAY
304 ns
"local-max"
ADDRESS
& ENERGY
Phase 3
192 ns
Phase 2
64ns
"front-end"
is free
crossbar switch
I/O <> DataWa
Data-controlled
ARRAY Processor
64 x 64 channels
CALORIMETER
CHANNELS
Phase 1
end of DATA transfer
from the Calorimeter
0
DATA Read
from A/D
crossbar switch
INPUT from Cal
Phase 0
Time
crossbar switch

Rapid improvements in performance of commercially available

- Digital Signal Processors and of
- Data-driven Array Processors

} Integrate Commercial Units into System

are an invitation to make a serious effort

- to efficiently integrate these commercial components
-in a design that satisfies the requirements of the applications in HEP.

The decision of developing a new VLSI special digital processor

- should be weighted very carefully
- because of the difficulty of providing all necessary software development tools.

RPC

Table 1 - Characteristics of RPCs	
plate bulk resistivity	$10^{11\pm1}$ Ω cm
electric field	~40 kV/cm
pulse charge	10^2 pC
pulse rise time	~3 ns
pulse duration	~20 ns
efficiency	~97%
discharge area	0.1 cm^2
recovery time	10^{-2} s
time resolution	~1 ns

2. Resistive Plate Chambers

The Resistive Plate Chambers, developped in Rome ten years ago, work at a uniform electric field of ~ 40 kV/cm between parallel electrode plates of a plastic phenolic material (bakelite) with a resistivity $\rho \simeq 10^{11}$ Ω cm. The plates, 2 mm thick, are kept separated at a distance of 2 mm by spacers of polyvinyl chloride. Gas tightness is insured by a frame of the same material. The sensitive volume is filled with a gas mixture of argon/butane plus a small percentage of freon 13B1 at normal pressure. The generating field electrodes are layers of a graphite varnish coating the outer surface of the plates. They are isolated from the read-out electrodes by a 300 μm thick film. A section of the chamber is shown in Fig. 1.

Sketch of a Resistive Plate Chamber

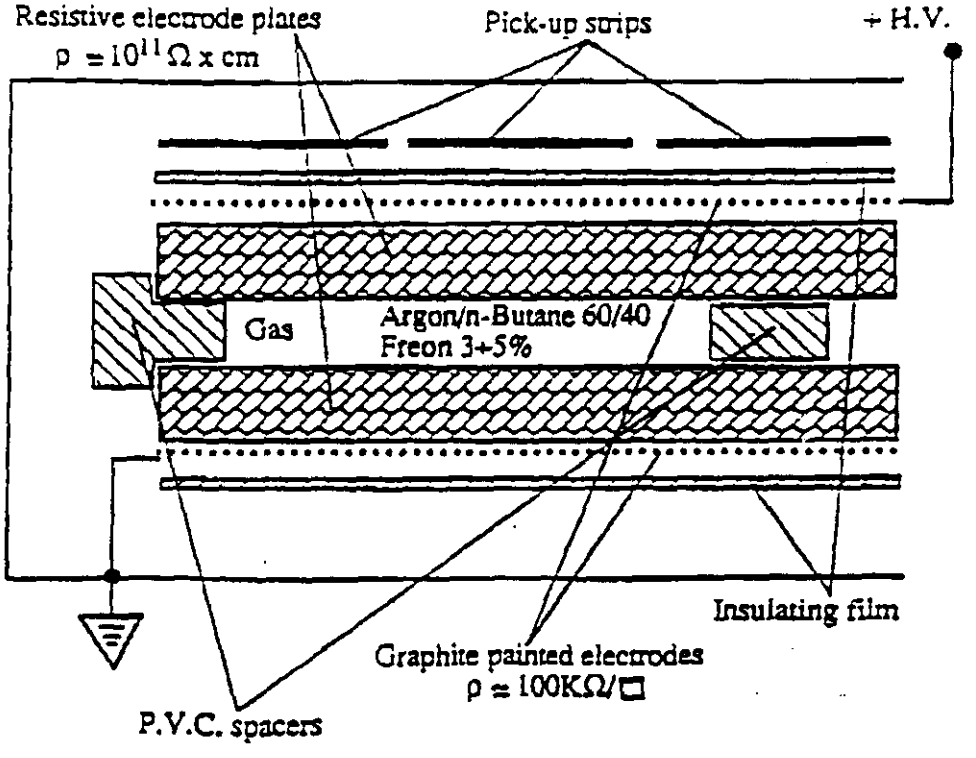

Fig. 1

Pless

CONCLUSIONS

1. USING RPCs ONE CAN GENERATE A P_t TRIGGER IN ABOUT 100 NANOSECONDS WITH A JITTER OF A FEW NANOSECONDS

2. TRIGGER LOGIC IS SIMPLE AND IS IN "REAL" TIME. THE INFORMATION FLOWS WITH THE PARTICLE

3. COSTS LOOK REASONABLE

4. THE Z COORDINATE AND THE RADIAL COORDINATE CAN BE MEASURED TO 1 MILLIMETER AND PROBABLY BE MEASURED TO 500 MICRONS

Resistive Plate Chamber R&D Collaborative Work

- Collaboration with Professor Irwin Pless's group at MIT.
  +BU + Brown + Indiana
- MIT will do the following:
  - Acquire an Italian bakelite RPC (1m x 2 m).
  - Set up a test stand to measure:
    - spatial resolution as a function of length along the readout strips,
    - time resolution
    - gas choice - non-flammable
    - noise
    - aging
    - high particle flux performance (< 100 Hz/cm^2 ?)
    - performance in high neutron flux (important for plastic based RPCs)
    - choice of readout electronics
    - choice of fast trigger electronics
  - Test facility with muon telescope, three component gas system, etc.
- LLNL will test glass-based counter on MIT test stand for comparison to the Italian RPC.

Resistive Plate Counter R&D at LLNL -

Craig Wuest, Elden Ables, Richard Bionta, Dan Makoweicki

- RPC R&D at LLNL is taking advantage of an extremely capable Chemistry and Materials Science Division.
  - We have expertise in coating a variety of dissimilar materials using a number of different technologies: e.g. sputtering of As on Pu.
  - We have identified a resistive soda-lime glass as a candidate for RPC plates (in place of the carbon-painted phenolic).
  - We will build a 25 x 25 cm^2 RPC in the first part of the program, based on the work of Cardarelli, et al., NIM A263 (1988).
  - Discussions with I. Pless of MIT have been initiated and a joint effort to develop RPC's is envisioned.
  - Larger 1 x 1 m^2 RPC's in the future.

Punchthru Rate Studies (Progress Report)

T. Bolton

Goals:

- Verify previous calculations for GEM
- Study feasibility of using Muon Layer 1
- Verify rates with proposed trigger strategies

(• Physics req. for η coverage ie $Z \to \mu\mu$ 800 GeV)

Tools:

- GEANT GEM geometry + tracking (M. Seman)
- ISAJET FOR Physics
- PCHTHR: Punchthru simulation from McNeil.
- Strategy:
  - Full tracking of all muons (primary, π/K decay)
  - Full tracking of punchthru products from back of calorimeter

T. Bolton

Preliminary Results

(Twojet Rate Isajet $P_\perp \geq 2$ GeV = 35.0 MHz)

Mean Rate of Hits

Barrel	Layer 1	83	kHz
	Layer 2	44	"
	Layer 3	33	"
Forward	Layer 1	1.3	MHz
	" 2	1.0	"
	" 3	.8	"

Mean $\langle P_\perp \rangle$ of hits = 580 MeV

Mean Preshower Multiplicity = .0133/event

03/09/91 11.34

BARREL Layer #1

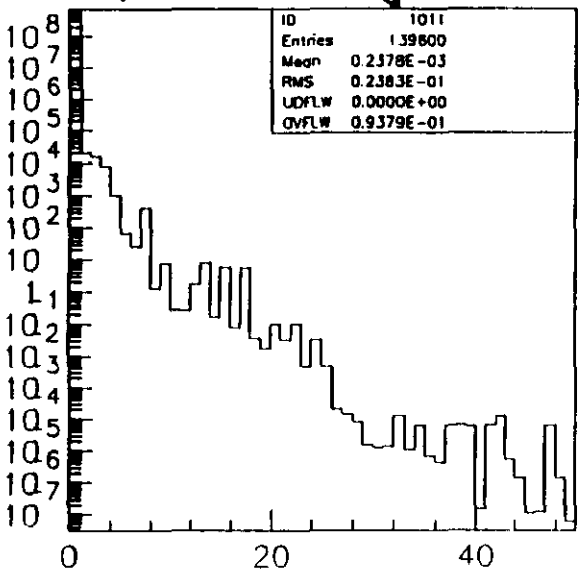

nzbarz1

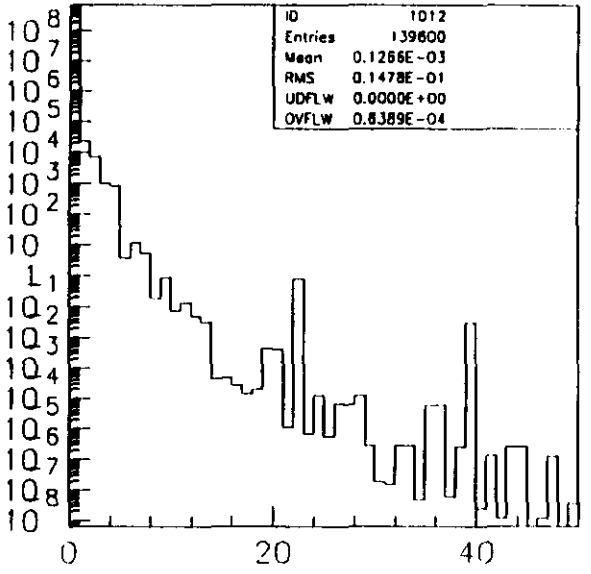

nzbarz2

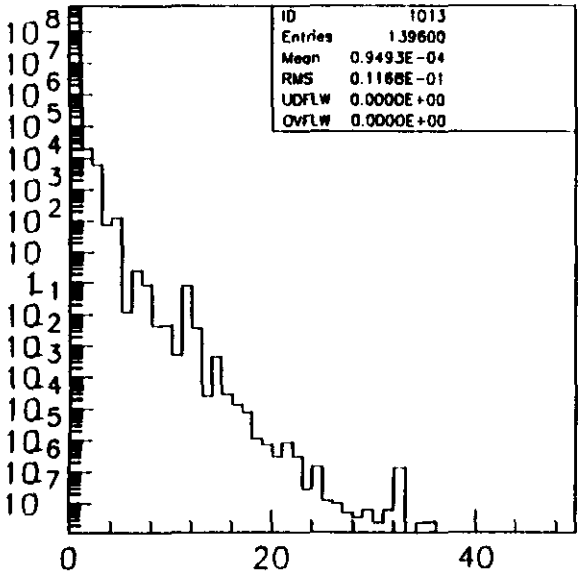

nzbarz3

Forward Layer #1

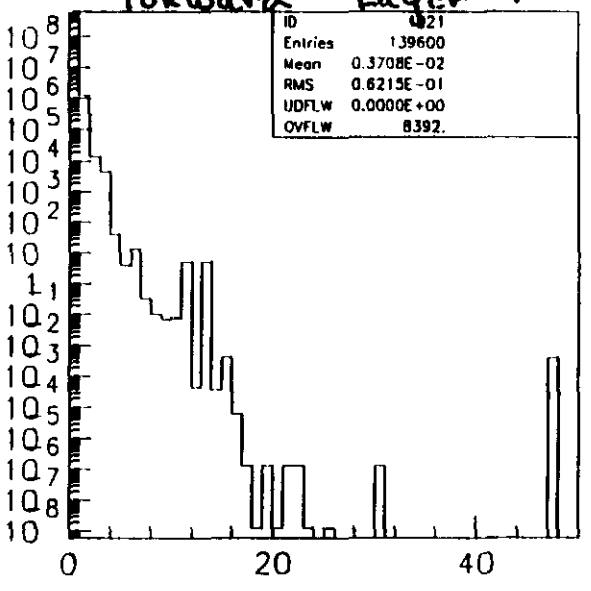

nznorz1

Ordinate = Rates in Hz

assuming $\mathcal{L} = 10^{33}\ cm^{-2}s^{-1}$

~~abcis~~

abcissa = # of hits

bar = barrel

nor = north end

sou = south end

TOTAL TWOJET rate

$P_T > 2$ GeV

$= 3.49 \times 10^8$

Fig. 1. Muon Trigger Strategies

M. Semen

D P H I AND RAYS TRIGGERS

***

D P H I IS A VALID TRIGGER IF THERE IS A COINCIDENCE BETWEEN PADS PHI3(i) AND ONE OF PHI2(i +/- thr)

WHERE thr = 0,1,2,3,....

***

R A Y S IS A VALID TRIGGER IF CALCULATED ANGLE BETWEEN RAY2 AND RAY3 IS SMALLER THAN A GIVEN THRESHOLD

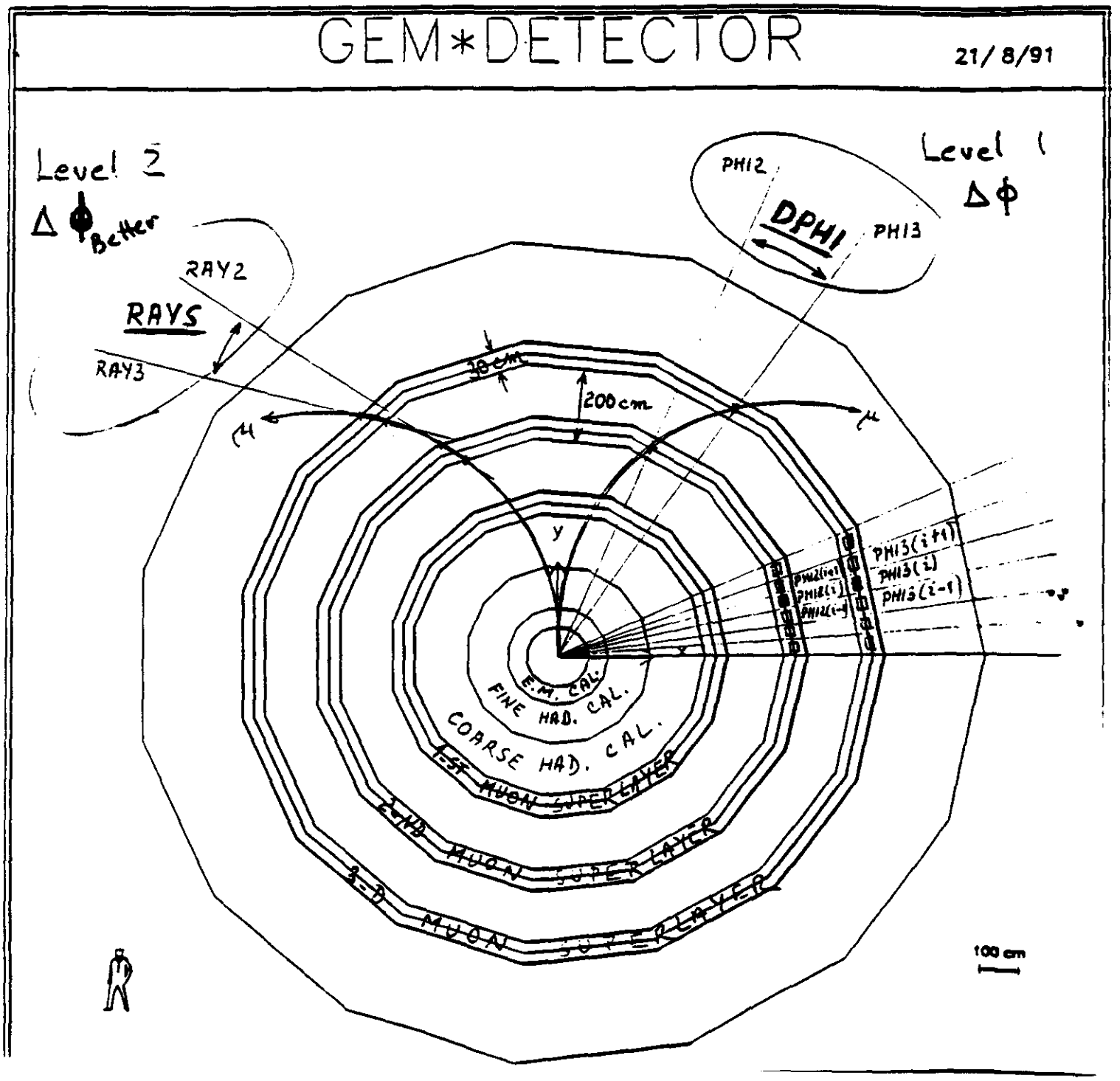

Fig. 2. Level 1 $\Delta\phi$ Trigger

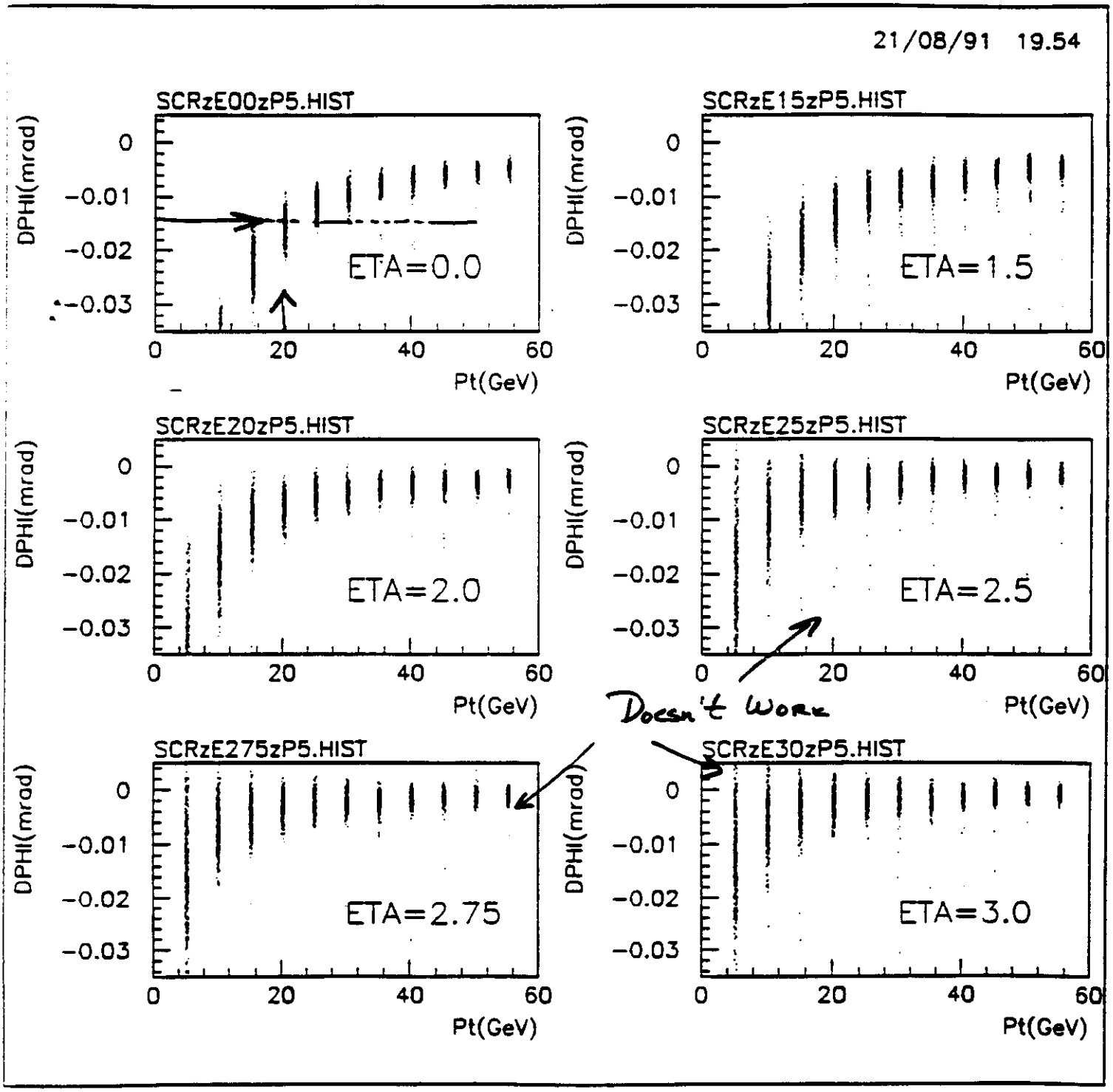

14.7.

D. REFOL = 0.1 cm

Level 2 "Ray Trigger"

$\Delta\phi$ Trigger

Baker

31/08/91 19.54

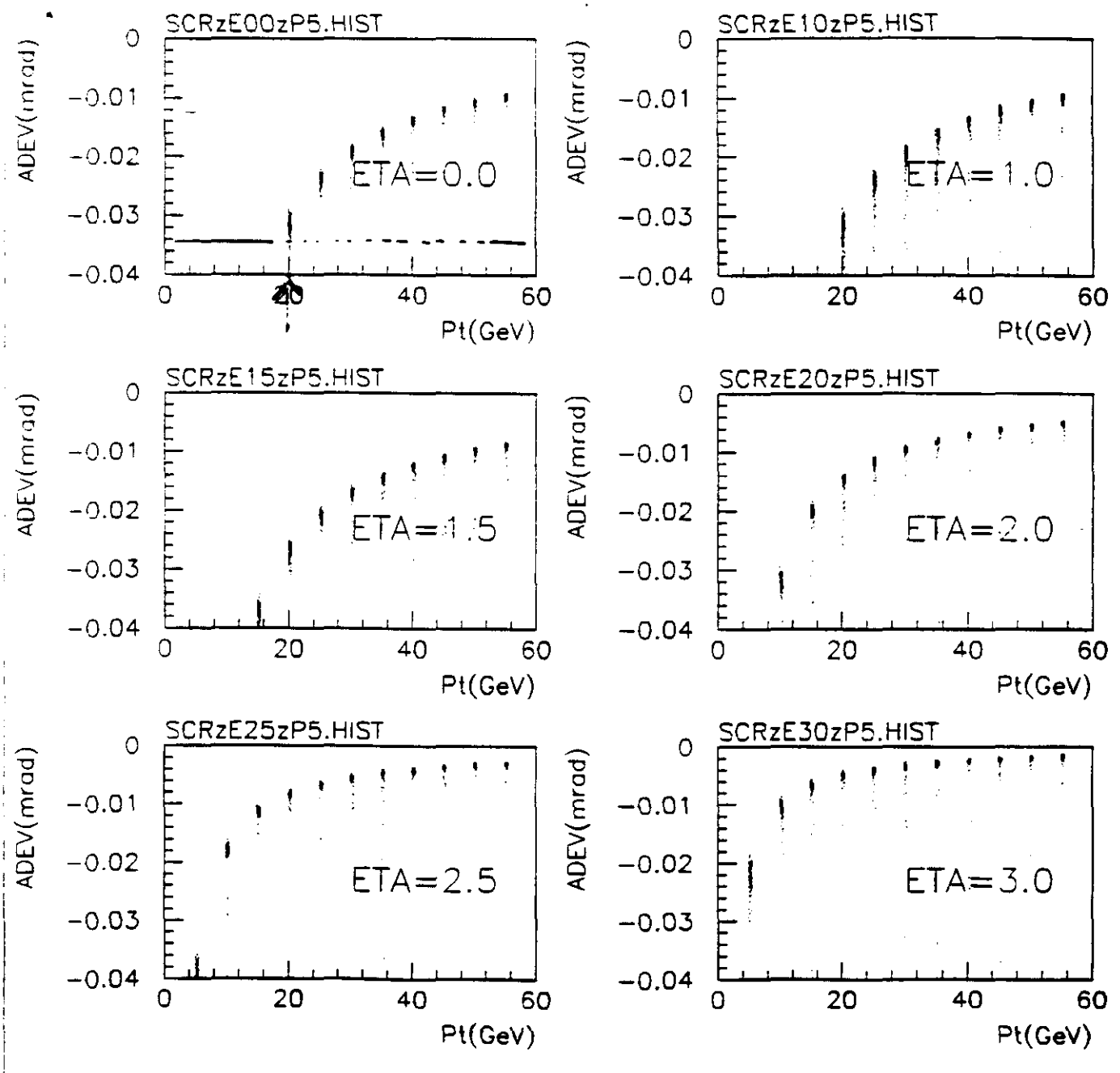

R & D PLANS

- Continue General Architecture Development
  + Trigger Strategies

- Analog Pipeline Development
  - Longer Delay Units
  - Integrate MUX ADC system

  ← Augment by SD + LHC

- Digital Pipeline Development
  - FAST ADC's

- Electro-optic readouts
  - Improved charge sensitivity
  - Cost reduction

- RPC (Resistive Plate Chambers)
  - Test resolutions + electrical properties
  - Build 1m x 1m glass plate device

- TRD Development
  - Prototype unit to check efficiency and rejection.

- DATA FLOW Studies
  ⇒ Required rates + technologies

Computing in High Energy Physics '91 Tsukuba City, Japan March 11-15, 1991.

A FAST CLUSTER FINDING SYSTEM FOR FUTURE HEP EXPERIMENTS

D. Crosetto

INFN, Torino, Italy.

Abstract

The recent rapid improvements in performance of commercially available Digital Signal Processors and Data-driven Array Processors, make attractive their efficient integration into the front-end trigger and data acquisition electronics of future detectors for High Energy Physics (HEP), in place of developing new VLSI processors for this special purpose. MIMD parallel hybrid processing system based on Data-driven Array Processors, Digital Signal Processors (DSP) and Transputers for trigger decision, data acquisition and compaction is described. The hybrid nature refers to the method of message passing based on both serial and parallel exchanges. The system is modular and suitable for all calorimeter sizes including the ones proposed in the R&D for the LHC experiments. The aim is to give full programmability for the trigger decisions and for the data compaction, over the entire calorimeter at the single-channel granularity level, with no boundary limitation. The fast cluster finding system is based on two cooperating levels, the higher one utilizing FDPP, and the lower one, the new data-controlled array processor for video signal processing, DataWave. The proposed architecture provides one DataWave Processing Elements (PE) for each calorimeter channel and one FDPP module for every 256 DataWave processing elements. These numbers have been chosen for an optimized design but may be changed. Fast inter-processor communication within the DataWave array overcomes the problem of overlapping areas, and effectively provides a continuous array of processing elements. Local maxima, along with their energy, are found in a very short time from the data-driven array processors, and are then easily selected and transferred, with the data of their region of interest, to a higher-level DSP array-processor system even if part of the data fall outside the region originally attributed to a particular FDPP.

1. Introduction.

Typical requirements for digital triggers and Data acquisition/compaction in Calorimetry of High Energy Physics Experiments can be summarized as follows (a more detailed description can be found in section 4):

(a) to load DATA from the calorimeter and free the front-end electronics for a subsequent acquisition;

(b) to find the geographical address of clusters (or local maxima corresponding to the center of an energy cluster derived from the full granularity), calculate their energies and apply different thresholds,

(c) to calculate the missing energy and the transverse energy of the event,

(d) to isolate the clusters found, and their region of interest, from the empty calorimeter channels, and calculate the cluster shape-factors (e.g. to separate pions from electrons).

The fast cluster finding system described herein is based on two cooperating levels, the higher one utilizing the FDPP (or FDPP_DM) Fast Digital Parallel Processing module [1], and the lower one, the new data-controlled array processor for video signal processing, DataWave [2].

Figure 1 shows an example of a general layout of a trigger and a data acquisition/compaction scheme with its related data-flow phases and timing for a typical calorimeter of future HEP experiments.

The DataWave array processing system is made of DataWave chips, (fig. 2) each one containing 16 identical, but individually programmable, processors working on the data flow principle and organized in a matrix form. Each cell is a RISC processor with 12-bit architecture which operates on the pipeline principle. The cells communicate with their four nearest neighbors via asynchronous parallel buses. The computing power of one processor is up to 125 MIPS, where an instruction may imply two operations, and the maximum data transfer rate via the processor boundaries is 750 MByte/s. The program memory of each processor is 64 words of 48-bits each.

The Fast Digital Parallel-Processing (FDPP) system is a modular system in which each node consist of one Digital Signal Processor (DSP) tightly coupled to one Transputer. Any number of nodes can be interconnected using the four serial links (1.2 Mbyte/s) provided by the Transputer, while any data source can communicate in a parallel manner with the DSP up to 10 Mbyte/s.

The Fast Digital Parallel-Processing Dual triple-port Memory (FDPP_DM) module has the same architecture

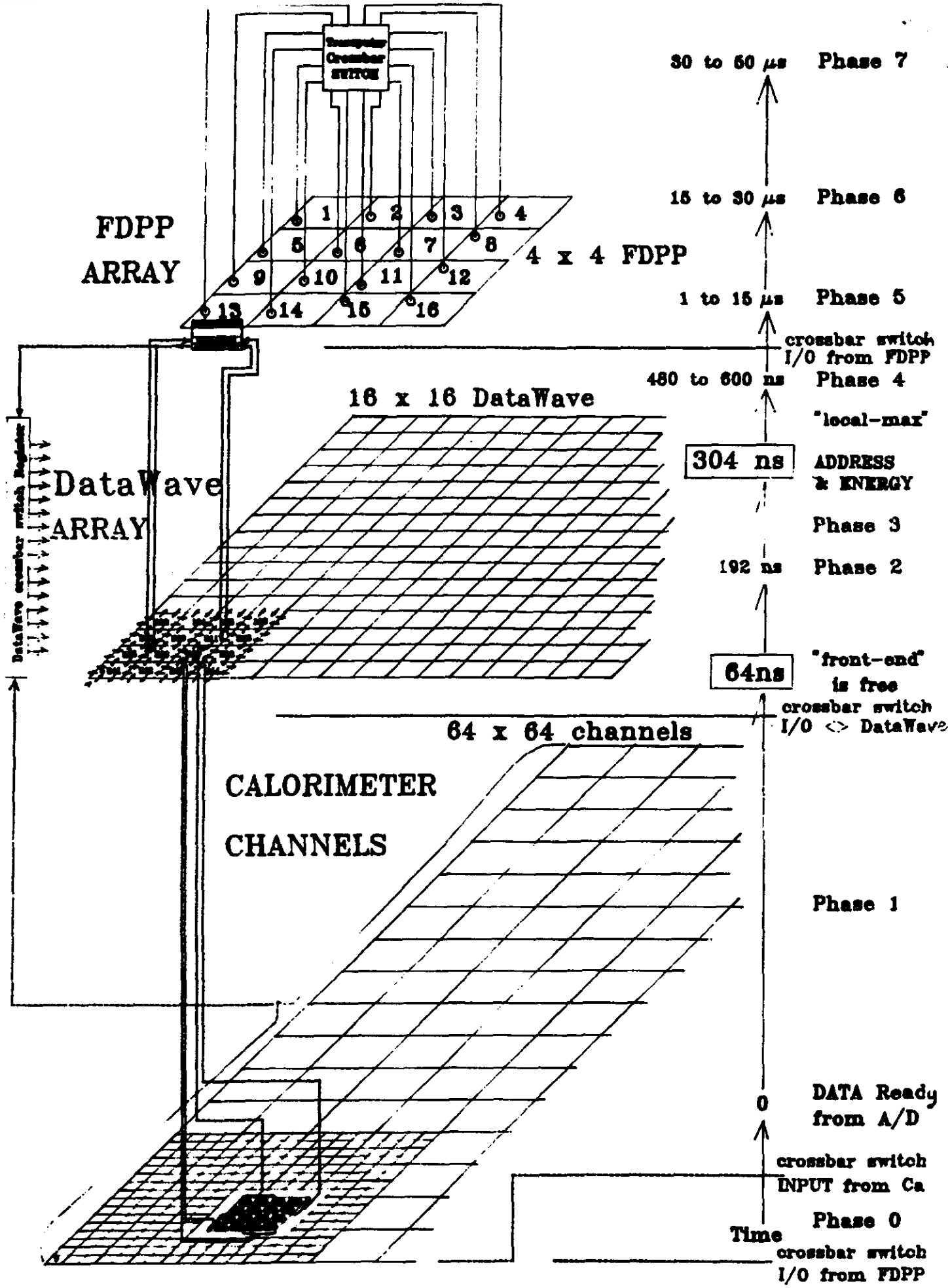

Fig. 1 Fast cluster finding system block diagram.

as the FDPP module with an additional internal direct-to-memory channel permitting data transfer at up to 150 Mbyte/s with either memory bank "X" or "Y".

There are three level of programmability:
(a) low level assembly code for the DataWave,
(b) assembly and "C" for the DSP32C, and
(c) high level language (OCCAM, C, FORTRAN, ADA) on the Transputer.

A crossbar switch is being designed to switch the parallel I/O ports of the DataWave chips to one of the following:
- the calorimeter input channels,
- the adjacent DataWave chips and
- the FDPP parallel array.

The design is presently waiting for the final specifications of the DataWave chip.

In the examined case, the Calorimeter channel values are digitized from A/D converters.

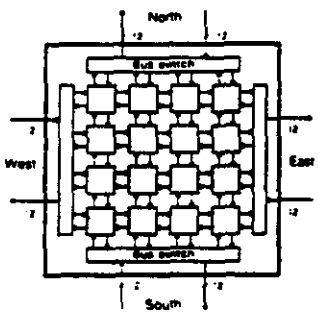

Fig. 2 DataWave chip architecture (courtesy of ITT).

The data-flow from the calorimeter with its associated timing (in parentheses) can be described as follows (see fig.1):

PHASE 0 The DataWave crossbar switch is set to INPUT from the FDPP (or FDPP_DM) array system which loads all programs and constants into the DataWave array.

PHASE 1 The DataWave crossbar switch is set to INPUT from the Calorimeter so that digital values can be transferred from the calorimeter to the DataWave Processing Elements (PE) 64 ns), next DataWave crossbar switch register is set to I/O between DataWave PE.

At this stage, the "front-end" electronics is free for the next acquisition (64 ns after digitized data was ready).

PHASE 2 Data received from the Calorimeter is exchanged between each DataWave Processor and its eight neighbors.

PHASE 3 The DataWave array finds all "local maxima", calculates their energies and compares them with a threshold. A local maximum is defined as a channel value greater than or equal that of any of its 8 nearest neighbors. "Local maxima" addresses and energies are then available at this stage (304 ns).

Total energy or transverse energy are calculated at this stage as partial results on 256 calorimeter channels. One of these two results can be obtained within the same time as the search of local maxima in a pipeline mode, while the other requires an additional 300 ns.

PHASE 4 The DataWave array transfers results of a 256-channel total energy or transverse energy determination, "local maxima" and their region of interest (which may extend beyond the area covered by the 256 channels) to the DataWave array exit which points towards the FDPP (480 to 600 ns). The DataWave crossbar switch register is set to I/O from the FDPP array.

PHASE 5 Total energy or transverse energy from 256 channels, "local maxima" and their region of interest are transferred from the DataWave array to the FDPP array (1 to 15 μs).

PHASE 6 The FDPP array (DSP part) calculates all cluster-shape factors to separate, for example, pions from electrons (15-30 μs).

PHASE 7 The FDPP (Transputer part) correlates the results and transfers them to the Crate Controller (30-50 μs).

2. State-of-the-art technology integrated in high-energy physics experiments.

Future experiments require electronic performance that may not yet seem available on the market. Much of the analog circuitry required for a given HEP application, is so specialized that it is impossible to find it among commercial components. Then the necessity to develop an ASIC or a VLSI circuit is unavoidable. For some very fast

and special combinatorial logic or a device with very few specialized instructions, it may really be necessary to develop a special chip.

For digital circuitry the situation is different, and before proceeding one should carefully investigate the latest technological advances in the field of programmable devices where progress is presently very fast, and make a serious effort to efficiently integrate these commercial components in a design that satisfies the requirements of the application. A decision to make a digital ASIC should be weighed very carefully because of the difficulty of providing all the necessary software development tools.

In order to efficiently integrate the commercial components (Data-driven array Processors, DSP and Transputers) in High Energy Physics applications, the following considerations have been and should be kept in mind:

(a) to find the optimum balance between the tasks to be executed and the processor characteristics.

(b) to find the best interconnection scheme (tightly coupled or loosely coupled) among processing elements in each processor array and between array processors.

(c) to define a flexible processor architecture with the possibility to change dynamically the topology of the system (e.g. from a tree structure to a mesh structure) on the high level of array processor and with a data flow based architecture on the lower level of array processors

The reason for having used two processors (Transputers and DSPs) on the higher level with different cost per Mflops, is because the AT&T DSP32C at a very low cost per Mflop can do most of the rapid calculations while the Transputer array at a higher cost per Mflop, gives an easier means to the user to distribute tasks over several processors (Transputers and DSPs) and to correlate results.

The low cost of the DataWave Processing Element (PE) gives instead on the lower level the possibility to make a scheme where there is one processor for each Calorimeter channel, ideal for rapid parallel calculations.

The features of the fast parallel I/O connection, associated with the interconnection scheme adopted in this system, provides a fast means to exchange data:

(a) from the calorimeter channels to the DataWave array;

(b) between PEs of the DataWave array, giving the full granularity of the calorimeter channels without boundary limitations.

(c) between DataWave array processors and the higher-level array of FDPP (DSPs and Transputers).

3. System modularity and flexibility.

The present system is modular in the sense that a "Logical Unit" is made of one FDPP (or FDPP_DM) module and 16 DataWave chips organized in a matrix 4x4 thus giving a platform of 256 DataWave Processing Elements organized in a matrix of 16 x 16. This choice does not introduce any boundary limitations in the DataWave Array but is simply a practical choice in associating the PE with the closest exit point to the higher-level of processors (fig. 1)

The higher-level Processors (FDPP or FDPP_DM) are linked to the Crate Controller (VME or IBM PC) and among themselves through the Transputer serial link (at 1.2 Mbyte/s max) or through the 32-bit parallel I/O port (up to 150 Mbyte/s max).

Any number of "Logical Units" can then be interconnected in a matrix scheme, regardless of the hardware platform used (VME, FASTBUS, etc.).

All timings given in this report should be independent of the Calorimeter size (100 to hundred thousand channels). As the size of the Calorimeter increases, the only time increases is the one required to transfer the data of the clusters found from the transputer to the Crate Controller.

4. Requirements on the calorimeter triggers and data compaction.

4.1. Triggers requirements.

From the requirements specified for triggers for the future colliders [3-5], one may conclude that simplified algorithms which execute in very short time should be capable of providing a reasonable selection. In the case of a calorimeter, the main algorithms are:

(a) Total Energy [4,5]

$$E_{tot} = \sum c_i E_i$$

(b) Transverse Energy [4,5]

$$E_T = \sum c_i E_i \cos\phi_i$$

where: "c_i" is the calibration constant for channel "i"
"E_i" is the signal for channel "i" and
"ϕ_i" is the angle of incidence of channel "i".

(c) Identify clusters or local maxima in the whole calorimeter [6-8], (a local maximum is found when a cell value is greater than or equal to that of any of its neighbors).

$$C > I_i \text{ for } i = 1,\ldots,8 \text{ (see fig. 3)}$$

I	I	I
I	C	I
I	I	I

$$E = \sum_{i=1}^{8} I_i + C$$

Fig. 3 Local maximum.

(d) Apply a threshold to the sum of the energies of the local maximum and of its neighbors.

$$\text{THRESHOLD} < \sum_{i=1}^{8} I_i + C$$

(e) Calculate the cluster shape factors: I/C, O/C, [6,7] (e.g. to separate pions/electrons)

$$I/C = (1/8 \sum_{i=1}^{8} I_i)/C$$

$$O/C = (1/16 \sum_{i=1}^{16} O_i)/C \qquad \text{(see fig. 4)}$$

4.2. Data reduction during acquisition.

To have the possibility to analyze more in detail each local maximum, that is a candidate to be a cluster, a relative large area (region of interest) surrounding the local maximum must be saved as useful data for further analysis. On the other hand, there is no need to transfer zeros from empty channels. The DataWave array is therefore capable of achieving a substantial reduction of the amount of data.

5. Performance of the system on real-time algorithms.

5.1. Finding "local maxima" on the DataWave array.

Each digital value of the calorimeter channel is transferred into a DataWave Processor. The DataWave array program to do this is shown in Table 1. In the first five lines calibration constants and thresholds are loaded into registers (r11 to r15). The next four instructions perform the following actions:

(a) each input value from the calorimeter (n) is multiplied by the relative calibration constant and accumulated

(b) the same value is also stored in local PE registers (r5-r9) and distributed to the adjacent PE. In the case of cell 0,0, the data are sent east (e) and south (s).

Table 1. DataWave Program to transfer input data into PE.

```
r2:     r11=C4
        r12=C5
        r13=C1
        r14=C2
        r15=THRES
/* START LOADING FROM READOUT ELECTRONIC */
        t0-     alu=alu+n*r11,   e=s=r9=n
        t1-     alu=alu+n*r12,   e=s=r8=n
        t2-     alu=alu+n*r13,   e=s=r5=n
        t3-     alu=alu+n*r14,   e=s=r6=n
/* END LOADING FROM READOUT ELECTRONIC */
```

In order to calculate the "local maximum", each processor needs to have the data of its neighbors in its own memory (see fig. 3). This task of transferring the data between processors is accomplished in a programmable way by the DataWave processors (Tables 1 and 2). The required time for this task is 128 ns. During the execution of the above program shown (see Table 2) partial calculation of the energy is also accomplished, thus only an additional 112 ns are required to have the energy of each "local maxima".

Table 2. DataWave program to exchange data with neighboring PE.

```
/* START TO EXCHANGE DATA WITH NEIGHBORING PE */
        t4-     r2=n,    w=r5
        t5-     acc=r8+r9
        t6-     r3=e,    acc=acc+r5
        t7-     s=r4=w, n=r5
        t8-     acc=acc+r3
        t9-     w=r5,    acc=acc+r6
        t10-    n=w,     r7=s
        t11-    r1=n,    acc=acc+r2
        t12-    acc=acc+r4       s=alu
/* END OF DATA EXCHANGE WITH NEIGHBORING PE */
```

The program listings for DataWave processor are derived from the examples reported in ref. [2], and should be considered preliminary as the DataWave chip is still under development.

Acknowledgements

The study and test of this project has been supported initially by the Computing Networking Division and successively by the Electronic and Computing in Physics Division. Additional support through a fellowship from the ASP (Associazione per lo sviluppo Scientifico e Tecnologico del Piemonte) for a physics student S. Buono, is gratefully acknowledged.

The author wishes to thank the experimental physicists of the SPACAL Collaboration for making their data available for these tests.

A special thank to Werbrouck for critically reading this document and for many helpful suggestions.

References:

[1] D. Crosetto. "Fast Digital Parallel Processing module" FDPP CERN - DD/89 - 33 (AC)

[2] K. Caesar, U. Schmitdt, S. Mehrgardt, T. Himmel. Parallel computing made efficient. Elektronik magazine 12/June 8, 1990

[3] C.W. Fabjan and T. Ludlam. Calorimetry in High-Energy Physics. Ann. Rev. Nucl. Part. Sci. Vol. 32 (1982)

[4] A.J. Lankford. Issues for trigger processing at high luminosity colliders. ECFA study week on instrumentation Technology for High-Luminosity Hadron Colliders, Barcelona 14-21 September 1989.

[5] P. Jenni. Aspects of jets and calorimetry at future hadron colliders. ECFA study week on instrumentation Technology for High-Luminosity Hadron Colliders, Barcelona 14-21 September 1989.

[6] R.K. Bock et. al.: Benchmarking computer architectures for HEP real-time algorithms, CERN - LAA/RT/88-08.

[7] S. Buono and D. Crosetto. Test results of real-time algorithms executed on FDPP with SPACAL data. CERN/ECP 90-6.

[8] R.K. Bock et. al.: Algorithms and image processing architecture for on-line electron identification from lateral profiles in SPACAL, CERN - LAA RT/90-01 May, 1990.

[9] SPACAL Collaboration, Proposal: "Scintillating fibre calorimetry at the LHC" CERN/DRDC/90-23

Crosetto

SUMMARY

1. Requirements on Calorimeter Triggers & Data acquisition

2. Integration of commercial components in High Energy Physics applications

3. Fast cluster finding system on two cooperating levels of Arrays Processors

4. Performance of the system on Real-time algorithms.

5. What is available today of the described system. (execution time of real-time algorithms on present and future systems are given)

Typical problems of Digital triggers & Data acquisition/compaction in Calorimetry of High Energy Physics.

For any number of channels:

1. Calculate the total energy and the transverse energy

2. Calculate the geographical address of clusters (local maxima).

3. Apply a threshold to the combined energy of a local maxima and of its neighbors.

4. Isolate from the empty calorimeter channels:
   - the clusters found along with their regions of interest and
   - calculate their cluster shape-factors (e.g. to separate pions/electrons).

FOCAL MONITOR
Euo(λ): 34.38 CeV

Rapid improvements in performance of commercially available

- Digital Signal Processors and of
- Data-driven Array Processors

are an invitation to make a serious effort

- to efficiently integrate these commercial components
-in a design that satisfies the requirements of the applications in HEP.

The decision of developing a new VLSI special digital processor

- should be weighted very carefully
- because of the difficulty of providing all necessary software development tools.

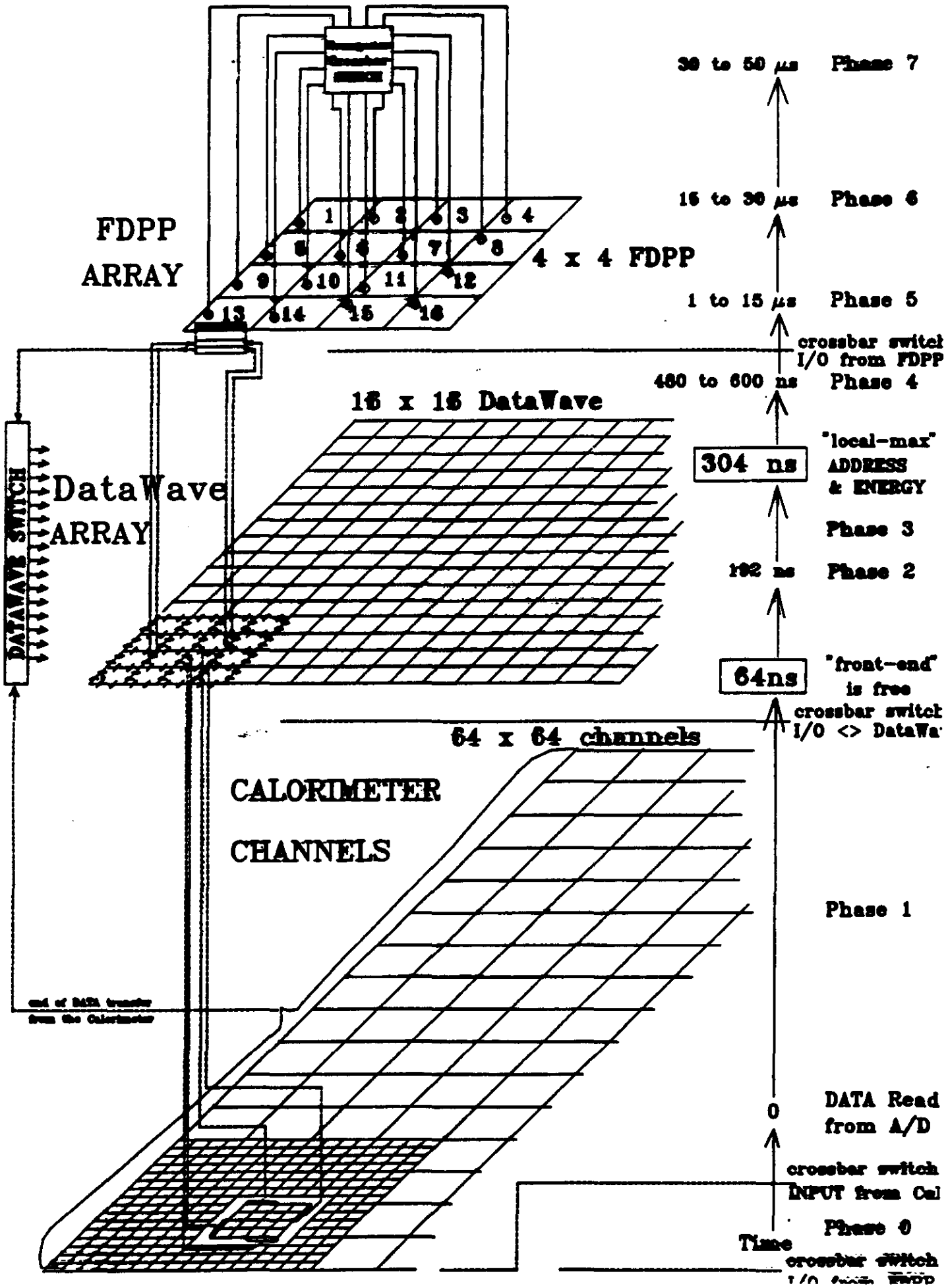
FDPP
ARRAY
4 x 4 FDPP
1
2
3
4
5
6
7
8
9
10
11
12
13
14
15
16
30 to 50 μs
Phase 7
15 to 30 μs
Phase 6
1 to 15 μs
Phase 5
crossbar switch
I/O from FDPP
480 to 600 ns
Phase 4
16 x 16 DataWave
DATAWAVE SWITCH
DataWave
ARRAY
304 ns
"local-max"
ADDRESS
& ENERGY
Phase 3
192 ns
Phase 2
64ns
"front-end"
is free
crossbar switch
I/O <> DataWa
64 x 64 channels
CALORIMETER
CHANNELS
Phase 1
end of DATA transfer
from the Calorimeter
0
DATA Read
from A/D
crossbar switch
INPUT from Cal
Phase 0
Time
crossbar switch

The fast cluster finding system is based on two cooperating levels of Array Processors:

- Higher level: FDPP

(Fast Digital Parallel Processing Module based on DSPs and Transputers)

- Lower level: DataWave

(Data-controlled array processor for video signal processing. Elektronik magazine 12/June 8, 1990)

module

FDPP

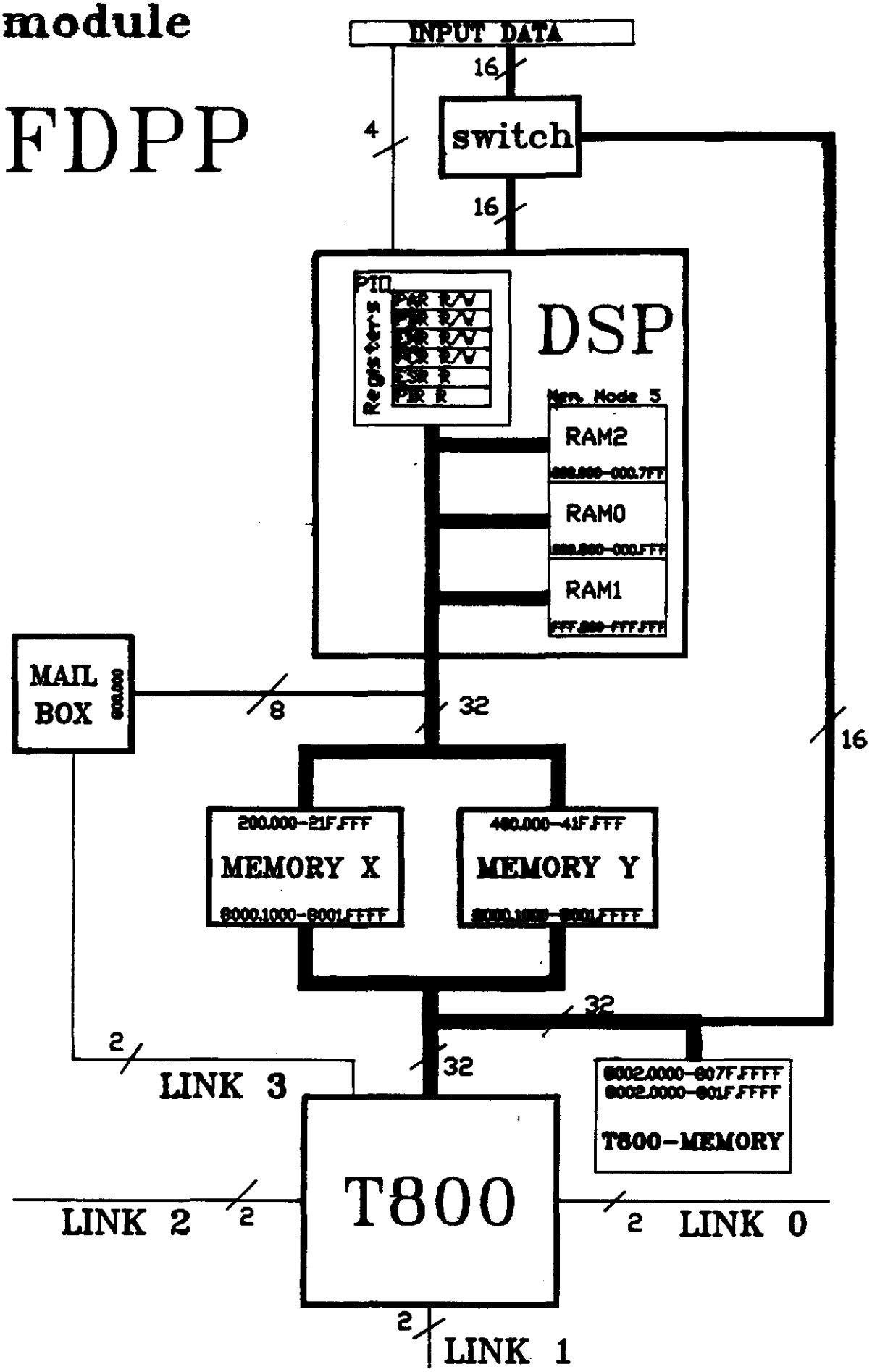
INPUT DATA
16
4
switch
16
PIO
Registers
PAR R/W
PBR R/W
PCR R/W
PDR R/W
ESR R
PSR R
DSP
Mem. Mode 5
RAM2
RAM0
RAM1
MAIL BOX
8
32
16
200.000-21F.FFF
MEMORY X
8000.1000-8001.FFFF
400.000-41F.FFF
MEMORY Y
32
2
LINK 3
32
8002.0000-807F.FFFF
8002.0000-801F.FFFF
T800-MEMORY
T800
LINK 2
2
2
LINK 0
2
LINK 1

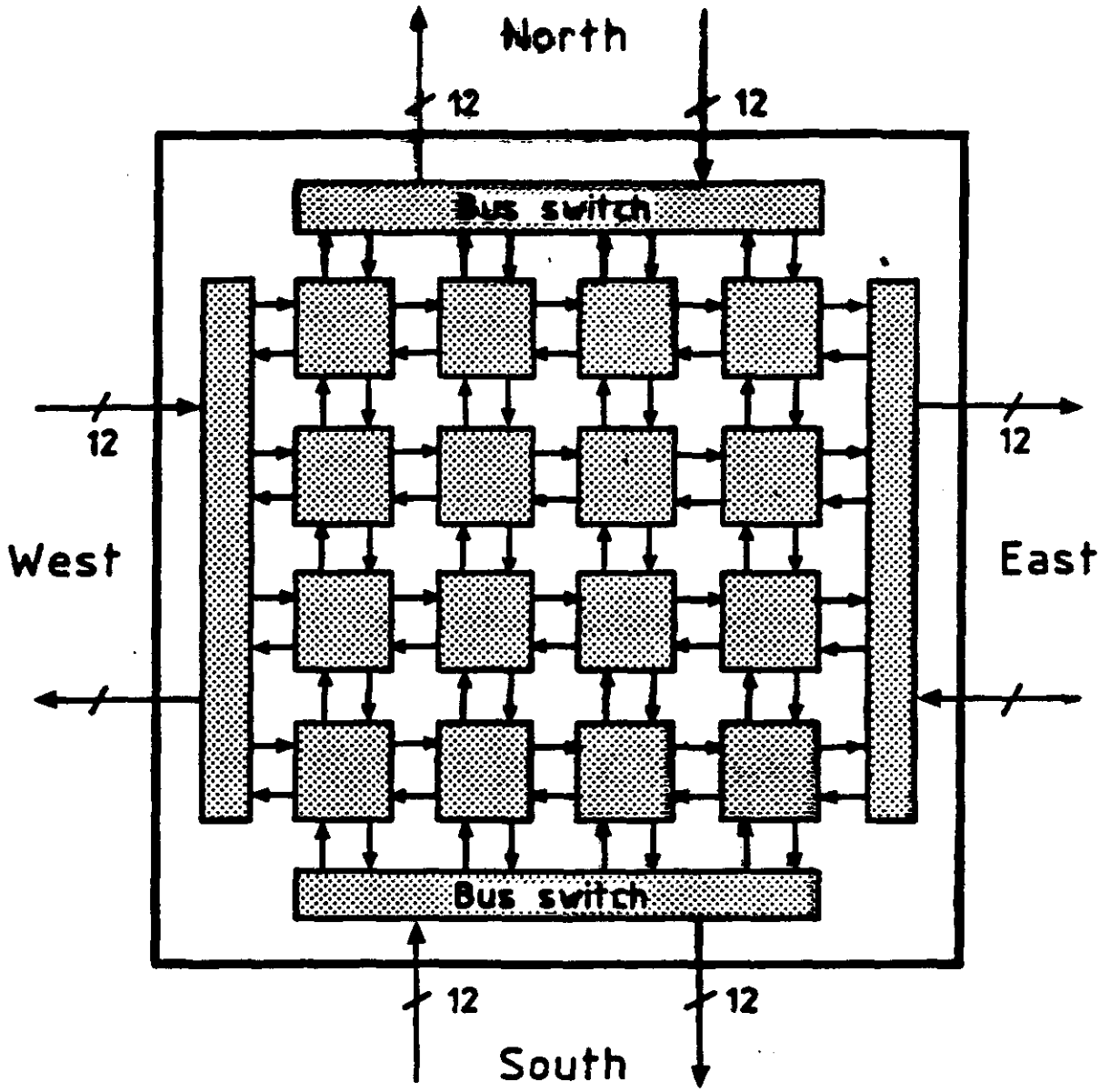
North
12
12
Bus switch
12
West
12
East
Bus switch
12
12
South

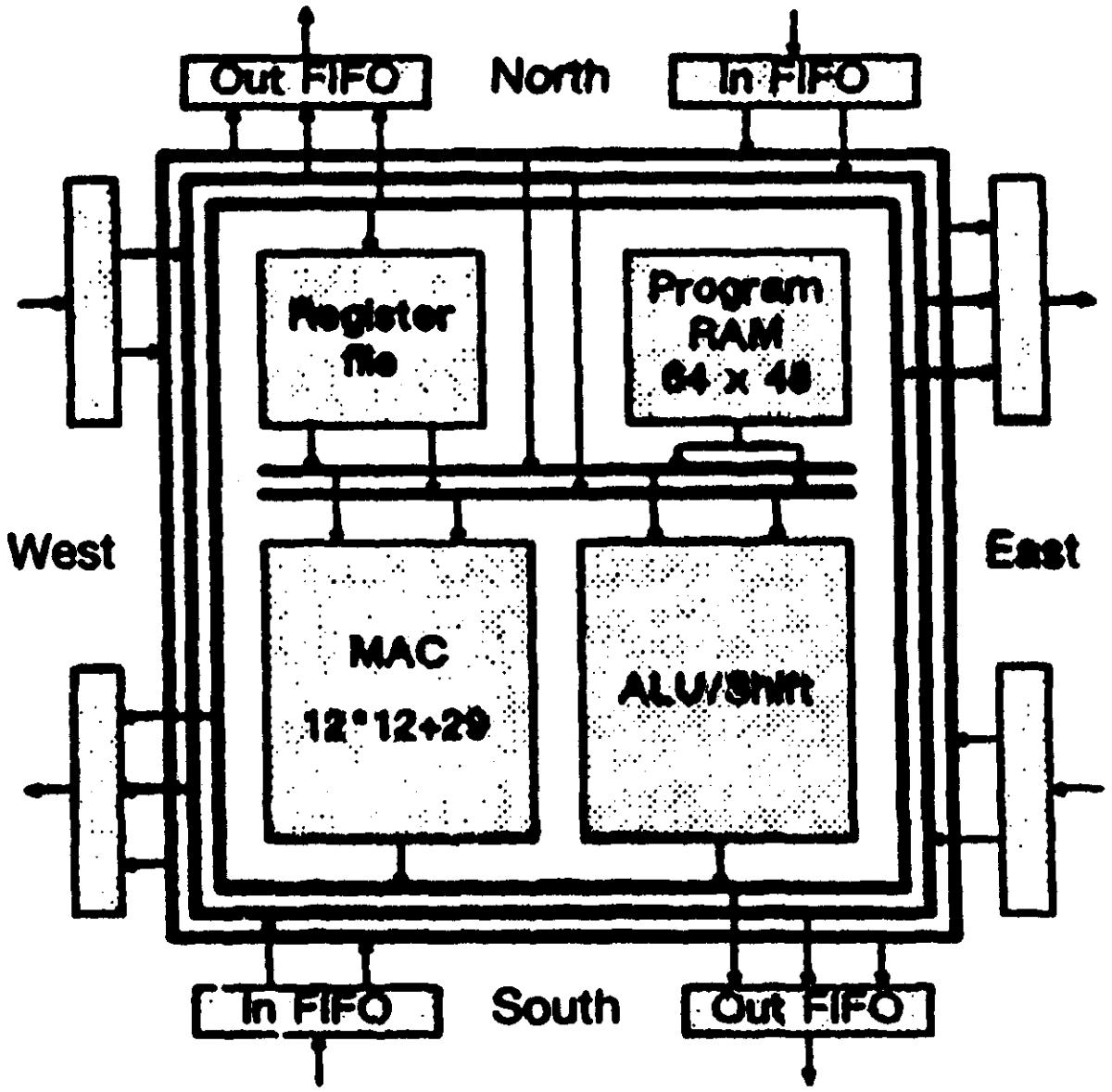

Fig. 5. The architecture of the cell covers all the main processor elements

DataWave chips

The one described in the magazine Elektronik 12/june 8, 1990 has:

- 16 identical PEs(in program also with one and 64 PEs)

- individually programmable

- working on the data flow principle and organized in a matrix form

- each PE is a RISC processor with 12-bit architecture which operates on the pipeline principle

- each PE communicate with their four nearest neighbors via asynchronous parallel buses

- each PE can have a maximum program length of 64 words of 48-bits each.

FDPP + DATAWAVE system

gives the possibility to realize a

FLEXIBLE ARCHITECTURE

1. MIMD PARALLEL HYBRID SYSTEM

(loosely coupled but with both serial and parallel exchange)
on the higher level array processor
(DSP + Transputers)

- with the possibility to change dynamically the topology of the system (e.g. from a tree structure to a mesh structure)
- with 1.2 Mbyte/s serial links
- with parallel channels of up to 150 Mbyte/s

2. DATA FLOW BASED

on the lower level array processor (DataWave)

- with 750 Mbyte/s maximum transfer rate between chips.

1. MIMD PARALLEL HYBRID SYSTEM

used for:

- distributing processes over several processors

- concentrating the processing power in the region of the detector where there are some interesting data.

2. DATA FLOW BASED

used in:

(a) CALORIMETER
- fast data correlation

(b) TRACKING DETECTORS
- should be possible to reconstruct tracks using the data flow principle:

Processing Elements execute programs when the input data is available.

- one DataWave Processing Element (PE)
- for each Calorimeter channel

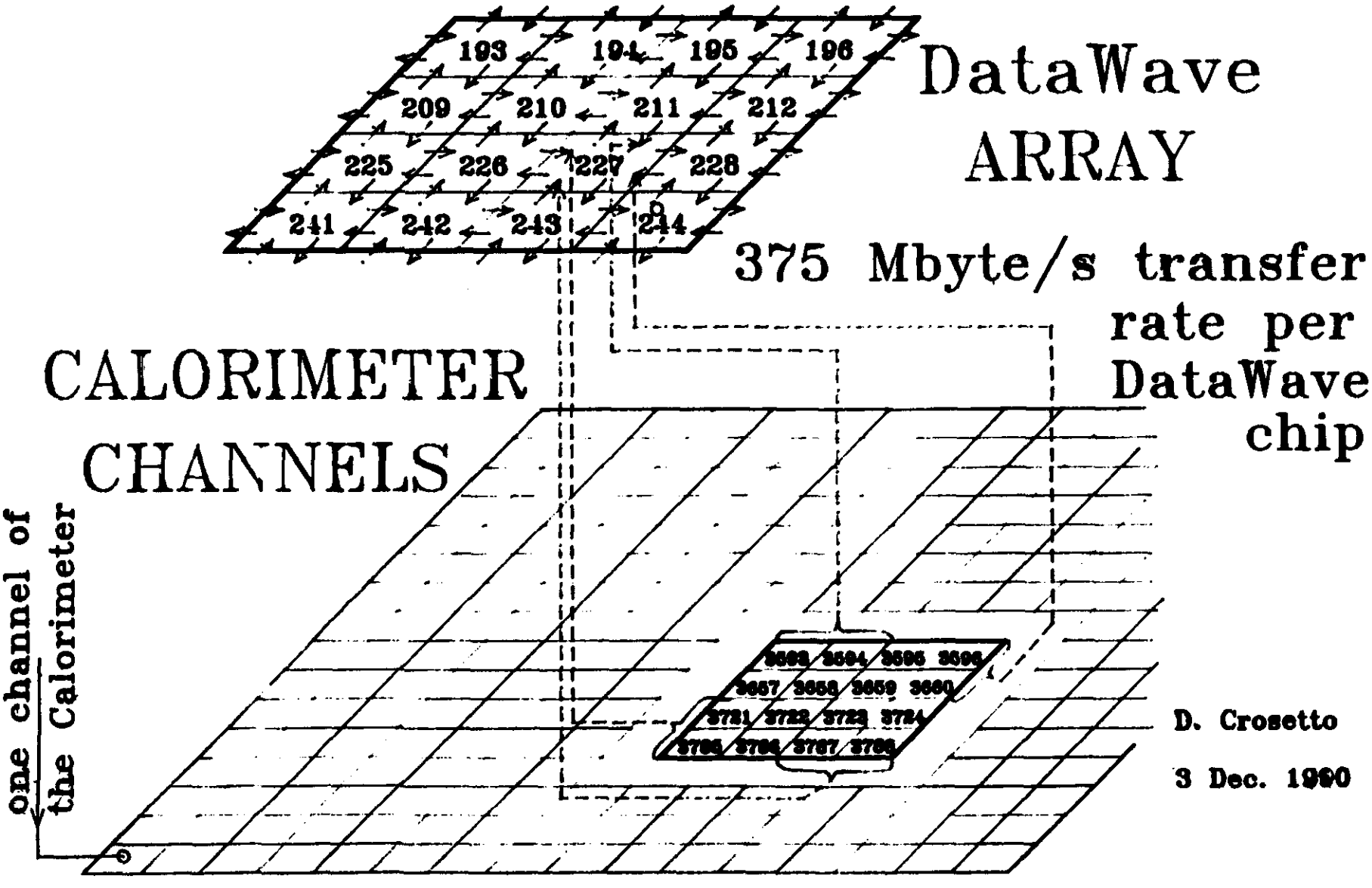

D. Crosetto

3 Dec. 1990

A "local maximum" is a channel value greater than or equal to its neighbors

I	I	I
I	C	I
I	I	I

$$E = \sum_{i=1}^{8} I_i + C$$

- the Calorimeter (A/D converters)
- and from neighboring DataWave chips

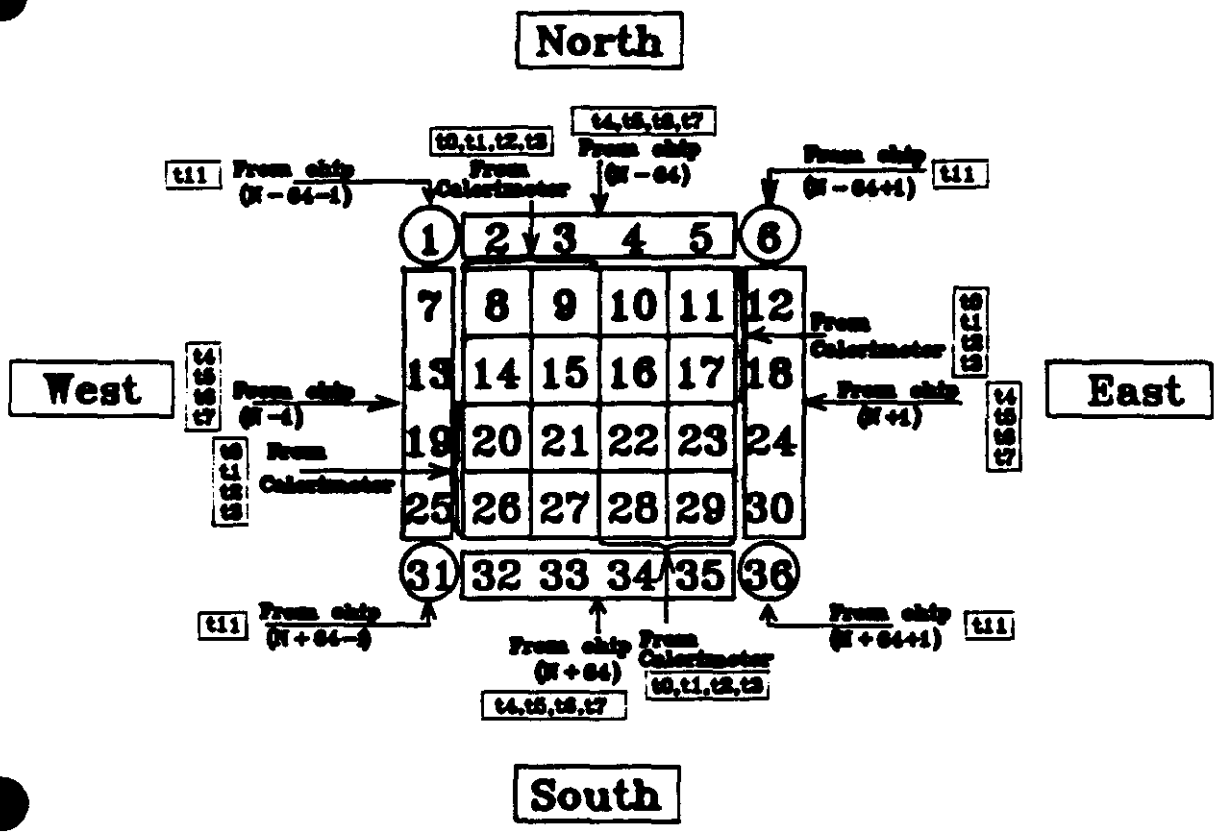

Each DataWave sends DATA to:
- neighboring DataWave processors

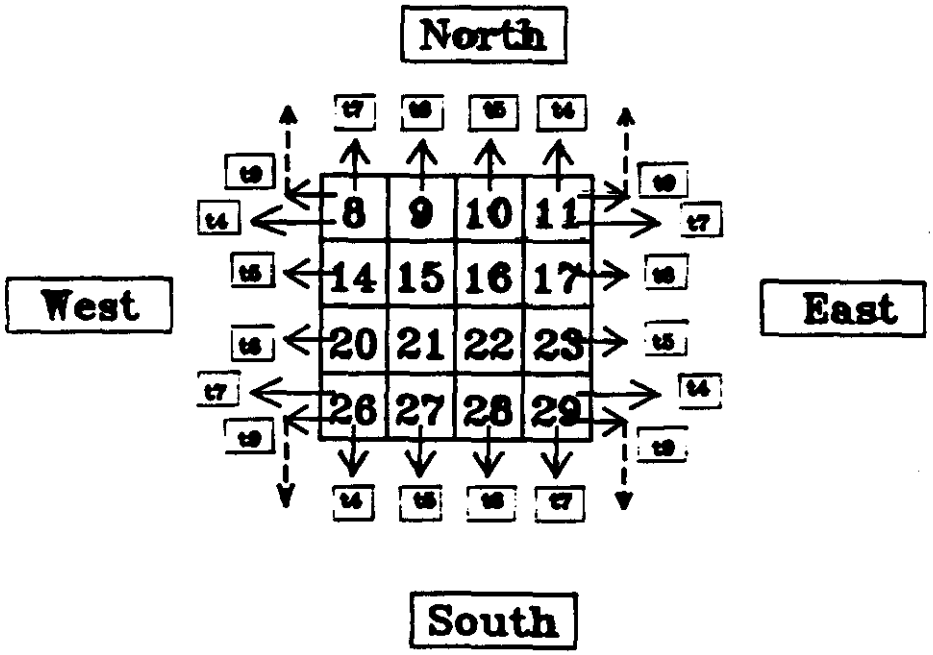

DataWave program to transfer input data into PE

```
/* START LOADING FROM READOUT ELECTRONIC */
    t0      alu=alu+n*r11,      e=s=r9=n
    t1      alu=alu+n*r12,      e=s=r8=n
    t2      alu=alu+n*r13,      e=s=r5=n
    t3      alu=alu+n*r14,      e=s=r6=n
/* END LOADING FROM READOUT ELECTRONIC */
```

DataWave program to exchange data with neighboring PE

```
/* START TO EXCHANGE DATA WITH NEIGHBORING PE
    t4      r2=n,               w=r5
    t5      acc=r8+r9
    t6      r3=e,               acc=acc+r5
    t7      s=r4=w,             n=r5
    t8      acc=acc+r3
    t9      w=r5,               acc=acc+r6
    t10     n=w,                r7=s
    t11     r1=n,               acc=acc+r2
    t12     acc=acc+r4,         s=alu
/* END OF DATA EXCHANGE WITH NEIGHBORING PE *
```

Fast inter-process communication within the DataWave Array
- overcomes the problem of overlapping areas,
- and effectively provides a continuous array of PEs.

Local maxima, along with their energy,
- are found in the DataWave array and
- are transferred, with the data of their region of interest,
- to a higher-level DSP array-processors system, even if part of the data fall outside the region originally attributed to a particular FDPP.

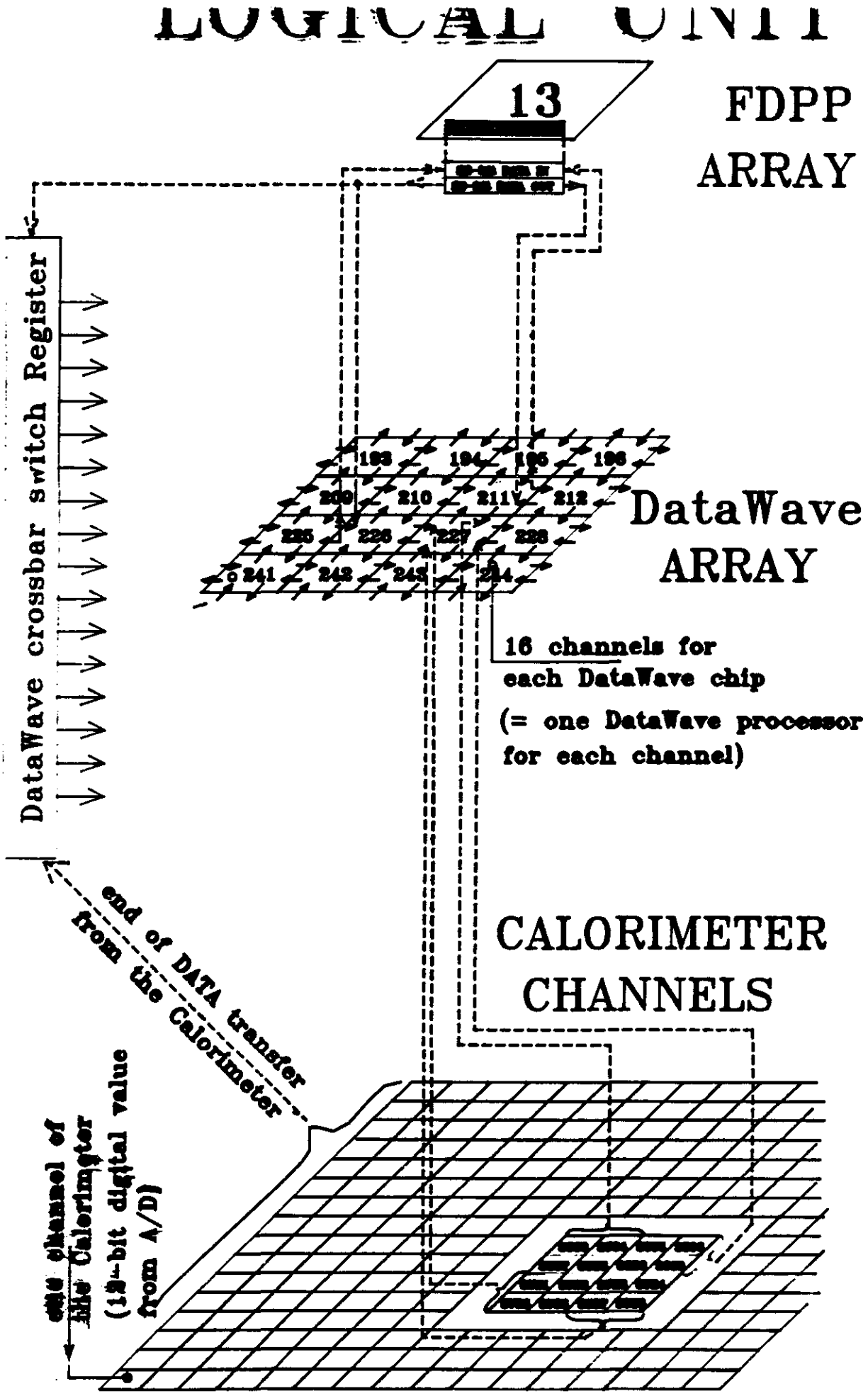
LOGICAL UNIT
13
FDPP
ARRAY
DataWave crossbar switch Register
DataWave
ARRAY
16 channels for
each DataWave chip
(= one DataWave processor
for each channel)
CALORIMETER
CHANNELS
end of DATA transfer
from the Calorimeter
(12-bit digital value
from A/D)

DataWave Communications
(controlled by the DataWave switch)

- down to calorimeter channel
  (proposed multiplex 4 channels
  on one cable unidirectional
  (16 ns for channel)

- across the other DataWave PE
  (North, East, West, South) NEWS
  bidirectionally (750 Mbyte/sec)

- Up to FDPP
  (bidirectionally 150 Mbyte/s)

(proposed 256 DataWave PE per upward link)

This choice does not introduce any boundary limitations in the DataWave Array but is simply a practical choice in associating the PE with the closest exit point to the higher-level DSP array-processors.

Performance of the whole system:

Full programmability over the entire calorimeter at the single channel granularity level, with no boundary limitations.

	TIME
- total energy cluster finding (address & energy)	304 ns
- Transverse energy (additional)	300 ns
- cluster shape-factors (e.g. to separate pions from electrons)	15 μs

Cost of the integration
- of commercial components (Data-driven array Processors, DSP and Transputers)
- in High Energy Physics applications.

Transputer	INMOS	T800	70	$/Mflop(4.5)
DSP	AT&T	DSP32C	7	$/Mflop(25)
Data-driven array processor	ITT	DataWave	3.?	$/Processor

Why not use only the cheapest components ?

Aim:

- Find the best balance between the tasks to be executed and the processor characteristics.

- Find the best interconnection scheme (tightly coupled or loosely coupled) among processing elements in each processor array and between array processors.

Low and to high end programmability

Level 1 (low-level)

DataWave Array Processors

- languages: assembly
- maximum program length of 64 words of 48-bit each

Level 2 (high-level)

- DSP part
  - languages: C or Assembly
  - maximum program length of 256 Kbytes
  - Library
  - Crosscompilers for MS-DOS, UNIX, VMS
  - Simulator: MS-DOS

- Transputer Part:
  - languages: OCCAM, C, FORTRAN
  - maximum program length of 8 Mbytes
  - compiler on Transputer
  - Debugger: postmortem

FDPP Development software

Algorithm 1

each FDPP

– calculates E, I/C, O/C (in floating point)

in 15 μs

SHAPE FACTORS

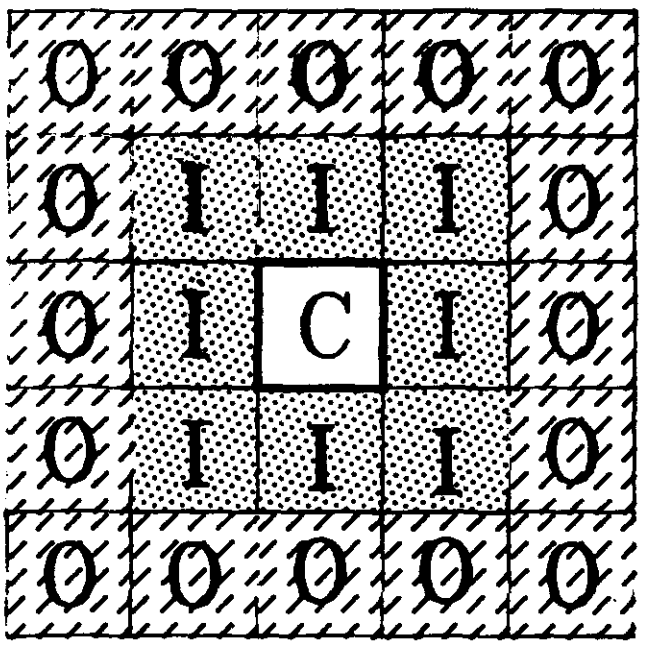

$$E = C + \sum_{i=1}^{8} I_i + \sum_{i=1}^{16} O_i$$

$$I/C = (1/8 \sum_{i=1}^{8} I_i)/C$$

$$O/C = (1/16 \sum_{i=1}^{16} O_i)/C$$

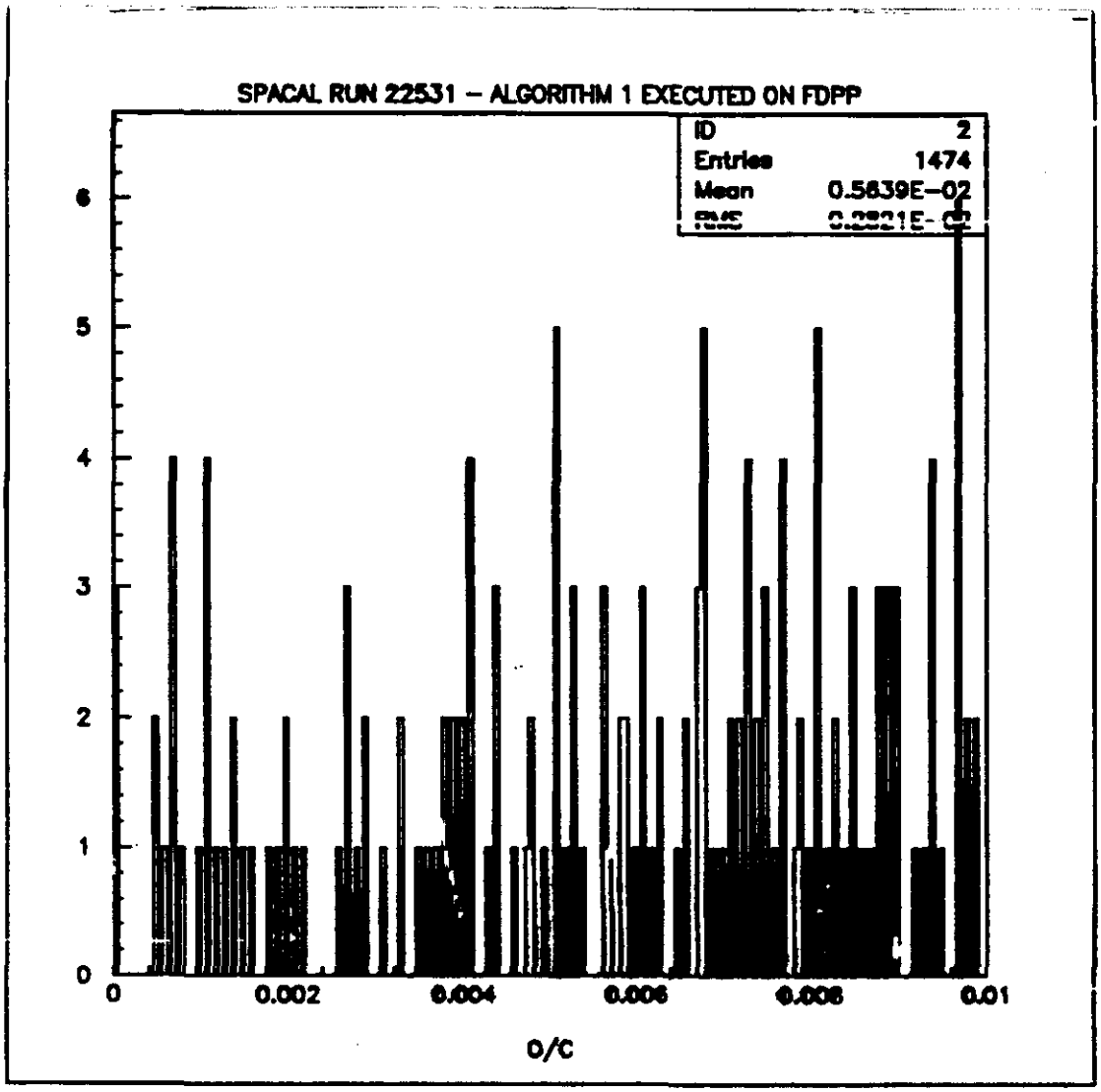
SPACAL RUN 22531 – ALGORITHM 1 EXECUTED ON FDPP
ID 2
Entries 1474
Mean 0.5639E-02
0
1
2
3
4
5
6
0
0.002
0.004
0.006
0.008
0.01
O/C

~ 2/1000

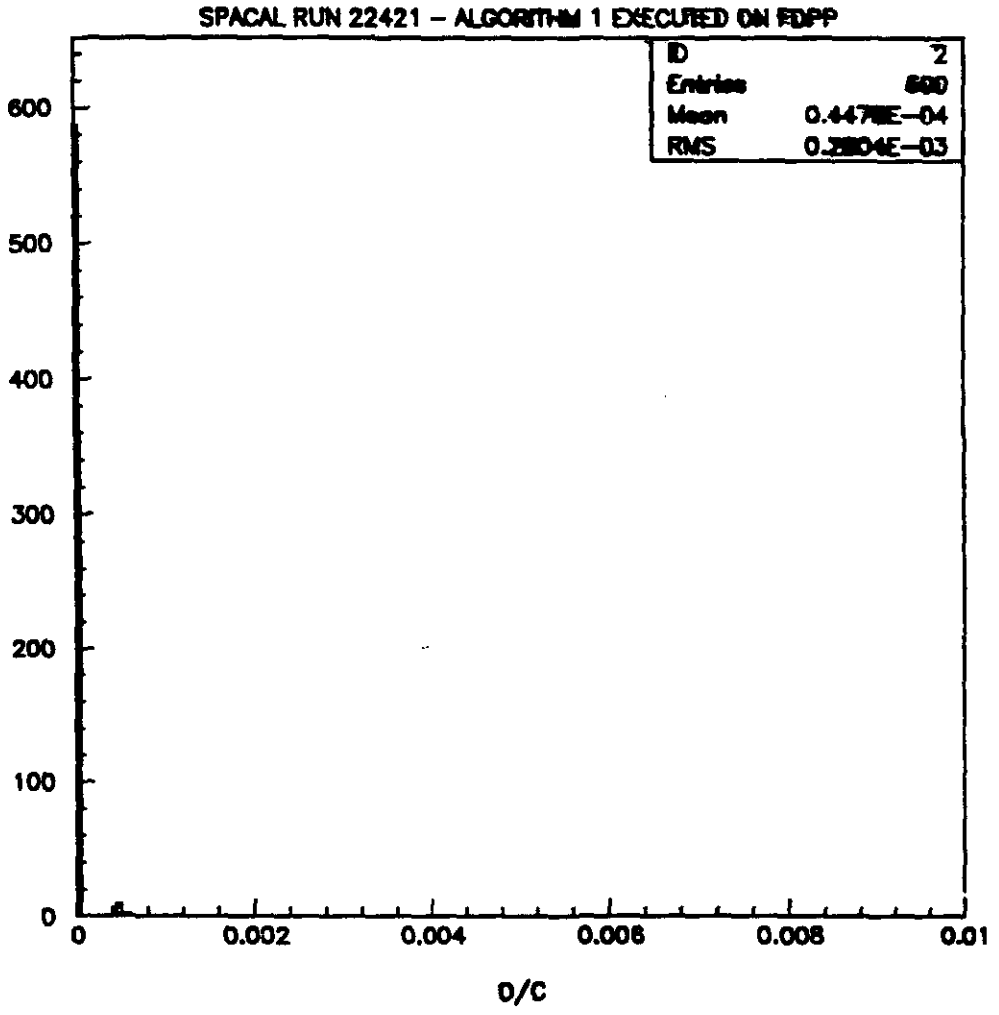
SPACAL RUN 22421 – ALGORITHM 1 EXECUTED ON FDPP
ID 2
Entries 600
Mean 0.4478E-04
RMS 0.3804E-03
600
500
400
300
200
100
0
0
0.002
0.004
0.006
0.008
0.01
D/C

Algorithm 2

each FDPP

- calculates Rp (in floating point)

in 15 μs

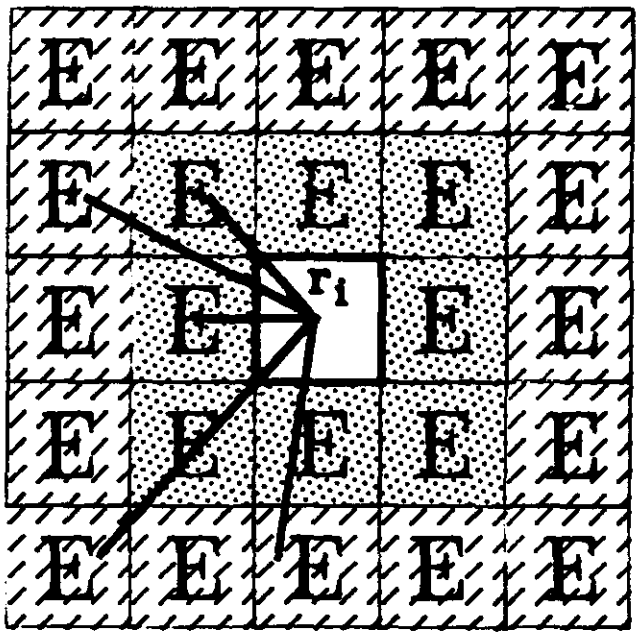

$$Rp = \frac{\sum_{i=1}^{25} r_i E_i^{0.4}}{\sum_{i=1}^{25} E_i^{0.4}}$$

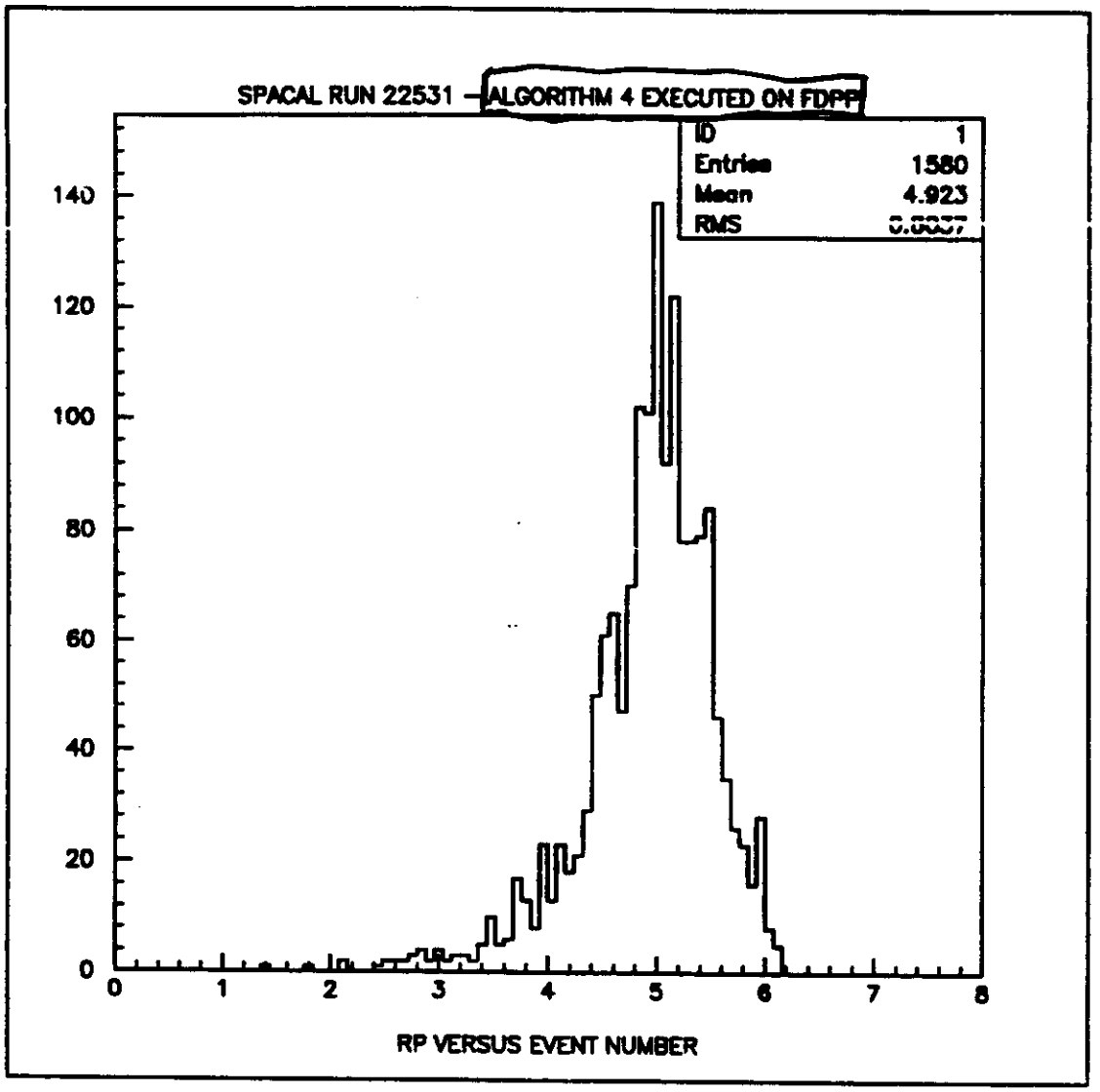
SPACAL RUN 22531 – ALGORITHM 4 EXECUTED ON FDPF
ID 1
Entries 1580
Mean 4.923
RMS
140
120
100
80
60
40
20
0
0
1
2
3
4
5
6
7
8
RP VERSUS EVENT NUMBER

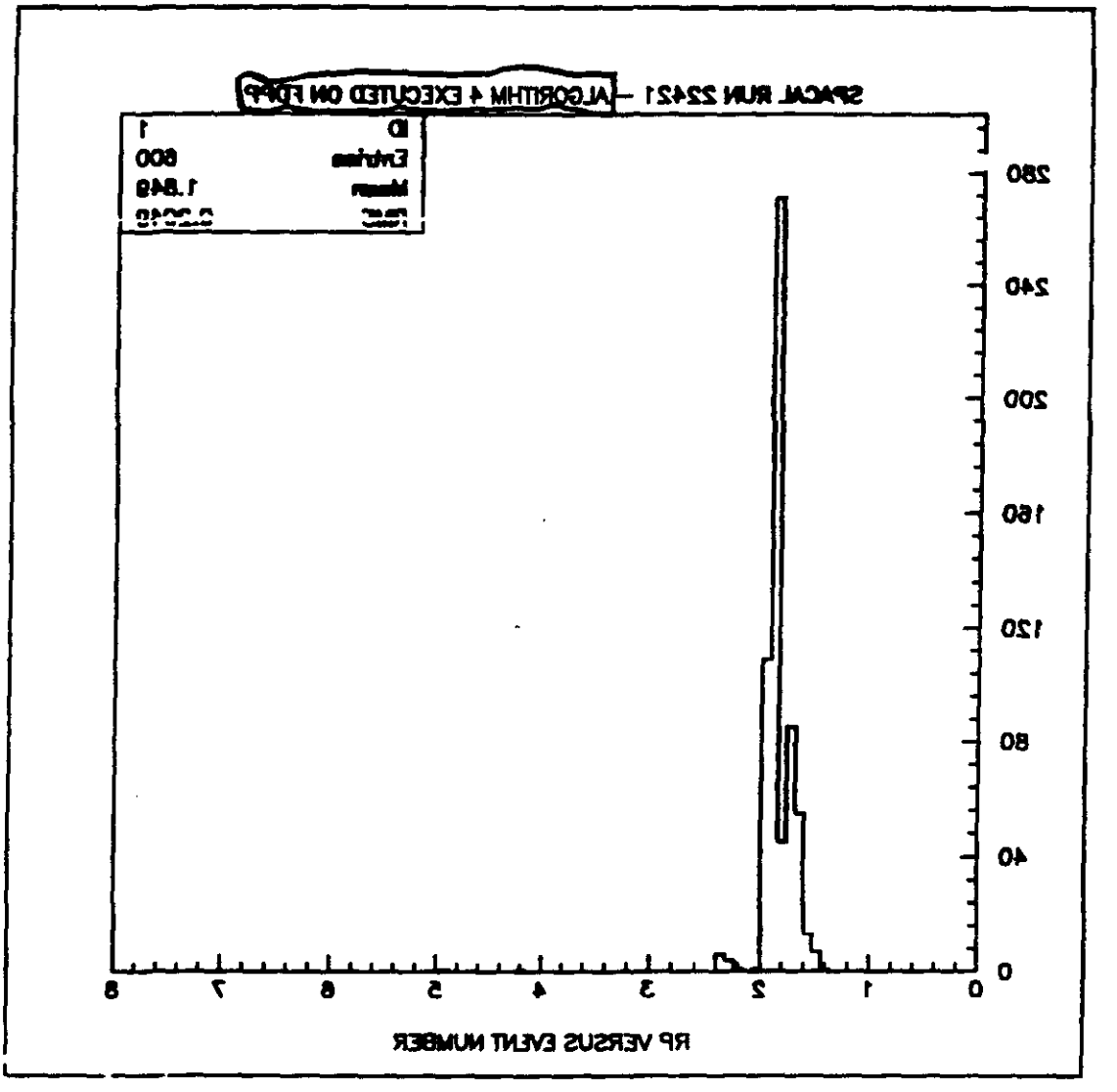
RF VERSUS EVENT NUMBER
0
40
80
120
160
200
240
280
0
1
2
3
4
5
6
7
8
ID 1
Entries 800
Mean 1.849
SPACIAL RUN 22421 — ALGORITHM 4 EXECUTED ON FDPP

Algorithm 1

each FDPP

- scans 100 channels
- finds local maximum
- calculate E, I/C, O/C

in 58 μsec

(electron events)

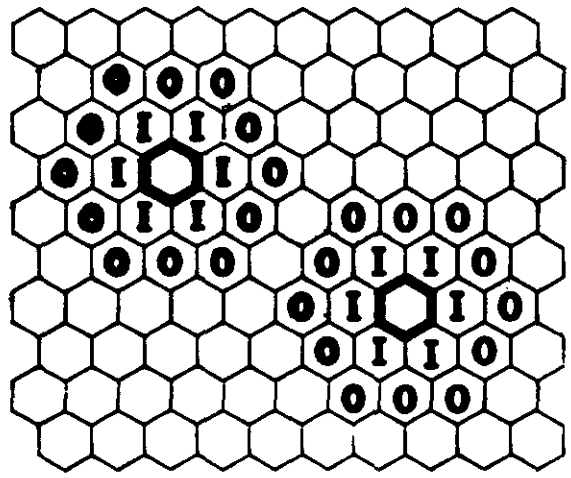

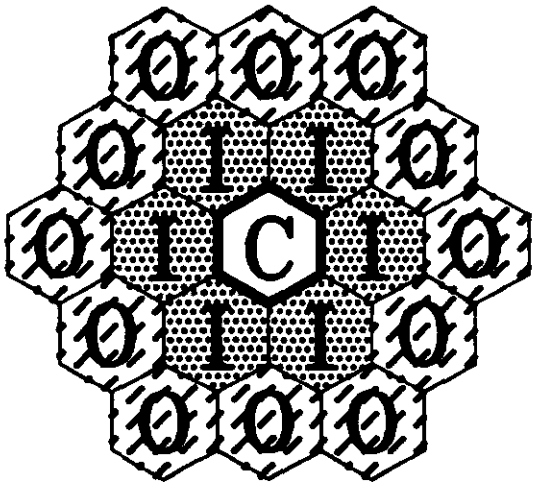

$$E = C + \sum_{i=1}^{6} I + \sum_{i=1}^{12} O$$

$$I/C = (1/6 \sum_{i=1}^{6} I)/C$$

$$O/C = (1/12 \sum_{i=1}^{12} O)/C$$

Algorithm 3

each FDPP

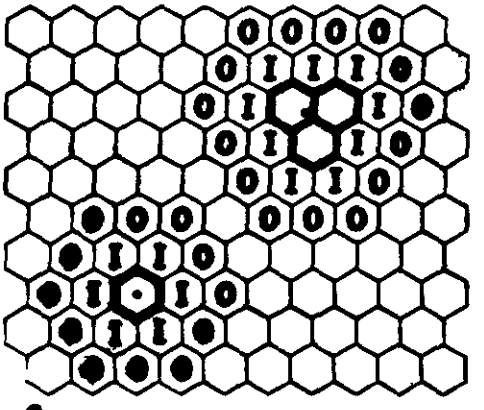

- scans 100 channels
- finds type of hit
- finds local maximum
- calculate E, I/C, O/C for different type of hit

in 62 μsec

(electron events)

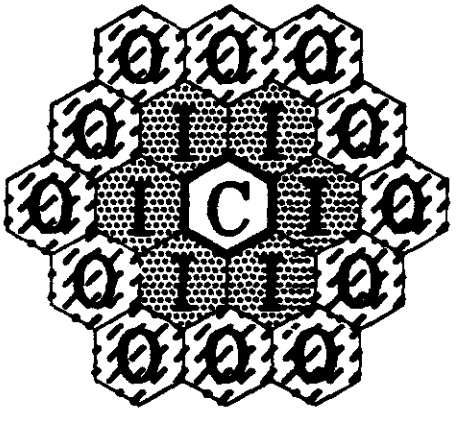

OR

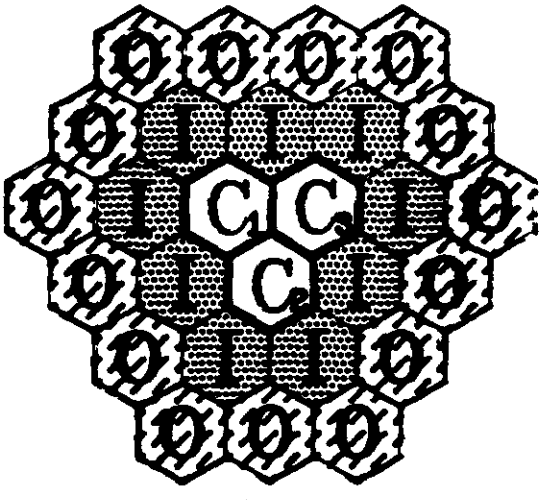

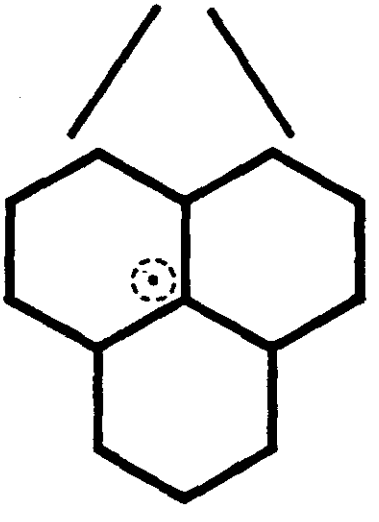

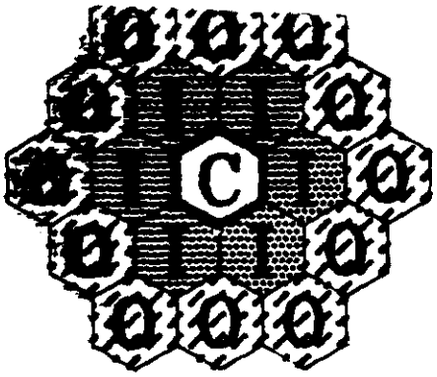

OR

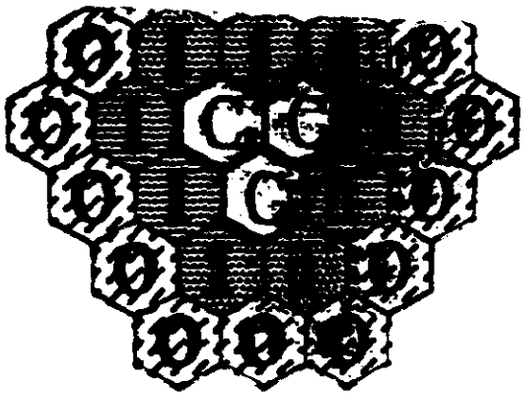

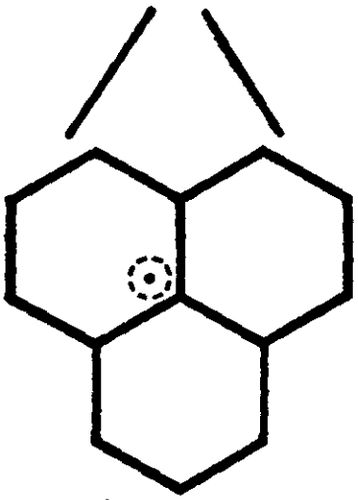

$C = C_1 + C_2 + C_3$

$$E_1 = C + \sum_{i=1}^{6} I + \sum_{i=1}^{12} O \qquad E_2 = C_1 + C_2 + C_3 + \sum_{i=1}^{9} I + \sum_{i=1}^{15} O$$

$$(I/C)_1 = (1/6 \sum_{i=1}^{6} I)/C \qquad (I/C)_2 = (1/9 \sum_{i=1}^{9} I)/C$$

$$(O/C)_1 = (1/12 \sum_{i=1}^{12} O)/C \qquad (O/C)_2 = (1/15 \sum_{i=1}^{15} O)/C$$

The same event N.3B from RUN 22531 on SPACAL (1990)

$E_1 = 27.25$ Gev	$E_2 = 28.25$ Gev
$(I/C)_1 = 0.1667$	$(I/C)_2 = 0.2874$
$(O/C)_1 = 0.1544$	$(O/C)_2 = 0.0977$

Which is ?

- the fastest
- the more flexible
- the more modular
- the simpler
- the more economical

way to interconnect them for these specific applications:

1) signal correlation in calorimeter
   (find region of interest)

2) track finding in traking detectors.

The Interconnection among

- high level processor arrays

- medium level processor arrays

- VLSI front-end chip arrays

and between the above arrays

is a challenging task

for future TRIG/DAQ systems

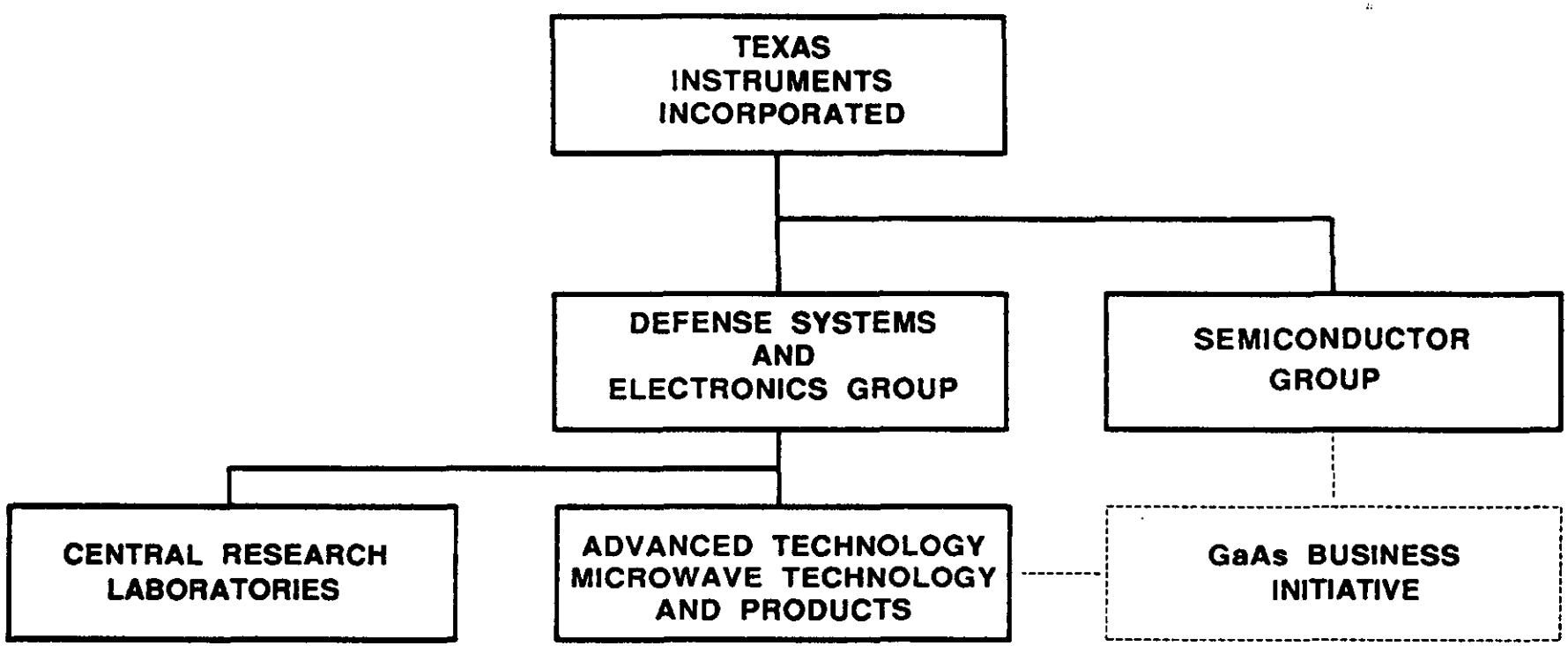

MICROWAVE & RF PROCESSES
MIXED EPITAXY & COMPONENTS
A/D CONVERTER DEMONSTRATION

MMIC
DIGITAL/ANALOG HBT
GaAs VLSI PROCESSORS
INTEGRATED DIGITAL/MICROWAVE

PERSONAL COMMUNICATIONS
FIBER COMMUNICATIONS
AUTOMOTIVE ELECTRONICS

GaAs AVIONICS SYSTEMS APPLICATIONS

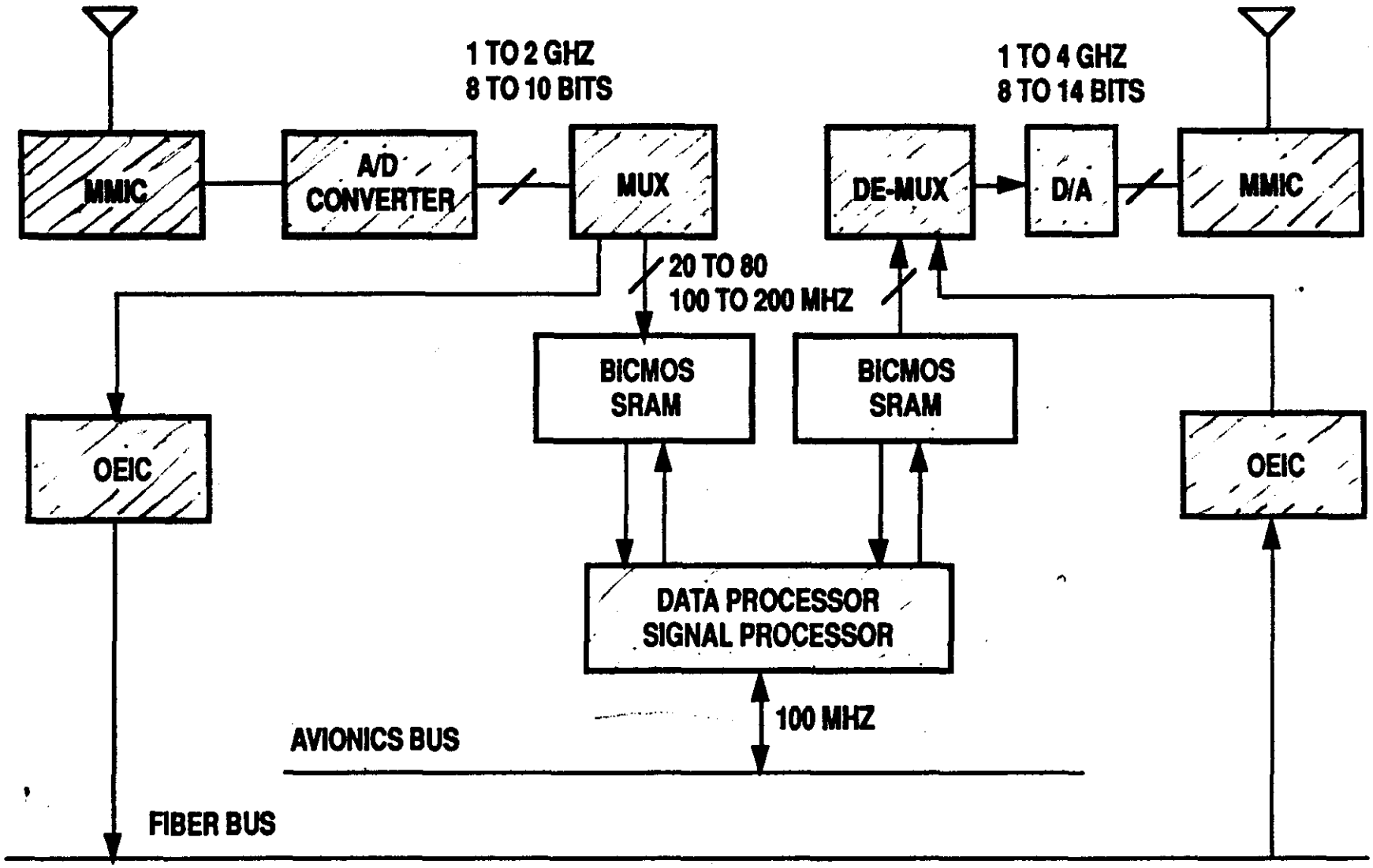

GALLIUM ARSENIDE SIGNAL PROCESSING

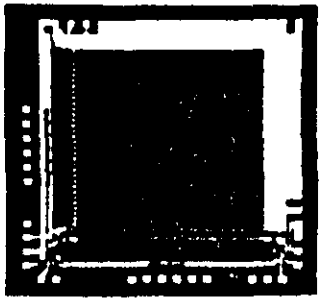

4K SRAM

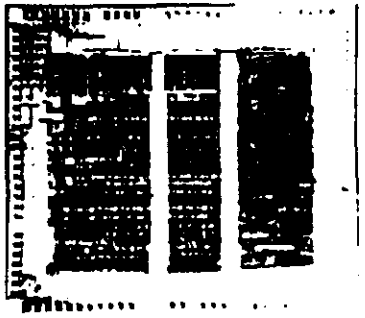

MIPS CPU

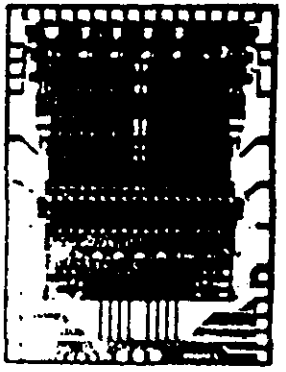

ADC

	4K SRAM	MIPS CPU	ADC
REQUIREMENT	4ns, 4K DRFM	RISC, 100 MIPS	12 BIT 20 MSPS
STATUS	4K DRFM ELEMENT 2.5ns ACCESS	DARPA CORE MIPS 150 MHz, 100 MIPS	PROCESS AND COMPONENTS DEMONSTRATED
PLANS	INTEGRATE W/HBT ADC FOR DIGITAL RF MEMORY	GaAs HBT 320/30 32 BIT FLOATING POINT DSP	E.O.-12 BIT 20 MSPS RADAR-8 BIT, 1.5 GSPS

DIRECT DIGITAL SYNTHESIZER/MODULATOR

MONOLITHIC ACCUMULATOR/ROM/DAC

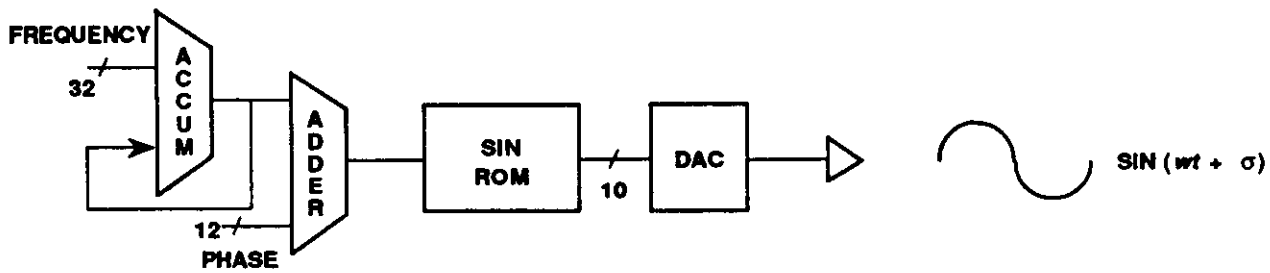

- @ F_C = 500 MHz, POWER = 2.5 W
- MAXIMUM CLOCK FREQUENCY, F_C = 500 MHz
- NYQUIST OUTPUT FREQUENCY 250 MHz
- FREQUENCY RESOLUTION 32 BITS, 0.1 Hz
- PHASE RESOLUTION 12 BITS, 0.1 DEGREES
- DIGITAL TO ANALOG 10 BITS
- UPDATE LATENCY 48 nSec

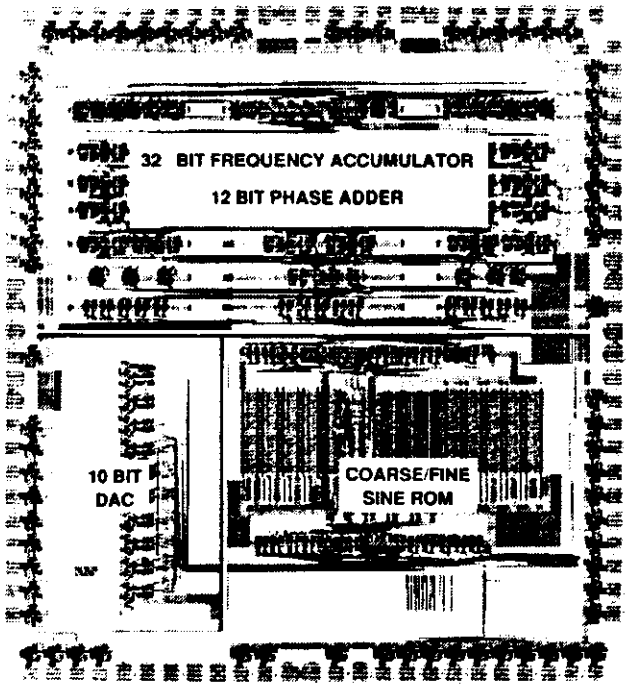

HUGHES

DARPA

TEXAS INSTRUMENTS

Objective

Design and fabricate HBT high sampling rate A/D and high resolution A/D

- 5 bit 2.5 Gsps
- 8 bit 1.5 Gsps
- 12 bit 20 Msps/watt

Approach

- Develop planar BIJFET process
- Design/fabricate 5-bit quantizers for 12-bit ADC building block
- Optimize ADC process/design
- Fabricate 12-bit 20 Msps ADC

Status

- Transferred ADC process to 3-inch GaAs pilot line
- Planar HBT process demonstrated 45% ADC yield
- Successfully tested 12-bit ADC subcircuits
- 1.2 Gsps 5-bit GaAs ADC demonstrated

Schedule

	Start	Complete
• Demonstrate 5-bit ADC	4/87	2/89
• Demonstrate scaled 5-bit	4/88	3/90
• Demonstrate 12-bit ADC	3/88	12/91

04278

HUGHES — TEXAS INSTRUMENTS — DARPA

GaAs HETEROJUNCTION BIPOLAR ADC TECHNOLOGY

KEY PARAMETERS

f_T	25 GHz
FEATURE SIZE	5x5 µm EMITTER
METAL PITCH	5 µm
ΔV_{BE}	±1mV
V_A	>100V

NPN HBT CROSS SECTION

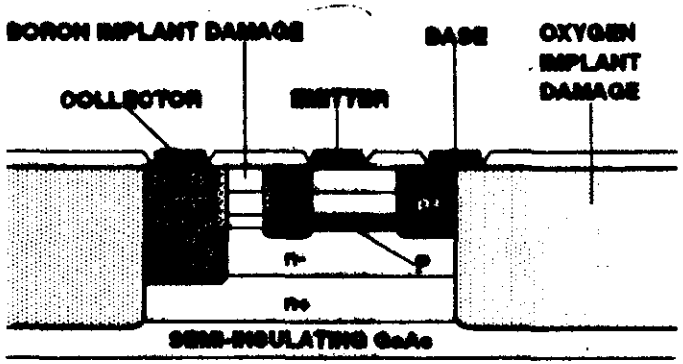

5 BIT, 1.2 Gsps FLASH ADC

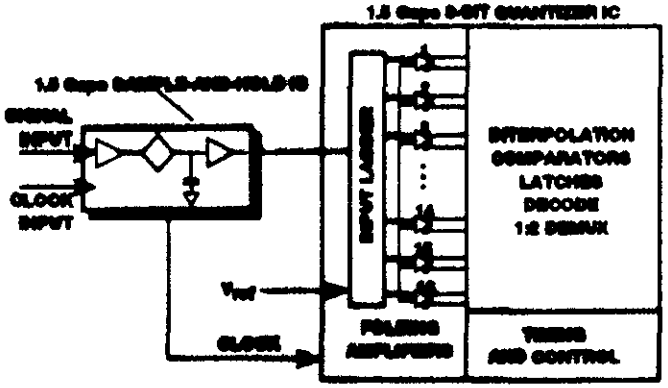

1.5 Gsps 8-BIT A-D CONVERTER

1070-C

Defense Systems & Electronics Group

MONOLITHIC 12 BIT 20 MSPS 4/5/5 SPFB CONVERTER BLOCK DIAGRAM

HUGHES

TEXAS INSTRUMENTS

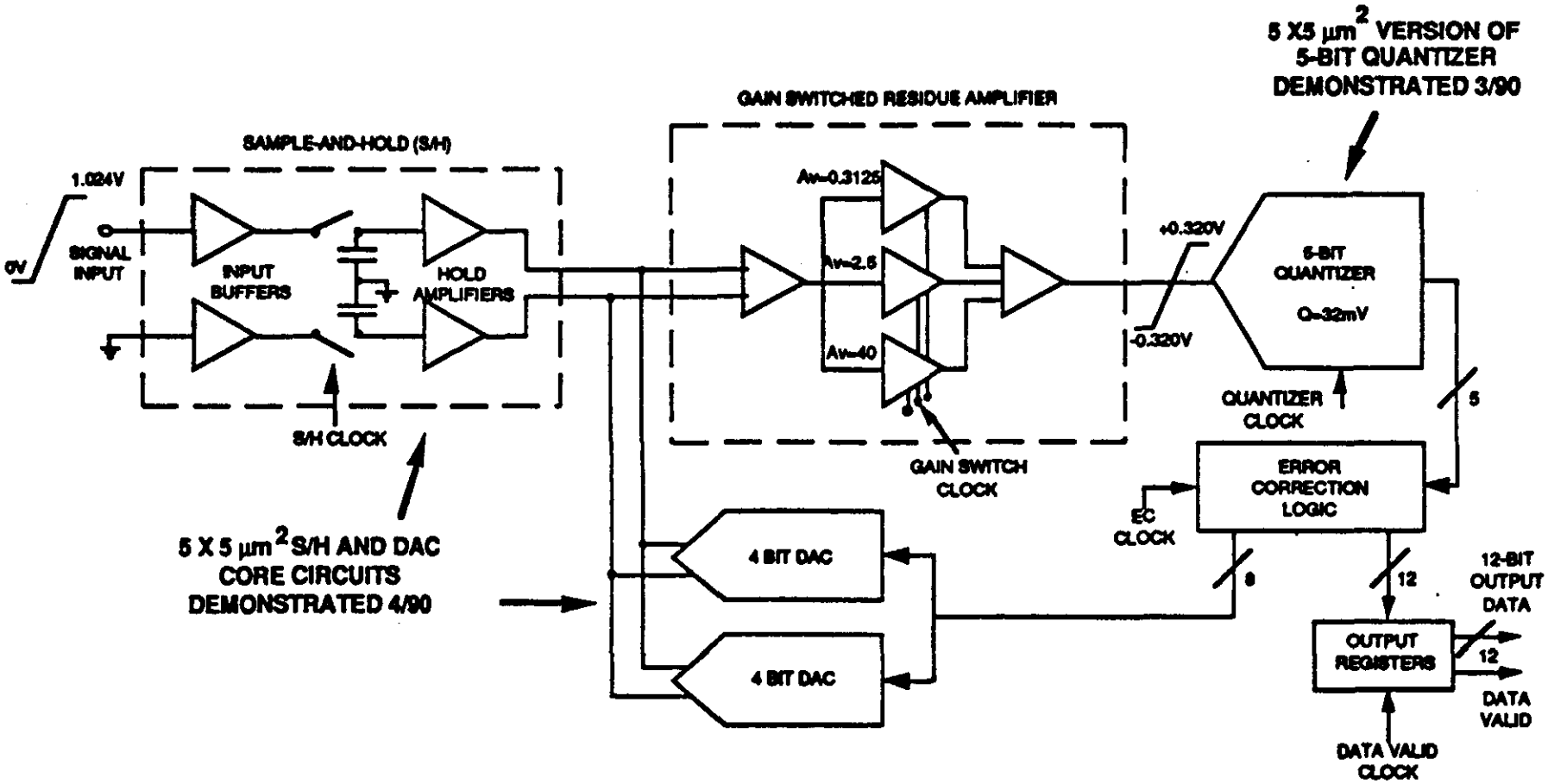

HUGHES

TEXAS INSTRUMENTS

DARPA / ONR GaAs HBT ADC

PARAMETER	12-BIT 20 MSPS ADC	8-BIT 1 GSPS ADC	5-BIT 2.5 GSPS ADC
ARCHITECTURE	SERIES-PARALLEL FEEDBACK (SPFB) 4/5/5	FLASH, ANALOG ENCODING (4 FOLD, 4 INTERPOLATION 64 COMPARATORS)	FLASH, ANALOG ENCODING (2 FOLD, 2 INTERPOLATION 16 COMPARATORS)
SPEED	20 Msps	1.2 Gsps	2.5 Gsps
LINEARITY	± 0.5 LSB	± 1 LSB	± 0.5 LSB
INPUT BANDWIDTH	-3 dB > 40 MHz	-3 dB > 500 MHz	-3 dB > 1 GHz
INPUT VOLTAGE RANGE	0 TO 1 V	± 1.28 V	± 0.32 V
OUTPUT DRIVE	TTL	DIFFERENTIAL ECL	DIFFERENTIAL ECL
OUTPUT DEMUX	N/A	2:1 OPTIONAL	2:1 OPTIONAL
POWER SUPPLIES	± 12 V, ± 7 V	± 7 V	± 7 V
POWER	3 WATT / 20 Msps	5 WATT	4 WATT
EMITTER SIZE	5 uM X 5 uM	5 uM X 5 uM	5 uM X 5 uM
DEVICE COUNT	2100 HBTs, 50 JFETs	~4000 HBTs	~1000 HBTs
DIE SIZE	280 mils X 210 mils	270 mils X 260 mils	100 mils X 150 mils

GaAs HBT MASKWORKS

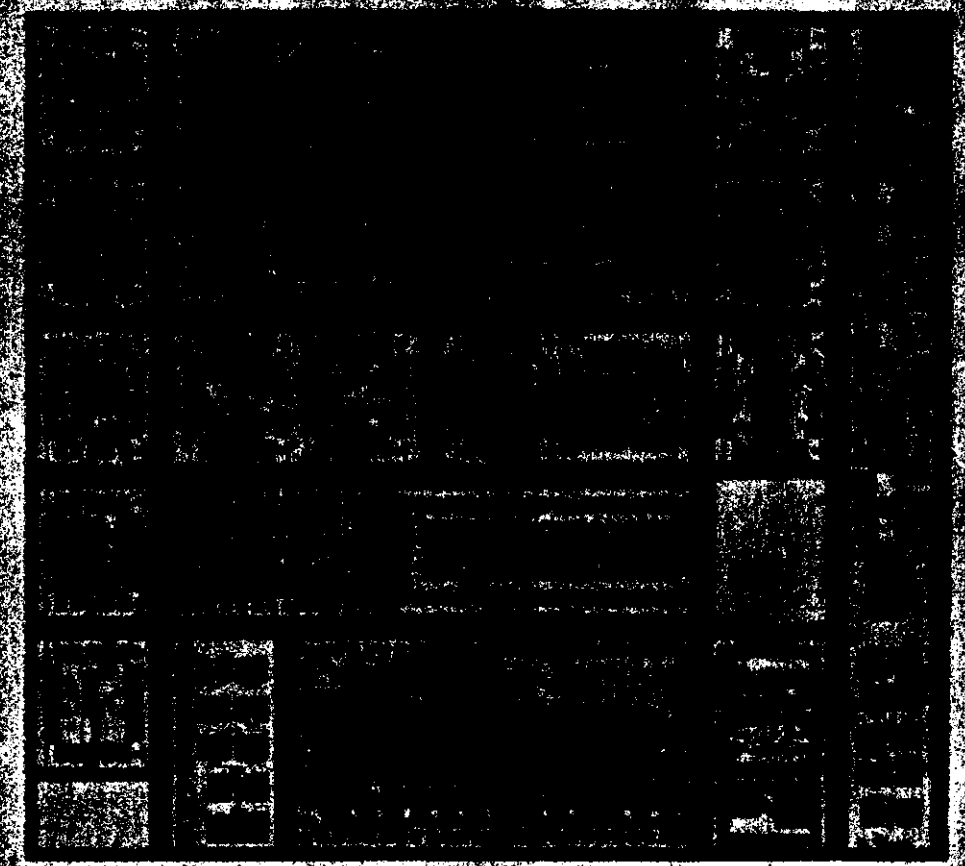

DIE SIZE, APPROXIMATELY 300 X 300

Defense Systems & Electronics Group

APS-137 (V) HIGH RESOLUTION RADAR
TEXAS INSTRUMENTS

OBJECTIVE

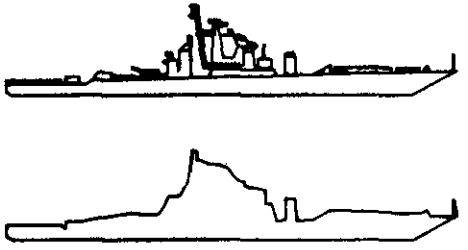

6 FOOT RESOLUTION

3 FOOT RESOLUTION

APPROACH

- DEFINE GaAs ASICS FOR MAXIMUM SYSTEM BENEFIT
- MODIFY SYSTEM BOARDS & SOFTWARE TO SUPPORT 2X (200 MHz) CLOCK
- DEVELOP TWO 270 MHz GaAs ASICS

	DATA BUFFER	DELAY GENERATOR
F_{MAX}:	270 MHz	270 MHz
COMPLEXITY:	13,000 GATES	1,000 GATES
POWER:	3.5 WATTS	1 WATTS
SPECIAL FEA.:	2K RES. FILE	PHASE LOCK LOOP

ACCOMPLISHMENTS

- SYSTEM HARDWARE AND SOFTWARE MODS COMPLETED
- SECOND PASS PARTS, APRIL, 100% FUNCTIONAL AT 200 MHz
- SYSTEM INTEGRATION STARTED
- 270 MHz GaAs ASICS NEEDED FOR JULY ASSEMBLY FOR SEPT. FLIGHT TEST

SCHEDULE

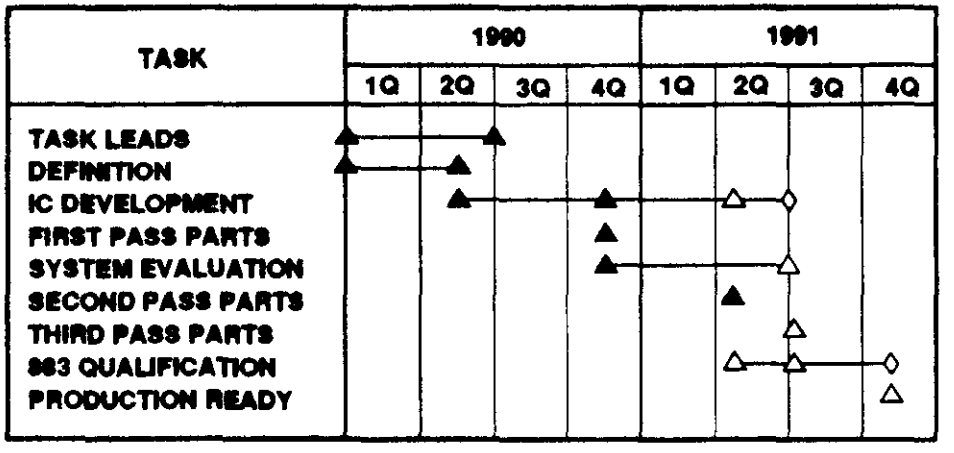

RECEIVER'S QUANTIZER FUNCTION

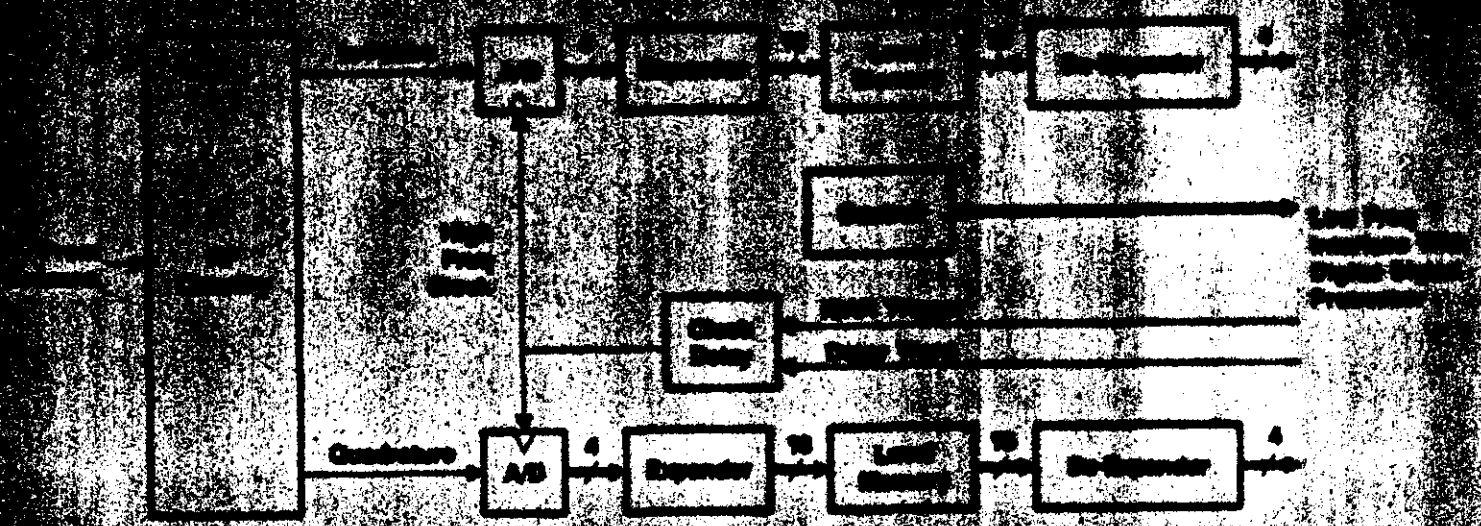

TEXAS INSTRUMENTS — GaAs SIGNAL PROCESSING TECHNOLOGY

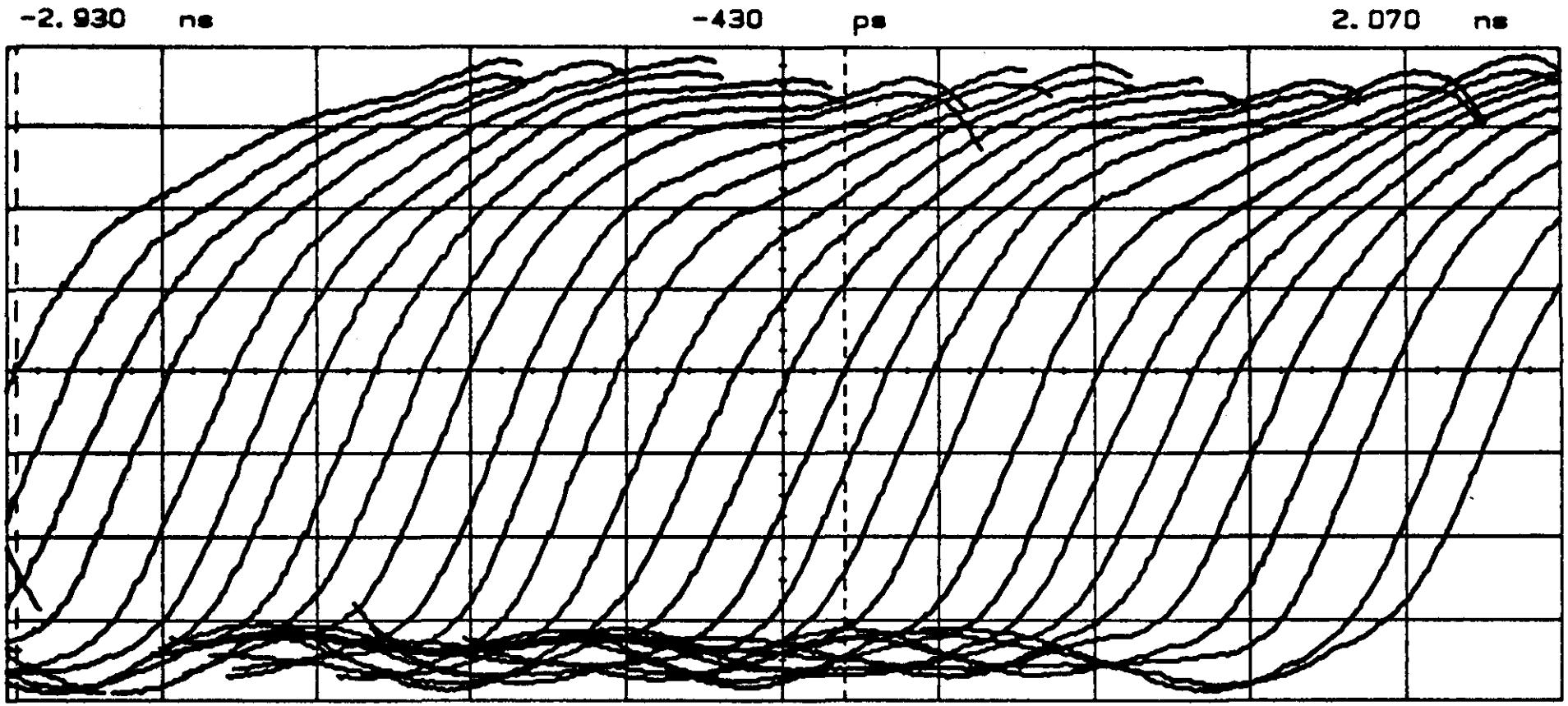

Ch. 1	= 125.2 mvolts/div			Offset	= -501.0 mvolts
Timebase	= 500 ps/div			Delay	= -430 ps
Start	= -2.900 ns	Stop	= -230 ps	Delta T	= 2.670 ns
Vmarker1	= -501.0 mvolts	Vmarker2	= -501.0 mvolts	Delta V	= 0.000 volts

HIGH SPEED GaAs MICROPROCESSOR PROGRAM
ELEMENTS OF HIGH PERFORMANCE COMPUTER SYSTEMS

LOGIC

- GaAs HETEROJUNCTION BIPOLAR
- DARPA CPU: 13,000 GATE, 150 MHz
- APS-137: 14,000 GATE, 200 MHz
- AN/PRC-126: 3,500 GATE, 500 MHz

ARCHITECTURE

- TMS320 FAMILY IS A COMMERCIAL LEADER
  - 60% WORLD MARKET IN DSP's
  - 32 BIT FLOATING POINT AND MULTIPLY IN C30
  - ADA SOFTWARE SUPPORT AND COMMERCIALLY DRIVEN TOOLSET
- SOI-320 20 MFLOP RADIATION TOLERANT
- HBT-320 PROVIDES SPEED AND RADHARDNESS GROWTH

MEMORY

- CMOS SRAM HAS BEST SPEED/POWER TRADE
- GaAs AND ECL SRAMS DRAW POWER CONTINUOUSLY
- BASELINE: LEVERAGE ALADDIN BICMOS SRAM (8 ns 100 MHz 16K X 9)
- 64 BIT BUS AND PIPELINED ARCHITECTURE ALLOWS VARIOUS 100 MHz SRAM OPTIONS FOR RISK REDUCTION

PACKAGING

- TI/GE AWARDED 1 OF 2 DARPA BAA's FOR MULTI-CHIP MODULE FOUNDRY
- HIGH DENSITY INTERCONNECT - GE PROCESS
  - TI WILL FOUNDRY AND COMMERCIALIZE
- Si ON Si - TI DEVELOPED
  - TRI-C30 DEMONSTRATION

GALLIUM ARSENIDE HBT DIGITAL SIGNAL PROCESSOR

GaAs HETEROJUNCTION BIPOLAR TRANSISTOR PROCESSOR

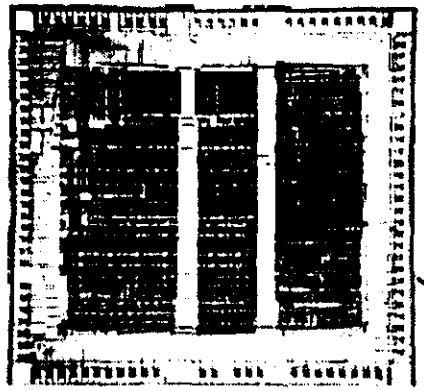

TMS320/30 DIGITAL SIGNAL PROCESSOR ARCHITECTURE

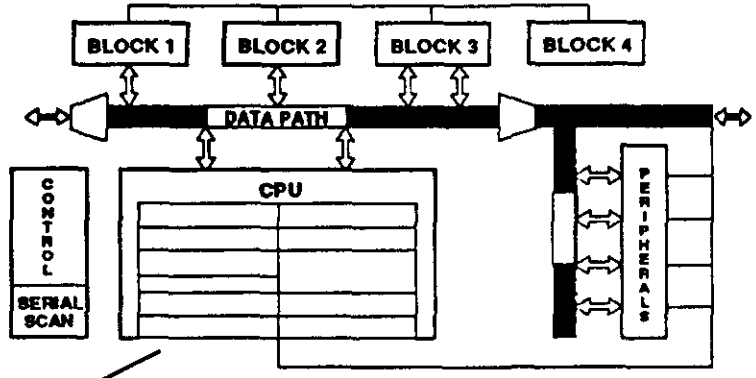

HBT 320C30
160 MFLOPS
80 MIPS

EPIC-III™ (0.5 μm) BICMOS
3.8ns 64K ECL SRAM

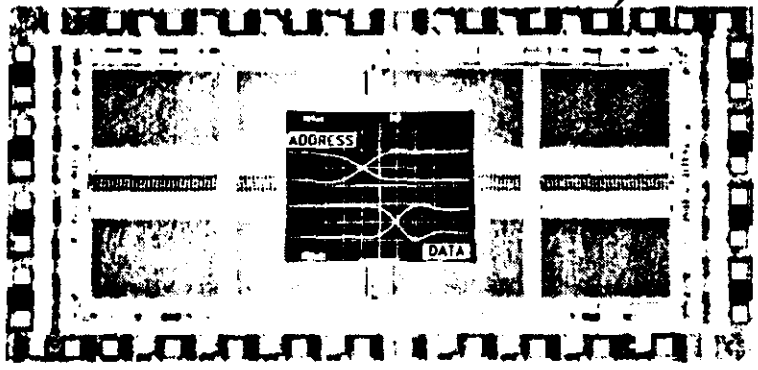

DUAL TMS320/30 WITH 3-D MEMORY

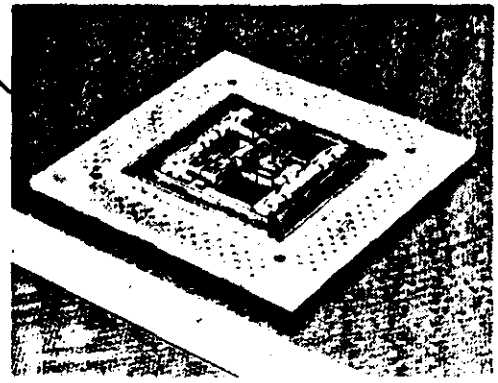

SSC SENSOR ADC DEVELOPMENT

STUDY PROGRAM (6 MONTHS)

ARCHITECTURE - SPARSE CODE / LOG ADC / SERIES VS. PARALLEL

RISKS - YIELD / SCHEDULE / PROCESS MATURITY

COSTS - DIE SIZE / DESIGN TO COST / PACKAGING / VOLUME FOUNDRY

PROTOTYPE DEVELOPMENT (24 - 30 MONTHS)

IC DESIGN / TEST ISSUES / PACKAGE PARAMETRICS / COST

PRODUCTION

FOUNDRY / COST REDUCTIONS / YIELD ENHANCEMENT

Lowry

Progress on E-O Modulators for Detector Readouts.

presented to
GEM Trig/DAQ Group.
9/4/91

Mark Lowry
LLNL

Electro-optics offers several advantages for SSC Instrumentation

The detector system must promptly acquire 10^6 channels of data at potential rate of 10^{15} bits/sec

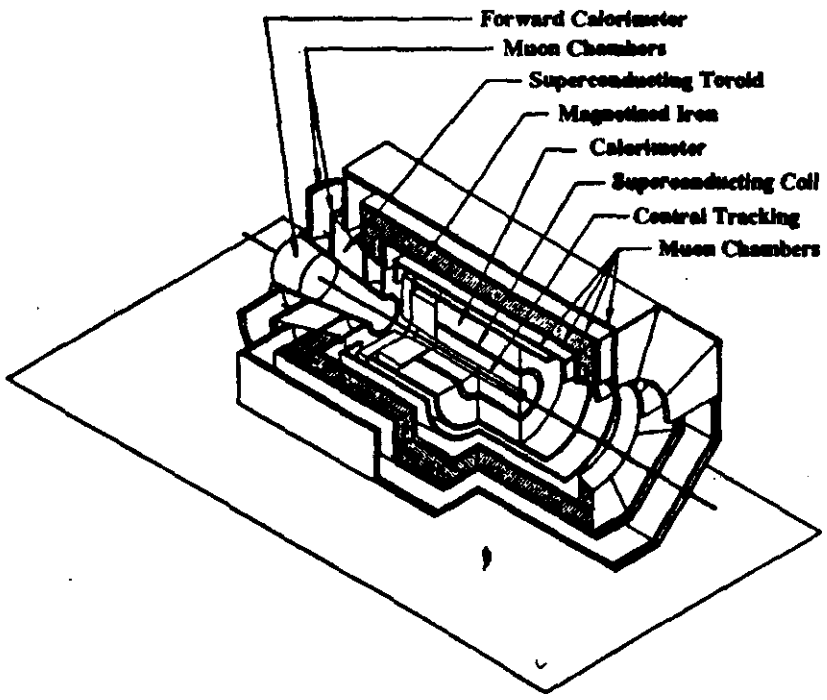

E/O Advantages:

- Fiber optics data links offer a compact cable-plan and minimal radiation scattering cross-section
- E/O systems are much more immune to EMI and grounding problems
- High bandwidth of E/O is important for potential high data rates
- Small size of E/O components is important for limited volume in detector
- E/O eliminates need for much electronics in the detector
  - space
  - thermal loading
  - radiation vulnerability
- Optical processing for fast trigger generation

Change to Light

The Mach-Zehnder Interferometric Modulator

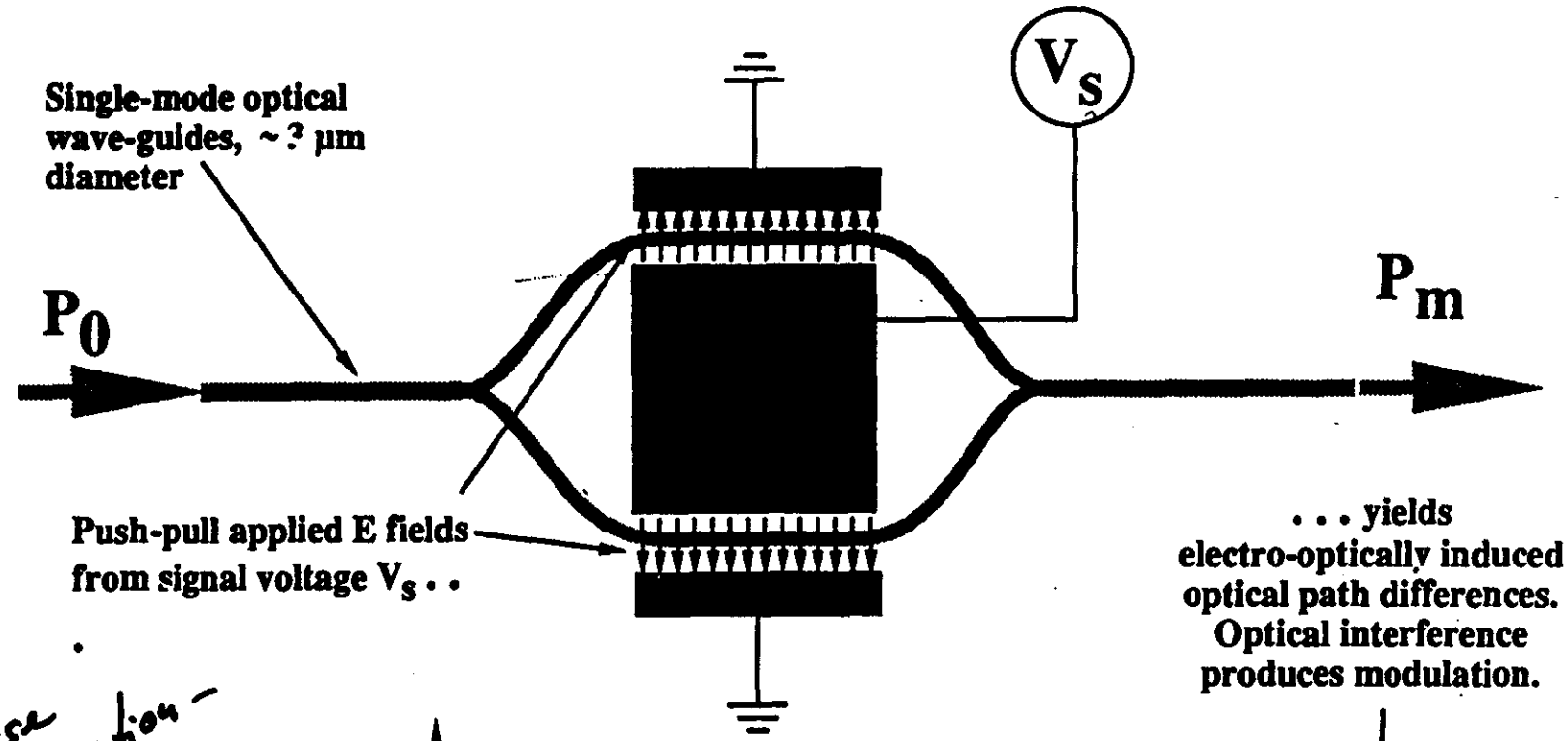

In-house LLNL fabrication - NTES/ERD

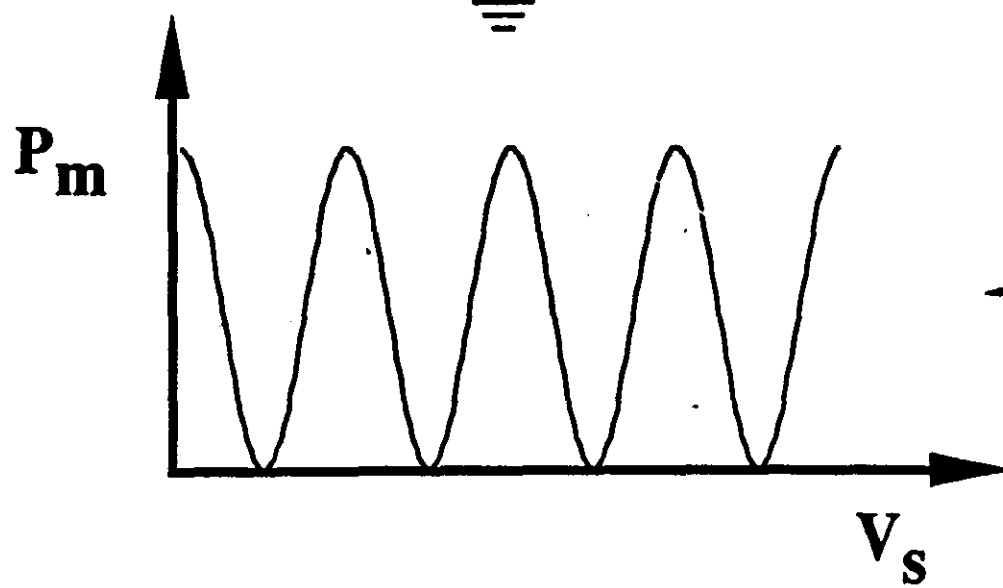

Modulator System Sensitivity

$$\frac{\delta Q}{Q_\pi} = \frac{\delta V}{V_\pi} = \frac{\delta P}{P_0}\,\frac{2}{\pi(1-\epsilon)}$$

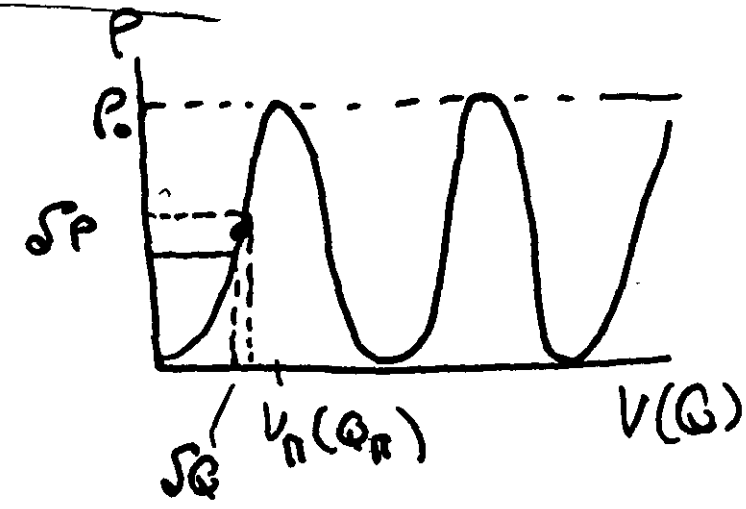

$M = V_\pi L$ ← electrode length ; $M = 14$ V-mm

$\rho = 0.85$ pF/mm

$Q_\pi = M\rho = 12$ pC

$\frac{\delta P}{P_0} \sim 1\times10^{-4}$ @ 10 MHz BW.

$\Rightarrow \delta Q = \underline{\underline{0.86 \text{ fC}}}$ @ 10 MHz BW. ; $\delta V \sim 1$ mV (50 Ω)

remember $\delta Q \sim \sqrt{\Delta\nu}$

& $\frac{\delta P}{P_0} \sim \frac{1}{\sqrt{P}}$

improvements underway ⇒ x2 to x3 better

Sensitivity vs. Bandwidth for E-O Modulators

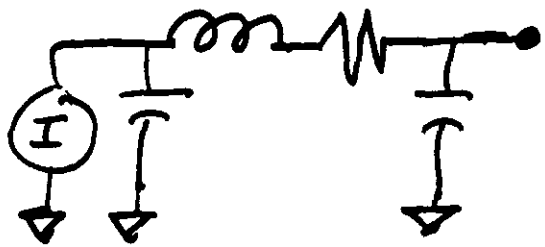

Zeroth order model for wire-chamber

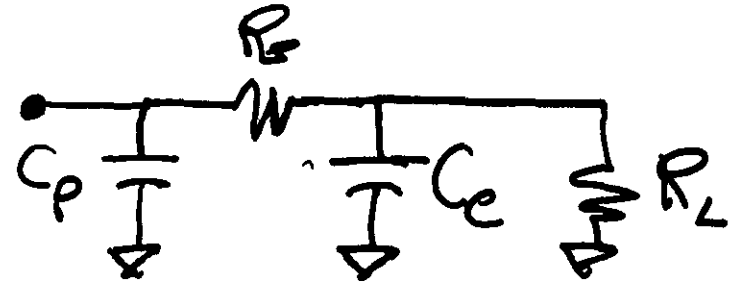

1st order model for modulator

C_p = parasitic capacitance

C_e = cap. of electrode 5-10pF

R_L = load resistance

- Modulation efficiency determined by voltage across C_e; higher $R_L \Rightarrow$ better efficiency.
- However $\tau_r \sim R_L(C_e + C_p)$
- Best sensitivity × Bandwidth product obtained with careful impedance matching

Our experimental demonstrations of LLNL E/O technology in the HEP environment have been very successful, and well received

.....concentrating on goals that would bolster credibility and quickly demonstrate institutional effectiveness.

- Sensitivity demonstration with 800 and 1300 nm systems
  dynamic range of 5 decades reasonable target, ref. 1
- First observation of muon chamber charge signals with E/O modulator without electronic preamp
  ... achieved with LLNL muon chamber, ref. 2
- Collaboration with MIT (Ulrich Becker, et. al. from Ting's group)
  -- demonstrated direct charge readout of drift tube--- no preamp !!
  -- measured Fe 55 decay spectrum
  -- demonstrated direct readout in B-field environment expected within the SSC detector
  ... at 0.8 Tesla no effect
  -- measured muon track resolution with modulator readout system
  -- familiarized key members of HEP community with technology
  -- ref. 3
- Radiation hardness demonstrated in collaborative experiment at LAMPF
  -- ref. 4

1) Mark Lowry, Eldon Ables, Richard Bionta, Ron Haigh, Keith Hugenberg, Ralph Kalibjian, Charles McConaghy, Darin Milton, Mark Rotter, andHal Schulte, *An Electro-Optical Imaging Approach to the Prompt Signal Processing Problem of Mega-Channel SSC Detector Arrays*, to be published in the proceedings of the Symposium on Dectector Research and Development for the Superconducting Super Collider, October 1990

2) E. Ables, R. Bionta, M. Lowry, D. Masquelier, K. McCammon, C. McConaghy, and C. Wuest, *Observation of Drift Chamber Signals Using a Mach-Zehnder Electro-optic Modulator*, accepted for publication in Nuclear Instruments and Methods in Physics Research , July 1991

3) to be published in NIM: joint LLNL/MIT paper ~ 75% written

4) to be published in NIM: joint LLNL/LANL paper. Data just now being analyzed- 120 megabytes

Electro-optic read-out of muon drift chambers has been performed at LLNL and MIT

paper in outline stage.

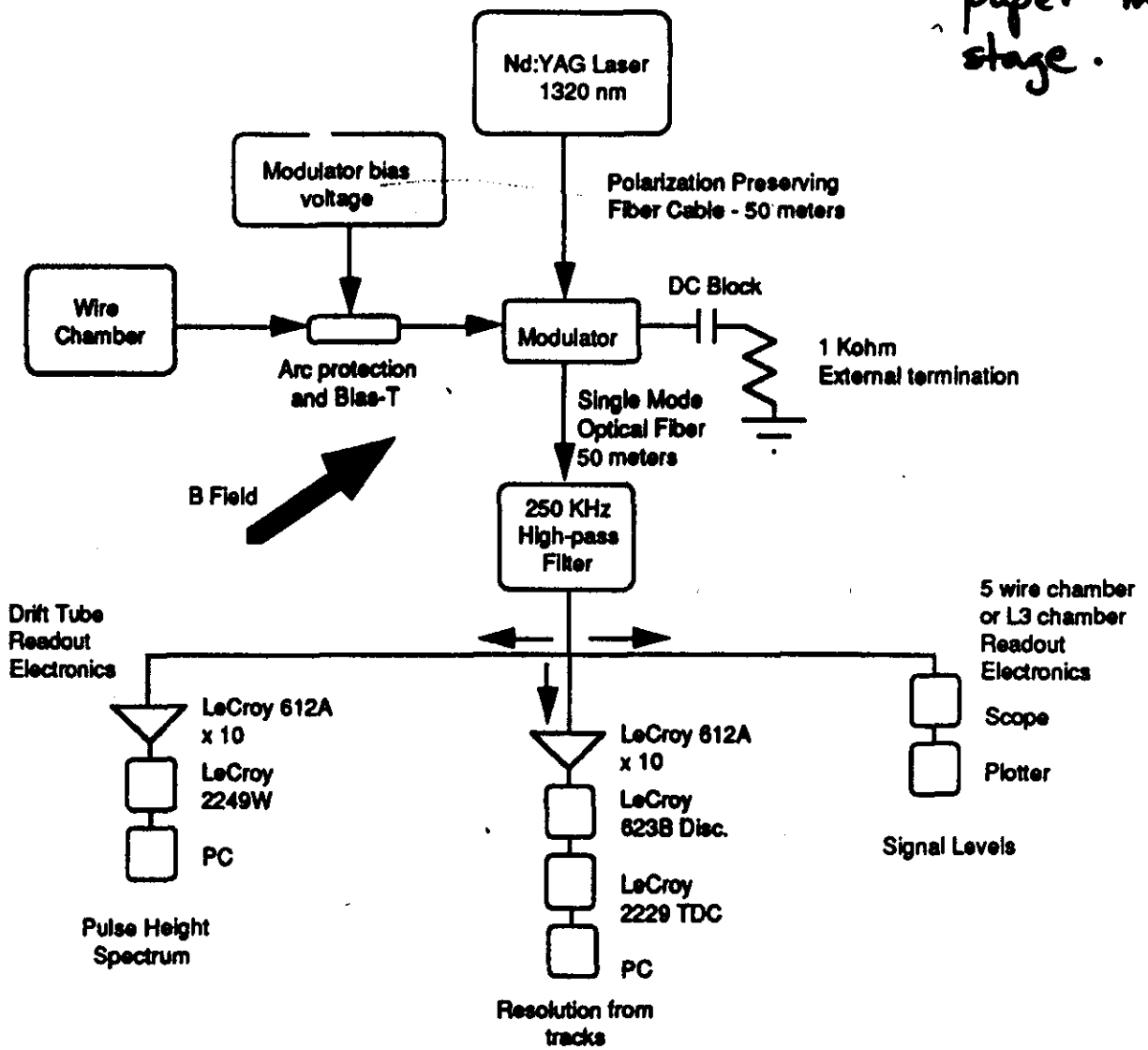

Comparison of 5-wire chamber signals from N2 laser tracks

NIKHEF amplifier

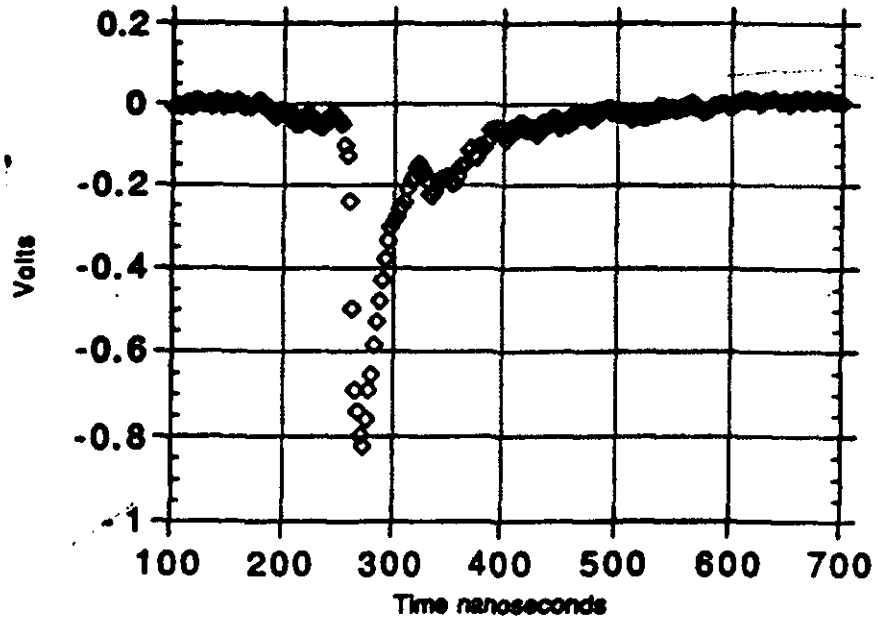

Modulator

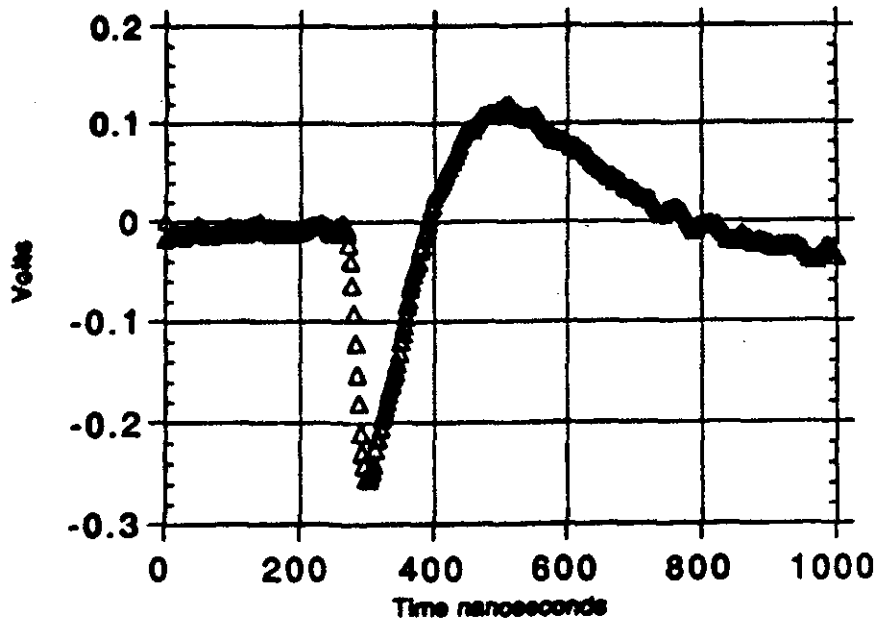

Comparison of Drift Tube Signals from Iron-55 X-rays

NIKHEF amplifier

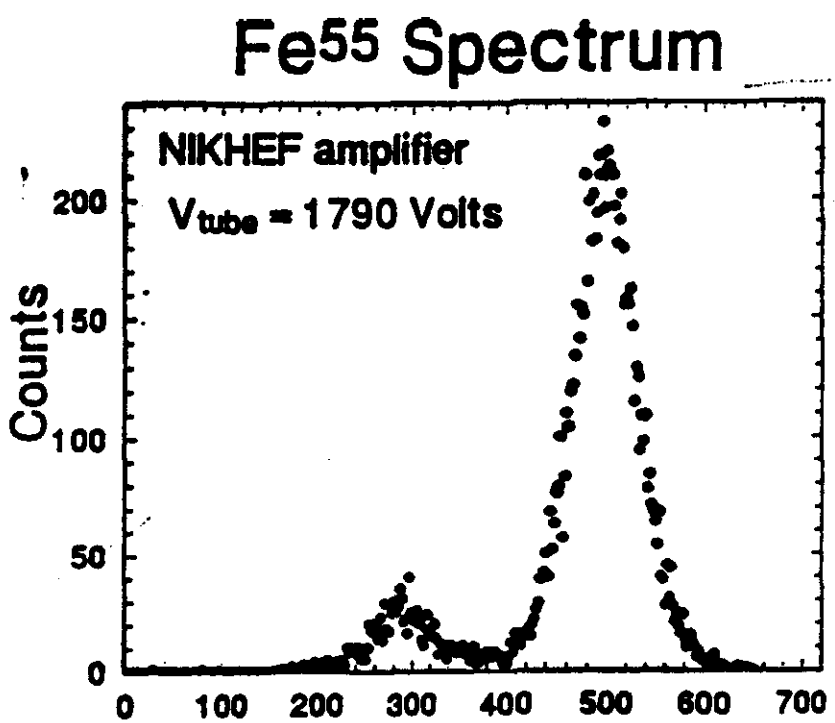

Modulator

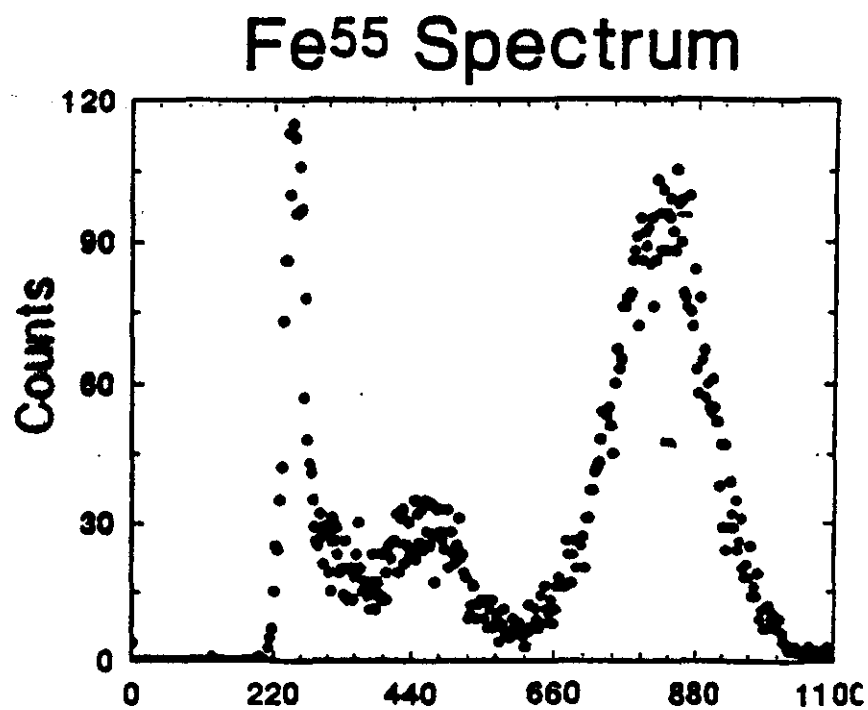

ADC channels

Effect of B Field on Electro-optic Modulator

Test Pulse injected into 5-wire chamber

B = 0 Tesla

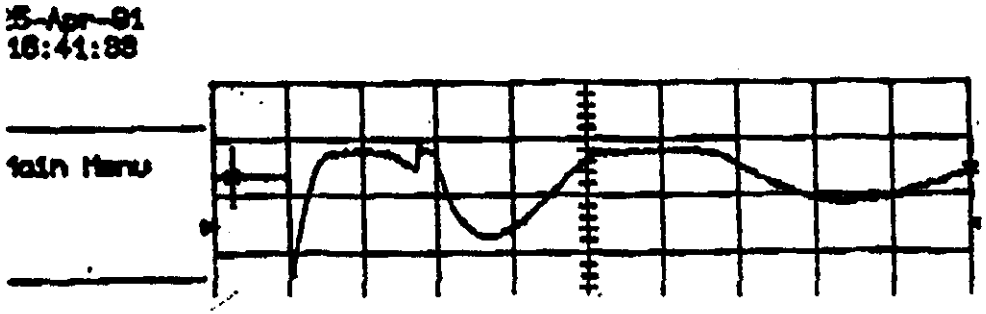

B = 0.8 Tesla

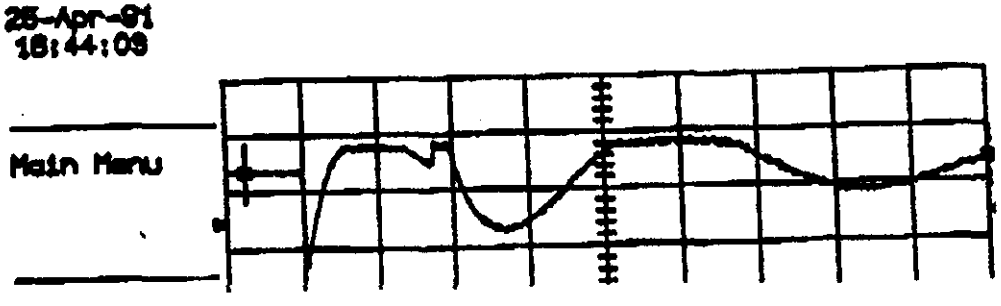

ringing due to poor impedance match: Inductive Bias-T was replaced by Resistive Bias-T for this measurement.

Modulator performance has been measured for ~10 SSC years of dose -

Mark Lowry, Kent McCammon, LLNL; Hans Ziock, Larry Rybancyk, LANL

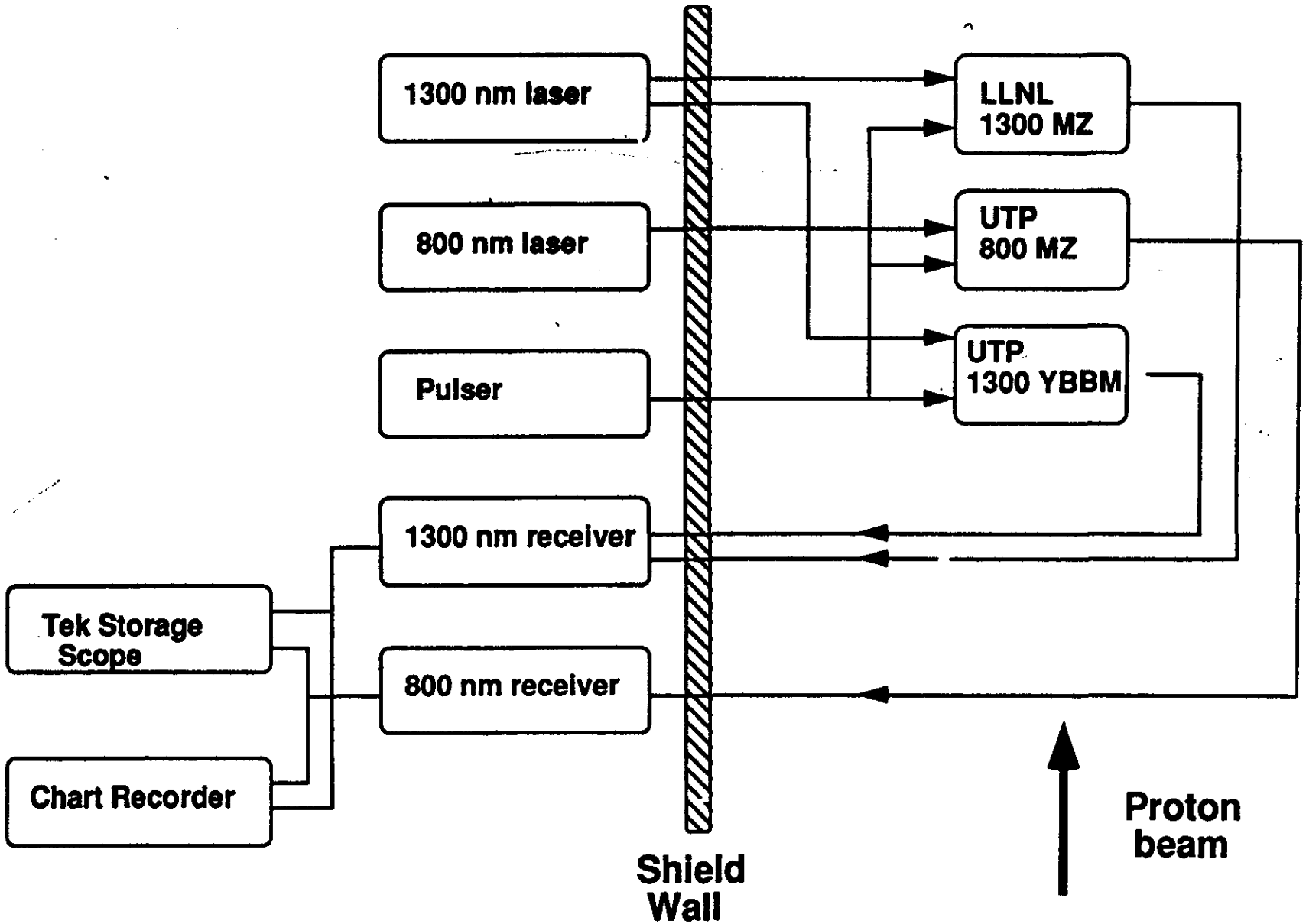

Modulator Electrical Calibration Waveform

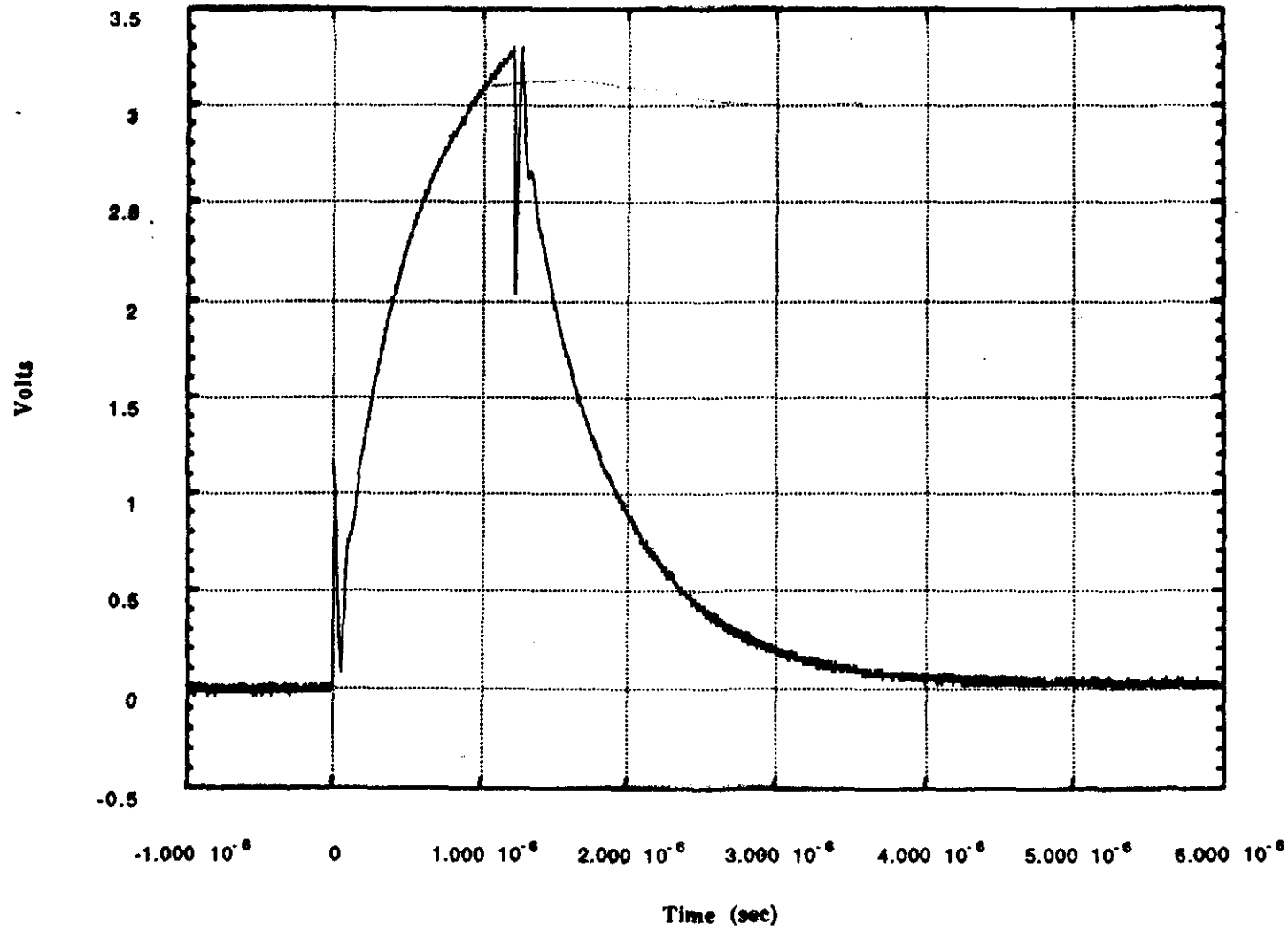

LLNL MZ output on 7/17 while being irradiated

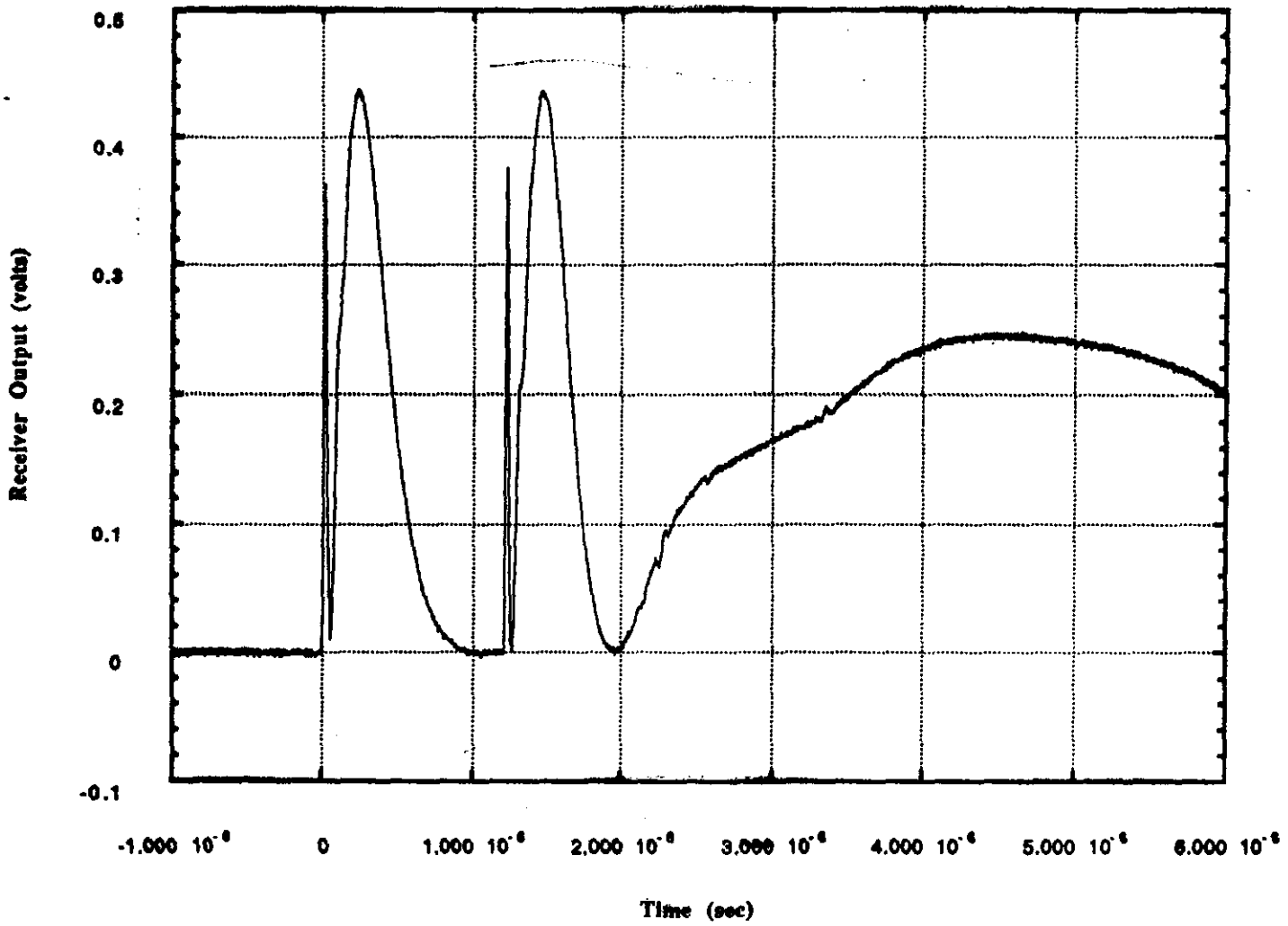

Our preliminary results indicate that radiation hardness is excellent for SSC applications

Experiment Conditions:

- LAMPF proton beam was source
- 650 MeV protons, I= 0.6-1.6 nA, ~ CW beam
- Irradiated 3 modulators
  - 800 nm and 1300 nm
  - spectrum of device designs
- 6.5 days of irradiation approximates 10 SSC years of dose

Preliminary Results:

- No radiation induced transient upsets observed (down to 1-5 mV levels) while the modulators were being irradiated (note upset threshold scales with dose rate)
- Some darkening of modulator/fiber may have been observed. Less than x2; more analysis required. Self-annealing will probably mitigate this at the lower dose rates at the SSC.
- Some operating point drift correlated with beam on/off. Scaling these effects with dose rate indicate minimal impact on SSC implementation.

Directions for E/O at the SSC

- Continue improvements in charge sensitivy
  -- x 2-3 on horizon

- Cost reduction initiative
  - industrial partner UTP ?
  - increase integration density
    model channel interactions
    produce multi-channel chip
  - automate packaging

- High-bandwidth Serialized data link demonstration
-- experimentally demonstrate time-division multiplexed system
  trading fiber and modulator count for bandwidth

– also look @ low-gain/low-power dissipation preamps.

- Develop cost models for parallel and serial approach
  -- apply to SDC and GEM

UCRL- JC 105645
PREPRINT

An Electro-Optical Imaging Approach to the Prompt Signal Processing Problem of Mega-Channel SSC Detector Arrays

Mark Lowry, Eldon Ables, Richard Bionta, Ron Haigh,
Keith Hugenberg, Ralph Kalibjian, Charles McConaghy,
Darin Milton, Mark Rotter, and Hal Schulte

This paper was prepared for submittal to the
Symposium on Detector Research and Development for the
Superconducting Super Collider
Fort Worth, TX
October 15-18, 1990

December 1990

Lawrence Livermore National Laboratory

This is a preprint of a paper intended for publication in a journal or proceedings. Since changes may be made before publication, this preprint is made available with the understanding that it will not be cited or reproduced without the permission of the author.

DISCLAIMER

This document was prepared as an account of work sponsored by an agency of the United States Government. Neither the United States Government nor the University of California nor any of their employees, makes any warranty, express or implied, or assumes any legal liability or responsibility for the accuracy, completeness, or usefulness of any information, apparatus, product, or process disclosed, or represents that its use would not infringe privately owned rights. Reference herein to any specific commercial products, process, or service by trade name, trademark, manufacturer, or otherwise, does not necessarily constitute or imply its endorsement, recommendation, or favoring by the United States Government or the University of California. The views and opinions of authors expressed herein do not necessarily state or reflect those of the United States Government or the University of California, and shall not be used for advertising or product endorsement purposes.

Observation of Drift Chamber Signals Using a Mach-Zehnder Electro-optic Modulator

E. Ables, R. Bionta, M. Lowry, D. Masquelier,
K. McCammon, C. McConaghy and C. Wuest

Lawrence Livermore National Laboratory

Abstract

A Mach-Zehnder electro-optic modulator has been used to read out the charge collected on drift chamber sense wires. The modulator sensitivity is sufficient to allow measurement of the pulse waveform without preamplification of any kind. We report here initial results and discuss on-going research and potential applications as well as projected performance improvements as we continue to optimize the system for drift chamber read-out.

As part of the L* detector collaboration, Lawrence Livermore National Laboratory has proposed that electro-optic modulators could be used in a number of detector sub-systems in the L* detector to be built at the Superconducting Super Collider, as well as other planned high energy physics detectors.[1,2] Recent advances in electro-optics coupled with the obvious advantages of utilizing modulated analog light signals carried on fiber-optic cables make this technology a very desirable option for the future generation of large detectors at SSC and LHC. Among these advantages are reduction of coaxial cable volume, reduction of ground-loop and noise pick-up, lower power consumption through the elimination of front-end preamplifier circuitry, the possibility of performing triggering algorithms using light signals rather than electrical signals, and increased density of sense elements.

Electro-optic modulators have been successfully used to read out the sense wire of a multiwire drift chamber built at LLNL. The read-out was performed by connecting a single sense wire of the drift chamber directly to the input of the modulator without a preamplifier of any kind. The drift chamber is a 1 meter long test chamber built with the same wire spacings as the L3 muon drift chambers at LEP.[3,4] 25 micron diameter gold-coated tungsten sense wires alternate with 50 micron diameter gold-coated tungsten field wires with a 4.5 mm spacing. Cathode (mesh) planes are located at a distance of 5 cm on either side of the sense/field plane and consist of 50 micron wires separated by 4.5 mm. The chamber cross section is shown in Figure 1 along with the voltages applied to the wires. A 100 microCurie cobalt-60 source was used to provide ionization tracks in the drift chamber gas - P10 (90% Ar, 10% CH_4).

An electro-optic modulator was arbitrarily connected to the third sense wire out of sixteen available sense wires. The circuit used to operate the modulator is shown in Figure 2. The main component of the modulator system is the integrated optical modulator, which is a basic Mach-Zehnder interferometric modulator as shown in Figure 3. Details of the modulator operation may be found elsewhere.[5] For the purpose of this discussion we note that the optical intensity output of the modulator varies sinusoidally as a function of the applied voltage (or charge) to the modulator electrodes. The applied voltage (or charge) creates an electric field over the optical waveguide regions, changing the index of refraction, and hence interferometrically modulating the optical intensity.

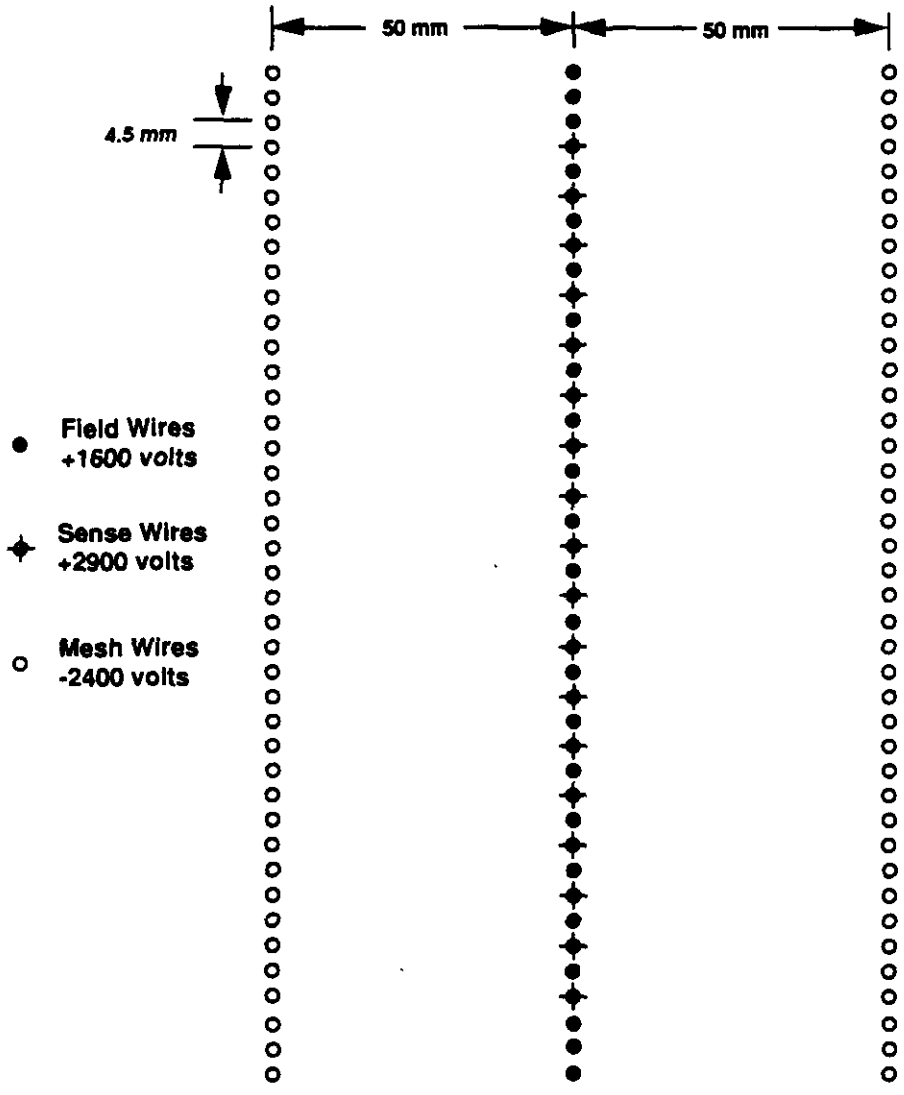

Figure 1. Cross section of muon drift chamber. The mesh and field wires are 50 micron diameter gold-coated tungsten and the sense wires are 25 micron diameter gold-coated tungsten. Mesh plane wires are all set to the same voltage. Field and sense wires alternate with the voltages as shown. The wires are 1 meter in length and are kept in 1 atmosphere of 90% argon and 10% methane. Sense wires are unterminated.

The modulator employed was a 20 GHz travelling-wave Mach-Zehnder modulator that was designed, fabricated and evaluated at LLNL. For this application, the standard 20 GHz modulator was packaged such that the electrical output of the travelling-wave electrode structure could be accessed via a standard high bandwidth Wiltron "K" connector. This modification allowed us to experiment with the value of the output impedance that was connected to the electrode structure.

At frequencies below about 1 GHz this modified modulator electrode structure is well represented by a simple "lumped element" circuit model. In this model the electrode structure itself may be viewed essentially as a capacitor to ground in parallel with the externally supplied termination impedance. To optimize charge sensitivity the

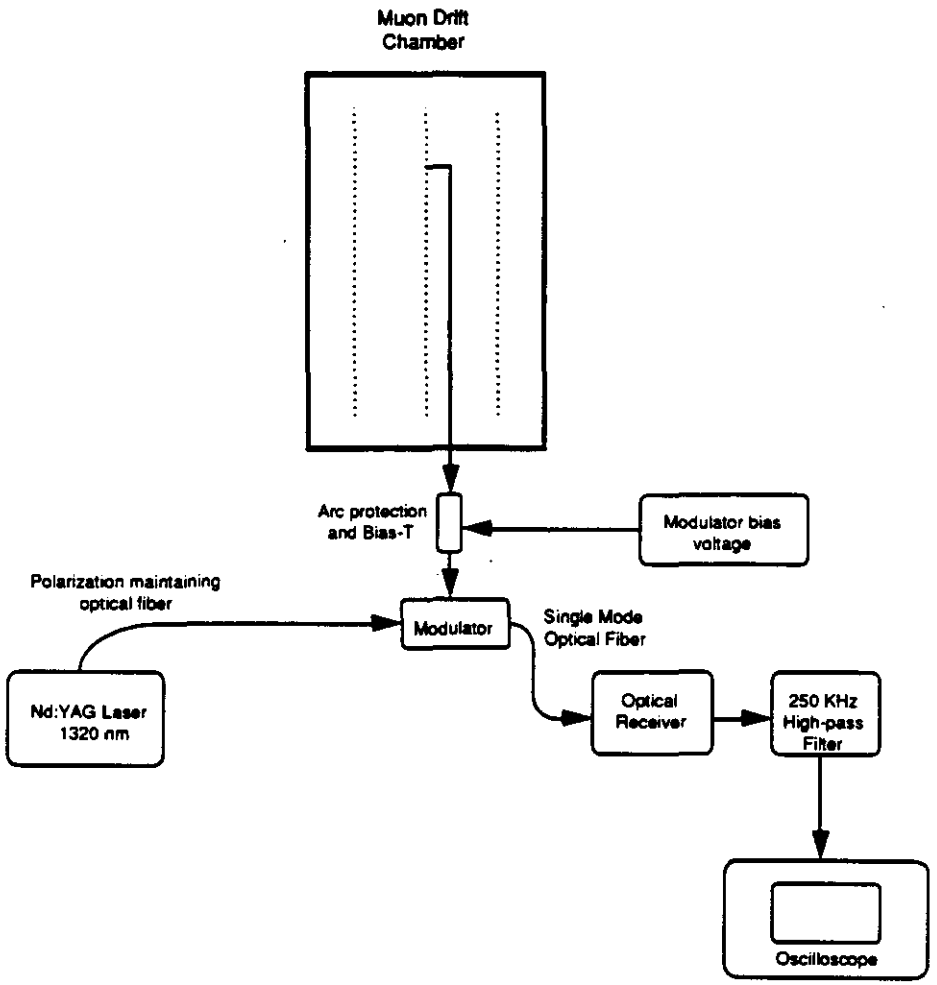

Figure 2. Electro-optic modulator drift chamber read-out system. The muon drift chamber sense wire is connected to a protection circuit and bias-T into the Mach-Zehnder interferometer. The Nd:YAG driving laser light is modulated, as detailed in Figure 3, by the charge collected on the sense wire and transported to the modulator electrode. A single mode optical fiber transports the modulated light to an optical receiver where it is sensed by a photodiode, amplified, filtered and displayed on an oscilloscope.

ionization detector output impedance must be matched to the modulator impedance. However, this modulator termination impedance also affects the modulator time response through the RC time constant of the modulator's electrical circuit model. Thus, to optimize both sensitivity and bandwidth, careful consideration must be given to detector/modulator impedance matching.

The modulator system used an Amoco Nd:YAG laser operating at a wavelength of 1320 nanometers to provide the carrier signal. The laser carrier passed through an optical isolator and half-wave plate. The half-wave plate was used to rotate the beam polarization for proper launching of the laser light into polarization-preserving (pp) optical fiber. The laser carrier travelled through a pp optical fiber jumper and into the pig-tailed lithium niobate waveguide of the modulator. The drift chamber sense wire was connected to the modulator through a 2.54 cm length of coax, a high voltage protection circuit, and bias T-connector. The bias voltage applied to the modulator set the operating point of the device on the sine-squared transfer curve. This bias voltage was set to the point of maximum device sensitivity - corresponding to the maximum slope

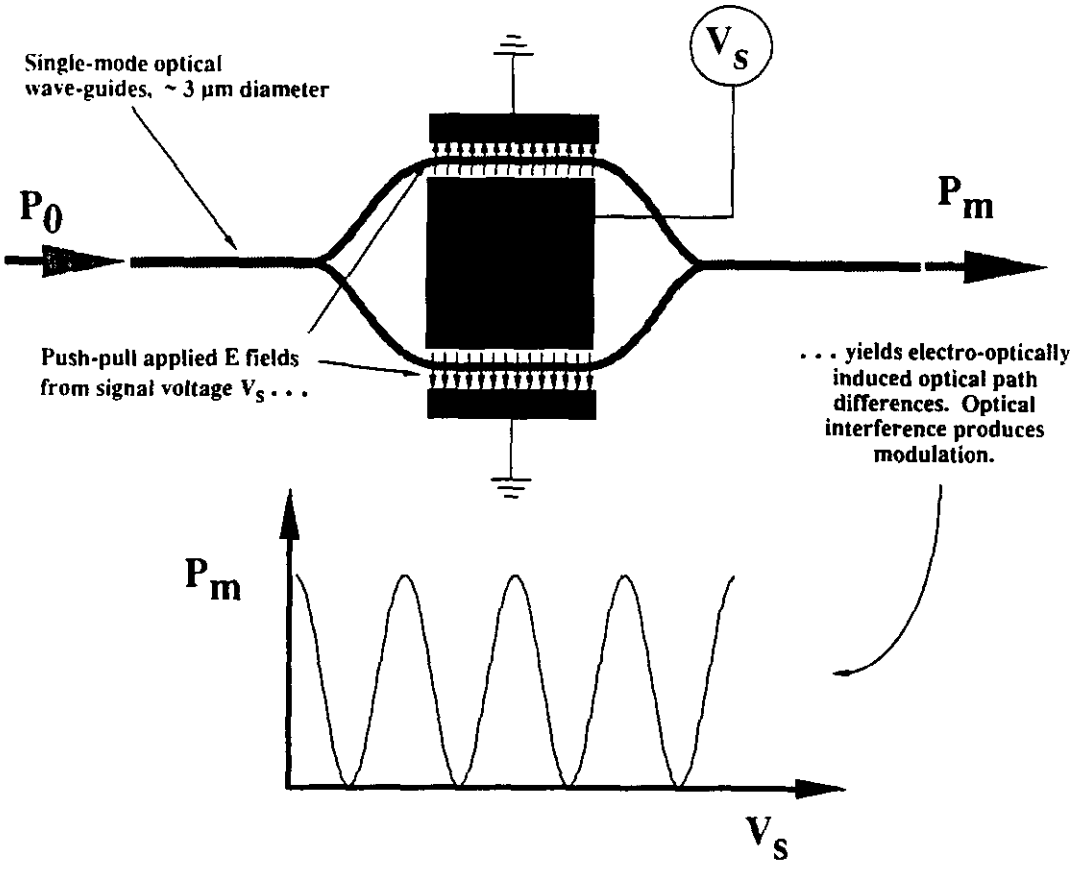

Figure 3. Simplified diagram of the operation of the Mach-Zehnder integrated optical modulator.

of the modulator response function. This setting is denoted as the half-power point. For the small signal levels typically read off the drift chamber sense wire, the modulator transfer curve was linear about the half-power operating point. If necessary, large signal responses can post-measurement linearized.

The charge pulse signal from the drift chamber sense wire developed an electric field across the modulator that produced a proportional optical pulse out of the device. The optical pulse propagated through a single mode optical fiber to a remotely located optical receiver. The photodiode and preamplifier in this receiver converted the optical signal to an amplified electrical signal.

After the receiver, the signal was high-pass filtered in order to attenuate the 150 kHz frequency noise introduced by the relaxation oscillations of the Nd:YAG laser source. This resultant signal was sent to an oscilloscope for observation and recording. Figure 4 shows a picture of the output of the modulator/receiver system. The pulses are clearly discernable over the noise.

In order to measure the gas gain in this particular drift chamber the electro-optic modulator was removed and in its place an EG&G Ortec 142 pre-amplifier was connected to the sense wire. The amplitude of the pulses generated in the chamber was measured visually by observing the output of the preamplifier on an oscilloscope. Knowing the gain of the preamplifier and the impedance of the circuit, we arrived at a gas gain of 1.2×10^6 for the particular operating conditions in this experiment.

While the signal-to-noise ratio (s/n) of the signal from this first attempt at reading out a drift

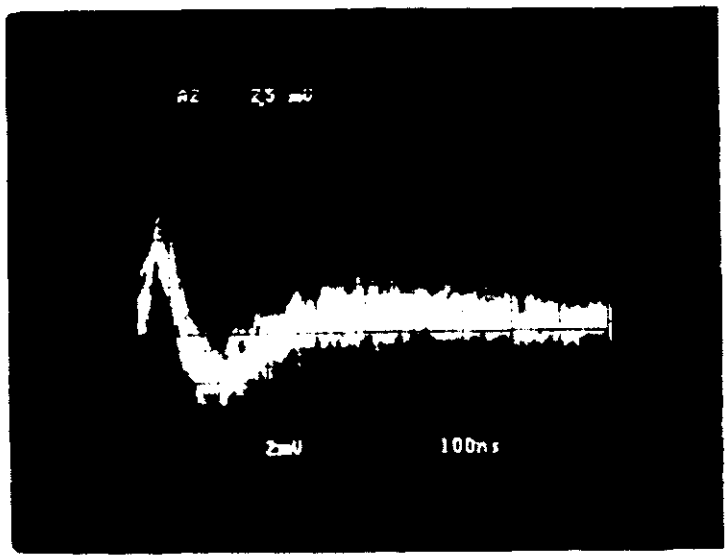

Figure 4. Oscilloscope picture of the output of the optical receiver for cobalt-60 gamma ray interactions in the drift chamber. The vertical axis is 2 mV/division and the horizontal axis is 100 ns/division. The exposure was for 1/4 second. The bandwidth of the signal is given by the RC time constant of the modulator's internal capacitance and the chosen termination resistor and has not been optimized.

chamber with an electro-optic modulator is not currently suitable for most applications, we note here that in continuing collaborative work with researchers at MIT we were able to achieve s/n ratios of ~ 30 from ionization tracks generated in drift tubes due to ^{55}Fe x-rays and clearly discern the two peaks of the ^{55}Fe x-rays in a pulse height spectrum.[6] Furthermore, in the LLNL/MIT work we experimented more extensively with detector/modulator impedance matching and were able to detect signals at significantly higher bandwidths, whereas the system described in this letter is still very far from being optimized for charge sensitivity, and bandwidth.

The sensitivity of the modulator system as a charge-readout device depends on several factors: the shot noise and thermal noise in the optical receiver, the slope of the interferometric response curve[1,5], the stability of the laser source, and the impedance matching between the ionization detector (drift chamber) and the modulator. We are currently making several improvements to the system that will be ready in the short term. We are stabilizing the previously mentioned 150 kHz relaxation oscillation, as well as lower frequency fluctuations in the laser source. The shot-noise floor is being lowered by using a detector and preamplifier in our optical receiver that are capable of handling higher optical power without adding to the thermal noise. Finally, we are working on ways of optimizing the impedance matching between the ionization detector and the modulator.

A longer term improvement will be realized with an increase of the modulator response slope. We are currently considering approaches ranging from redesigning the modulator electrode structure to completely different device architectures.

In summary, we have detected and followed the charge off a drift chamber sense wire directly using a Mach-Zehnder electro-optic interferometer without preamplification. The gas gain of about 10^6 implies that the interferometer system in this configuration is sensitive to charge at a level of about 0.1 picocoulombs. The application of this technology could significantly reduce the amount of electronics, cabling and power consumption in large detector arrays. In addition, optical processing of the signals generated by electro-optic read-out of drift chamber systems could be performed. Taking into account all of the refinements that are currently being pursued we expect improvements in the sensitivity of the modulator to the charge generated in ionization drift chambers by a factor of 10 to 100.

Acknowledgements

Work performed under the auspices of the U.S. Department of Energy by the Lawrence Livermore National Laboratory under Contract W-7405-ENG-48.

References

1. M. Lowry, et al., "An Electro-Optical Approach to the Prompt Signal Processing Problem of Mega-Channel SSC Detector Arrays," UCRL-JC-105645, prepared for submission to the Symposium on Detector Research and Development for the Superconducting Super Collider, Fort Worth, TX, October 15-18, 1990.

2. R. Bionta, et al., "Liquid Scintillator Calorimetry: A Research and Development Proposal," submitted to the Superconducting Super Collider Laboratory, December, 1990 (unpublished).

3. U. Becker, et al., "Resolution Study for Large Drift Chamber Systems," Nucl. Instr. Meth. 220, pps. 338-342 (1984).

4. D. Antreasyan, et al., "The L3 High-Resolution Muon Drift Chambers: Systematic Errors in Track Position Measurements, Nucl. Instr. Meth. A252, pps. 304-310 (1986).

5. M. Lowry, et al., "Electro-Optic Transient Imaging Instrumentation Development at Lawrence Livermore National Laboratory: Implications for SSC Instrumentation Development," to be published in the proceedings of the Symposium on Detector Research and Development for the Superconducting Super Collider, Fort Worth, TX, October 15-18, 1990.

6. U. Becker, et al., to be published.

UCRL- JC 105645
PREPRINT

An Electro-Optical Imaging Approach to the Prompt Signal Processing Problem of Mega-Channel SSC Detector Arrays

Mark Lowry, Eldon Ables, Richard Bionta, Ron Haigh,
Keith Hugenberg, Ralph Kalibjian, Charles McConaghy,
Darin Milton, Mark Rotter, and Hal Schulte

This paper was prepared for submittal to the
Symposium on Detector Research and Development for the
Superconducting Super Collider
Fort Worth, TX
October 15-18, 1990

December 1990

Lawrence Livermore National Laboratory

This is a preprint of a paper intended for publication in a journal or proceedings. Since changes may be made before publication, this preprint is made available with the understanding that it will not be cited or reproduced without the permission of the author.

DISCLAIMER

This document was prepared as an account of work sponsored by an agency of the United States Government. Neither the United States Government nor the University of California nor any of their employees, makes any warranty, express or implied, or assumes any legal liability or responsibility for the accuracy, completeness, or usefulness of any information, apparatus, product, or process disclosed, or represents that its use would not infringe privately owned rights. Reference herein to any specific commercial products, process, or service by trade name, trademark, manufacturer, or otherwise, does not necessarily constitute or imply its endorsement, recommendation, or favoring by the United States Government or the University of California. The views and opinions of authors expressed herein do not necessarily state or reflect those of the United States Government or the University of California, and shall not be used for advertising or product endorsement purposes.

An Electro-Optical Imaging Approach to the Prompt Signal Processing Problem of Mega-Channel SSC Detector Arrays

Mark Lowry, Eldon Ables, Richard Bionta, Ron Haigh, Keith Hugenberg,
Ralph Kalibjian, Charles McConaghy, Darin Milton, Mark Rotter, and Hal Schulte
Lawrence Livermore National Laboratory
Livermore, California 94550

Introduction

The physics demands of high luminosity at the SSC and the sometimes subtle measurements required to elucidate new physics will undoubtedly tax existing instrumentation. As is the case with most experimental fields, new physics follows from better measurement concepts and technologies. We expect this to be the case with the SSC as well. In what follows, we offer a glimpse of what may be possible using some of the recent results from the emerging technologies in the field of electro-optics.

A Proposed Electro-Optic System Architecture

The large number of channels required for SSC instrumentation and the temporal resolution required lead quite naturally to the consideration of electro-optical imaging techniques.[1] This is particularly true with the need to establish reliable and prompt event triggers that are based upon total energy and event topology, as we shall see with the system outlined in Figure 1.

Here we start with more-or-less conventional HEP detectors that yield charge as the measurement output. This charge is then used to modulate an externally provided optical carrier signal (amplifiers and pulse shaping may not even be required, as will be seen in what follows). The basic ideas regarding the optical modulator are discussed in ref. 1 . The optical carrier may be supplied by some, hopefully small, number of fibers that provide optical power to a chip containing many of the modulators discussed in ref. 1. The optical power division is accomplished on a chip as well (perhaps monolithically integrated with the modulator chip). This large

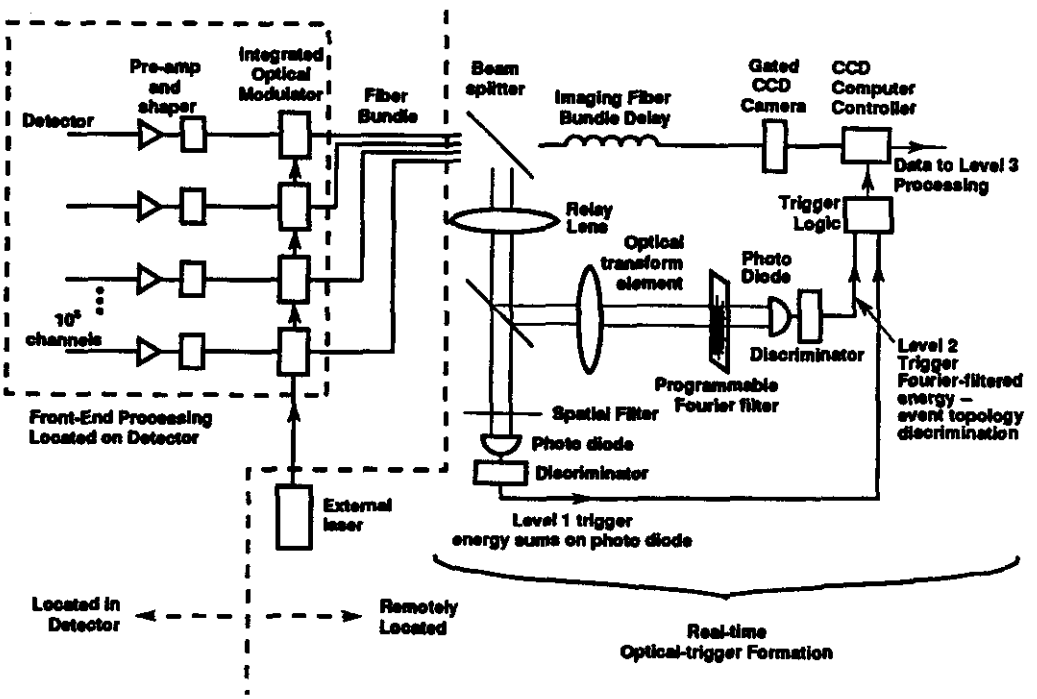

Figure 1. Proposed electro-optic system architecture for high luminosity data acquisition at the SSC. Some key features are the use of ultra-sensitive integrated-optical modulators and the use of optical pattern recognition for trigger formation.

* This work was performed under the auspices of the U.S. Department of Energy by the Lawrence Livermore National Laboratory under contract number W-7405-ENG-48.

number of independent optical channels (perhaps as many as 100 are possible per chip) are brought off chip in individual optical fibers. These optical fibers are arranged in an imaging bundle—such that image information is preserved. In the event of a hit, this bundle is then the conduit of a transient image that propagates to the level-one trigger.

The first step in the trigger generation process is to pick-off a portion of the image power through use of a conventional optical beam splitter. Let us call these beams, after the splitter, the trigger image and the major portion the record image. The trigger image can be split into two beams. In the case of data from a calorimeter, one leg of the trigger beam can be spatially filtered with a filter whose optical density is graded as, $\sin(\theta)$, where θ is the angle with respect to the beam direction for that pixel element. As this filtered image is relayed optically to a large area photodetector, the output charge from the photodiode is then a prompt measure of the total transverse energy—the delay for this part of the trigger formation is just the response time of the photodetector; a few nanoseconds is easy.

The second portion of the trigger image can be used to perform relatively complex event topology discrimination through the use of well-established optical pattern recognition techniques. The most straight-forward technique applies again to the case of calorimetry. By applying the optical Fourier transform to the second trigger image—realized conveniently with the use of simple optical lenses[2]—one can perform spatial frequency filtering operations by simply placing the appropriately patterned spatial transmission filter in the Fourier plane (by using the new technologies of spatial light modulation,[3] the characteristics of this frequency filter could be conveniently controlled electronically). The output of the spatial filter is then relayed to another large area photodetector. The prompt optical sum performed by this photodetector is a measure of the energy content only of features of the event that have a frequency content that is matched to the spatial filter in the Fourier plane. This then allows us to discriminate promptly (a few nanoseconds) on the basis of event topology, as well as total event energy. It should be noted that optical processing has at least one precedent[4] in HEP instrumentation.

Perhaps this optical pattern recognition may be extended to the case of tracking detectors. It may be possible to use the optical Hough transformation to detect the existence of stiff tracks. The Hough transformation maps straight lines into points—one coordinate of the point being the line's angle with respect to the abscissa, and the other is its distance from the origin. Using techniques similar to the optical Fourier transformation, the Hough transformation may be accomplished optically.[5,6] It may prove possible to optically correlate this trigger with the calorimeter information to provide an elegant and comprehensive trigger, promptly, and with little or no electronics in difficult environs. It must be pointed out that all the optical Hough transformation work that we have seen to date is accomplished with a mechanically rotating optical element, and thus would be far too slow for HEP instrumentation. However, there may be a way to realize the transform in optical fashion instantly, and we are currently exploring that possibility.

We have thus far painted a simple picture of Fourier optics techniques. Our laboratory measurements to date—and some reflection on the Fourier optics theory—would suggest that performing the Fourier transform of the image from an optical fiber bundle may be very difficult. Basic Fourier optics work is done with the use of simple apertures, and the optical wavefronts employed are coherent. In our case, the individual image pixels have probably suffered large relative optical phase shifts. These phase shifts lead to severe interference noise in the Fourier plane. We can suggest three possible ways around this relative phase shift problem.

First, the fact that our optical carrier was derived from a single laser (or perhaps a phase locked set of lasers) may allow us to adjust these relative phases such that when we arrive at the Fourier plane the relative phase shifts have been compensated. Further, the use of integrated optical devices as our signal encoding mechanism may provide a convenient solution. The most fundamental form of optical modulation is the phase shifter. In fact, the Mach-Zehnder modulator discussed in ref. 1 is composed of two such devices. A phase shifter could be employed in each channel to compensate these phase shifts in response to the input from a feedback mechanism. Another phase compensation technique would be the use of a holographic element in the image plane after the bundle, this element could be used to compensate the optical phases of the individual image pixels by focusing the image onto this holographic phase plate.[7] We are exploring both of these phase compensation techniques, and hope to carry-out experiments soon. Finally, the partially coherent image from the fiber bundle could be transformed into an incoherent image. This may be achieved by imaging the fiber output unto an image intensifier. The image intensifier output is then incoherent light from the phosphor screen. Then the incoherent image could be processed using incoherent processing techniques. This offers the added advantage of allowing the image information to be gated; however, to retain the speed of the optical processing fast phosphors must be used—so, the gain of the intensifier may then become an issue.

The remaining beam, the record image, can be refocused onto another imaging optical fiber bundle, and be allowed to propagate for however long is required for complete trigger formation. After trigger formation, the image is captured by a gated ultra-fast readout CCD imager. Image readout times of 10 μs for 10,000 pixels with a dynamic ranges of 1,000 are attainable with today's technology. Extended dynamic ranges could be attained by using a slightly higher power optical carrier and splitting the record image with a 10:90 beam splitter and recording both images.

The advantages of using this electro-optical imaging approach are several:

- The transmission media (small diameter optical fibers with approximately $1cm^2$ cross-sectional area per 10,000 fibers) offers low radiation scattering, and a mechanically manageable cable plan.

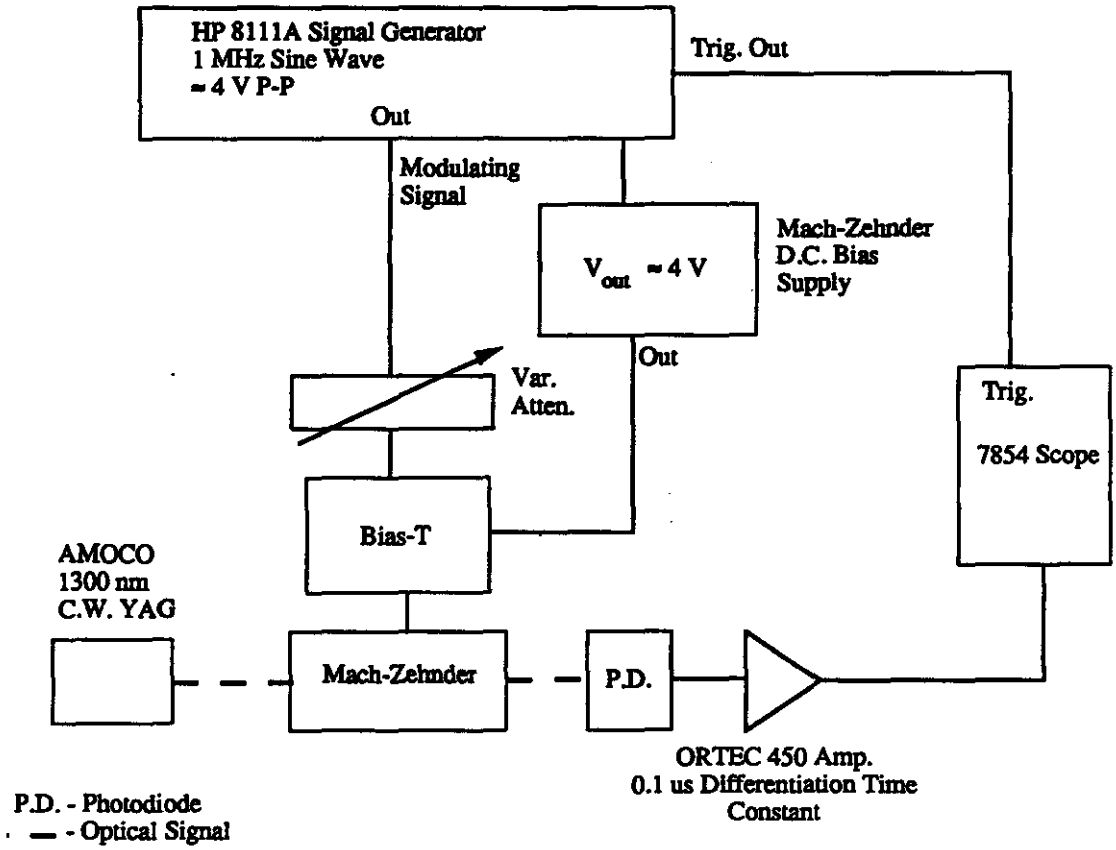

Figure 2. Experimental layout for Mach-Zehnder dynamic range measurements.

- Since all channels are brought outside in parallel, triggering architectures become very flexible and amenable to modification in the future.
- Ground-loops and other forms of EMI become less of a problem.
- The modulators and fiber medium easily support the required temporal response.
- The power consumption can be much less than 1 mW per channel for the power-dissipation critical inner-tracker applications.
- The fiber medium conveniently provides signal delay to accommodate the trigger formation time.
- The potential for operation without amplifiers (discussed in detail below) adds greatly to system reliability—particularly for the high radiation environments.
- Optical pattern recognition and optical summing techniques can be applied for prompt trigger formation.

While this total system architecture is quite attractive in many respects, we should not overlook the value of any one of the roughly three major subsystems: the optical modulators, the image processing techniques, and the fast CCD data capture. We will spend the rest of the paper addressing the optical modulators.

Integrated Optical Modulator Results

While we have been pursuing instrumentation development with modulators for several years, we have only recently considered them in the context of HEP experiments. To that end, we set out to understand how they might best be used in HEP experiments. A potential application of the technology is in calorimetry experiments, where exceptional dynamic range is required. We have made measurements of dynamic range at 800 nm, using 2x2 modulators, and measurements at 1300 nm using Mach-Zehnder modulators. Due to the limited space, we will only discuss the Mach-Zehnder measurements here.

The experimental setup is outlined in Figure 2. We used a sine-wave electrical input for convenience, but the conclusions should apply to pulse operation as well. The bandwidth of the system was limited by the amplifier at 1.5 MHz. The bias applied to the modulator was adjusted by observing the signal-to-noise of a very weak signal; at the point of maximum signal-to-noise, the bias voltage level was fixed. Figure 3 shows the result of three different levels of electrical attenuation (on the sinusoidal input signal) ranging from 0 dB to 80 dB (voltage). Even with 80 dB attenuation (x10,000), the output signal from the modulator is easily seen on the scope trace. For the 0 dB trace, the negative going portion of the sinusoidal input is distorted as it passes through the minimum

in the sinusoidal response function (see ref. 1), however the positive going portion does not go through the response peak (indicating that the modulator was not biased precisely at the half-power point). Concentrating on the positive going portion of the sinusoid, we see that the input signal goes through a dynamic range of at least 10,000. At the lowest input signal level (80 dB attenuation), the signal is still much above the noise. By analyzing the rms noise of our system with the light beam blocked, and with the beam unblocked but no modulation signal, we find that at the attenuation value of 10,000 the ratio of the peak signal to the noise due to just the laser/modulator combination is ~ 4. However, these noise measurements were made from scope traces of the same time scale as Figure 3; here the noise bandwidth is determined by the amplifier roll-off at 1.5 MHz, and the record length at the low end; we find this to be 1.3 MHz. Extrapolating to the case of a 10 MHz bandwidth (more suitable for most SSC applications), we find that this increase in bandwidth should lead to a noise increase of a factor of ≈ 2.77. Thus operating with a bandwidth of 10 MHz, we would expect to find a dynamic range of ≈ (4/2.77)(10,000) or slightly more than 14,000. Further, since we know that this signal can be linearized, we can establish a linear relationship between the optical power from the modulator and the input voltage to the modulator.

At this point, it is convenient to discuss the relationship of the charge (or voltage sensitivity) to the parameters of the carrier modulator system. The optical power output of most modulators can be conveniently described by

$$P=P_0F(V) \qquad \text{eq. 1}$$

where $P_0 = \eta P_{in}$ is the maximum carrier power out of the modulator—when $F(V)=1$, η is the insertion loss, P_{in} is the input optical power, and $F(V)$ is some modulation function of charge or voltage. The uncertainty of the measured optical throughput, ∂P, is made up of three contributions: carrier power instabilities, detector noise, and amplifier noise. We may lump these uncertainties together into the total uncertainty in the measured power, ∂P. The voltage uncertainty due to fluctuations in the measured optical power is given by

$$\delta V=(\delta P/P_0)/(dF/dV) \qquad \text{eq. 2}$$

assuming that ∂P is small compared to P_0, and dF/dV is not close to zero. Any fluctuations from the modulator itself[8] are then added in quadrature with this uncertainty to arrive at the total uncertainty in the measured voltage.

For the case of the Mach-Zehnder, reproducing eq. 1 from ref. 1 we note that

$$P=\eta(1-\varepsilon f(V_s))P_{in}\sin^2\left(\frac{\pi V_s}{2V_\pi}+\phi\right)+\eta\varepsilon f(V_s)P_{in} \qquad \text{eq. 3}$$

where P is the modulated optical power output, P_{in} is the input optical power, V_S is the applied signal voltage, V_π is the voltage required to modulate from a minimum to maximum (1/2 of an interference fringe), η is the device insertion loss, ε is the low voltage modulator extinction and usually $\varepsilon < 0.01$, ϕ is

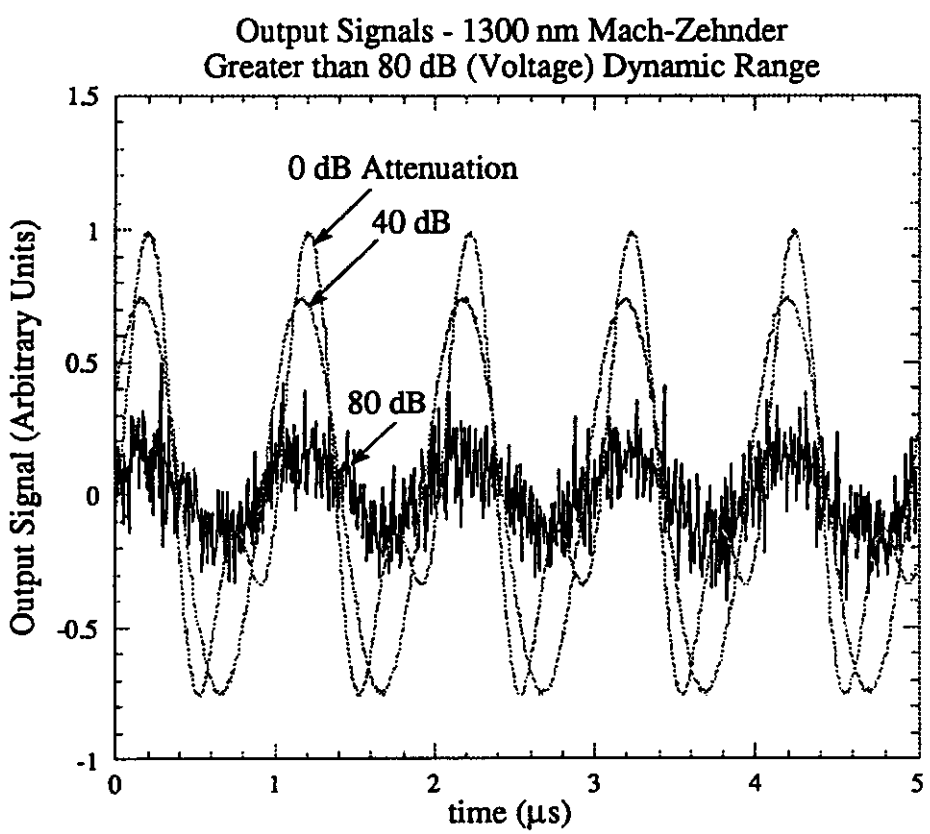

Figure 3. Results of Mach-Zehnder dynamic range measurements. A dynamic range well in excess of 10,000 is demonstrated.

the quiescent phase shift of the device, and f is a phenomenological function that describes the behavior of the modulator extinction at high modulation voltages "f" is very nearly 1 except at voltages much larger than V_π[9]. With dF/dV at its maximum (i.e., at the half-power point, in the Mach-Zehnder case), we find,

$$\frac{\delta Q}{Q_\pi} = \frac{\delta V}{V_\pi} = (\delta P/P_0)\frac{2}{\pi(1-\varepsilon)} \qquad \text{eq. 4}$$

so the voltage (charge) uncertainty is proportional to the relative optical power uncertainty, scaled by $V_\pi(Q_\pi)$.

For the measurements shown in Figure 3 extrapolated to 10 MHz, $\delta v/v_\pi$= 1/(dynamic range) = 1/14,000 = 7.1×10^{-5} Equivalently, $\delta Q/Q_\pi = 7.1\times10^{-5}$ Alternatively one may extract the relative optical power uncertainty using eq. 4, $\partial P/P_0=1.1=10^{-4}$. The modulator used for the measurements in Figure 3 was an in-house designed and fabricated high-bandwidth traveling wave Mach-Zehnder. In general, for SSC applications it appears that lumped element electrode structures may be preferred; to understand the charge sensitivity possible for SSC applications let's consider the lumped element case. Becker[10] discusses a figure-of-merit for lumped-element modulators: $M=V_\pi L$, where L is the length of the electrode structure. Becker finds that M= 14 V-mm and that the capacitance/electrode length ρ =0.85 pF/mm . Thus, one can easily calculate the amount of charge deposited on the electrode structure to yield a voltage of V_π; $Q_\pi=M\rho$=12 pC. Applying this to our dynamic range measurements above yields the result that the minimum charge that we are capable of detecting would be 12 pC/14,000 = 0.86 femtocoulombs. This assumes our value of the relative optical power uncertainty extrapolated to 10 MHz bandwidth, and the Q_π of a lumped element modulator structure. We are further making the tacit assumption that the electrode termination resistance is large enough (or actively gated) so that the charge will not dissipate on time scales consistent with the desired bandwidth.

It is useful to consider the shot noise (counting statistics) limitations on the dynamic range. For our optical power level of ~ 5 mW—at the Mach-Zehnder bias point, a projected bandwidth of 10 MHz, at a wavelength of 1300 nm, and a detector quantum efficiency of 90%, the shot noise is easily calculated using the usual Poisson distribution assumption. Given these circumstances we find that the shot noise fluctuations in the measured optical power would be 1.8×10^{-5} of the average power, i.e. $\partial P/P=1.8\times10^{-5}$, where ∂P is the fluctuations in the measured power (assuming only shot noise) and P is the average measured power. So we are a factor of 6.1 away from realizing a shot noise limited system. For the ideal optical shot-noise limited system, operating, with an optical power of 5 mW at the receiver, the charge sensitivity could be as good as 0.14 femtocoulombs. However, at these low charge levels, we are probably approaching the level of the thermal charge fluctuations in the modulator capacitance: at room temperature with a capacitance of 5 pF the thermal noise would be of order 1000 electrons or 0.16 fC (see ref. 8).

The dependence of the sensitivity on the slope of the modulation function , eq. 2, has led us to consider resonant modulator structures. These structures exhibit a modulation function that consists of resonances, i.e. the device is characterized by a "Q"—or finesse in the optical vernacular. These kinds of devices may be of interest where extremely high charge sensitivity is required but dynamic range is not. Most tracking detectors, by virtue of their necessarily small volumes, would seem to fall into this category.

This kind of modulator is very simple in design. It consists of a single waveguide with dielectric mirrors deposited on the input and output facets of the chip to form an optical cavity. The resonances in transmission are a function of the ratio of the optical length of the cavity and the optical free-space wavelength. For a Fabry-Perot modulator, the modulation function, in analogy with eq. 2 can be derived by following Born and Wolf[11] but including a loss factor,

$$G(\delta)=\frac{(1-R)^2e^{-\alpha L}}{(1-Re^{-\alpha L})^2+4Re^{-\alpha L}\sin^2(\delta/2)} \qquad \text{eq. 5}$$

where α is the optical loss coefficient, R is the reflectivity of the cavity ends, δ is the optical phase difference; $\delta=4\pi nL/\lambda$, where n is the refractive index. Electrodes are then deposited on either side of the single waveguide. The electrodes are used to modulate the index of refraction and hence the optical length of the cavity. Thus, this structure can be used as a tuneable monochromater or a very sensitive modulator that responds to applied voltage or charge.

Figure 4 shows data taken at LLNL from an integrated optical Fabry-Perot modulator of LLNL design and fabrication. Here the resonance is clearly seen. In this figure, the finesse, *F*—the ratio of the free spectral range (distance between peaks) to the FWHM of the resonance—is approximately 12. This data was acquired by scanning the optical spectrum; which is equivalent to applying a voltage or charge. One can easily relate the finesse of this device to the maximum slope of the modulation function. An analytic expression is possible from eq. 5, however, the essential point can be made with far less algebra, by approximating the resonant peaks with triangular spikes. If we constrain the peak of the spike to correspond to the peak of the resonance and also force it to pass through the FWHM of the resonance, we arrive at a very simple approximation for the slope of the resonant peak, especially for a finesse that is large,

$$\frac{dG}{dV} \approx F/(2V_\pi) \qquad \text{eq. 6}$$

where *F*- is the finesse. Applying eq. 2, we may calculate the voltage and charge uncertainties (hence, theoretical sensitivities) for the Fabry-Perot modulator as,

$$\frac{\delta Q}{Q_\pi} = \frac{\delta V}{V_\pi} = (\delta P/P_0)\frac{2}{F} \qquad \text{eq. 7}$$

Naturally, this sensitivity scales with the inverse of the finesse which can in principal be made quite high. Given the same optical noise parameters of our MZ measurements and using the finesse value from Figure 4, we would estimate under these conditions that the charge sensitivity of the FP modulator would be 0.3 femtocoulombs or ~ 2000 electrons.

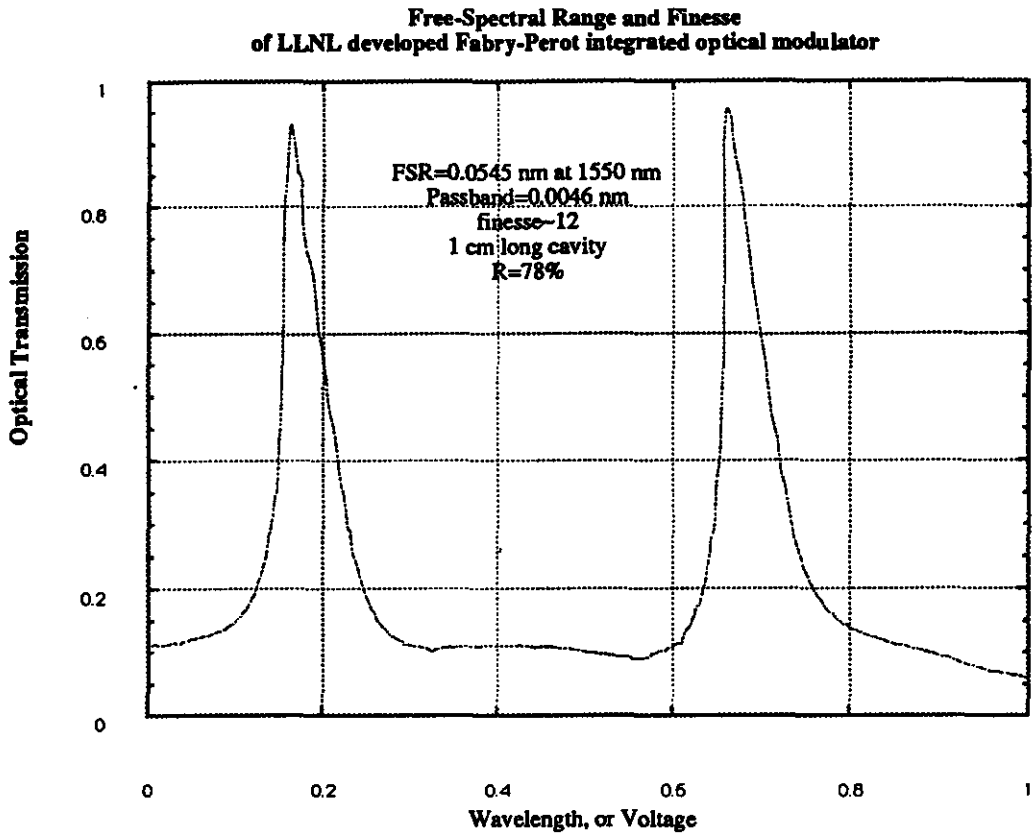

Figure 4. The modulation shape function for a Fabry-Perot structure. Note the resonant peaks in the response.

The sensitivity leverage of the resonant Fabry-Perot modulator is clear. We could presumably extract even better performance from a FP with a higher finesse and/or shot-noise limited optical detection, however we are again approaching the level of the thermal noise in the electrode structure itself (ref. 8).

A word of caution about such resonant structures is in order: Their excellent sensitivity may come at the price of significant instability, with respect to temperature in particular. However, it may be possible to compensate these instabilities with a feedback mechanism or conceive device designs that are self compensating, yet resonant—the Mach-Zehnder is an example of a self-compensating structure, unfortunately it is not resonant. The Mach-Zehnder's two parallel paths pass through the crystal so closely that any temperature-induced optical path change is experienced identically by both. Perhaps it is possible to design a resonant structure that also has this feature.

Modulator Power Dissipation

For many SSC applications, the power dissipated by subsystem elements is critical. For the case of the modulators, the dissipated power is from two sources the optical carrier and the charge driving the modulator. As we shall see, the most significant component is the optical power.

The optical power dissipation will be approximately equal to $(3/2)P_0$—on the order of 1/2 of the input optical power will probably be lost due to inefficiencies in optical coupling, and operation at the half power point will then account for an additional $1/2P_0$.

The energy dissipated due to the modulating charge is calculated as $q^2/2C$. Since the MZ will be the least sensitive of the two devices discussed here, we will consider it as the worst case. Taking C=2.55 pF and assuming $q=Q_\pi=12$ pC, we find that there will be 28 pJ of energy dissipated per "hit," maximum. Then, if every pixel registered a hit every beam crossing, the dissipated power from the charge would be 28pJ/1.6 nS = 1.8 mW. However, since the detector elements that *are not* hit far outnumber those that *are*, on average, this power dissipation term will be reduced by a couple orders of magnitude. So we would expect the charge dissipation power to be of order 10 microWatts, or less, on average. It should be pointed out that no matter how the charge is readout the energy must be dissipated.

While on the subject of power dissipation it should be noted that given the ultimate shot-noise limited system, where the optical noise goes as $P_0^{1/2}$, there will be a trade-off between noise--hence, sensitivity—and optical power dissipation. This tradeoff should be considered when determining the optimum modulator design for a particular SSC application.

System Costs

There is not space here for a comprehensive discussion of projected costs. However, it is clear that without significant advances in integration density (number of modu-

lators per chip) and automated packaging techniques the per channel costs will be prohibitive. We hope to pursue, with industrial partners, both of these critical areas.

Radiation Sensitivity

While some encouraging data on the radiation sensitivity of these integrated optical modulators does exist,[12] there is much that remains to be done at SSC dose-rate levels. And we have begun a program of investigation for this important issue for modulators at the SSC.

Conclusions

We have presented dynamic range, and sensitivity data for two distinct classes of integrated optical modulator. These measurements demonstrate that these devices may prove very useful for both calorimetry and tracking. Further, we have outlined a comprehensive electro-optical imaging system architecture that includes a novel and elegant optical approach to trigger formation and the means of capturing the triggered event data.

As high energy physics moves into the twenty first century with the completion of the Superconducting Super-Collider, we believe that only by incorporating the best and most sophisticated technology available will the physics move forward as efficiently as possible. We hope that we have demonstrated, in a substantive fashion, that electro-optics has a very large role to play.

Acknowledgements

We would like to thank Dan Marlow of Princeton University for many helpful discussions and much encouragement. Thanks are also due to Maged Atiya of Brookhaven for his encouragement and critical evaluation of some of these ideas. We also appreciate the time and consideration given by several researchers to some aspects of this work during a recent visit to Brookhaven: Veljko Radeka, Paul O'Connor, Venetios Polychronakos, Howard Gordon, William Willis, and Wilfred Cleland. David Nygren from Lawrence Berkeley Laboratory has also provided useful discussion and encouragement. As relative newcomers to the field, we gratefully acknowledge the help of many HEP researchers, too numerous to list, who attended the '90 Snowmass meeting and played an important role in shaping some of these ideas through their interest and constructive criticism.

We thank Richard Becker of Integrated Optics Circuit Consultants for useful discussions on modulator sensitivity.

At LLNL, we would like to thank Hye-Sook Park for her suggestion of the optical Hough transformation, Stan Thomas for useful discussions about current image intensifier technology, Wolfgang Stoeffl and Craig Wuest for their interest, and Orrin Fackler, Chip Britt, and Tony Chargin for their interest and encouragement.

References

1 M.E. Lowry, B. A. Jacoby, and H. F. Schulte, *Electro-Optic Transient Imaging Instrumentation Development at Lawrence Livermore National Laboratory: Implications for SSC Instrumentation Development*, in these proceedings (previous paper).

2 J. W. Goodman, *Introduction to Fourier Optics*, McGraw-Hill, San Francisco (1968)

3 W. P. Bleha, L. T. Lipton, E. Wienen-Auner, J. Grinberg, P.G.Reif, D.Casasent, H.B.Brown, and B.V.Markevitah, *Application of the Liquid Crystal Light Value to Real-Time Optical Data Processing*, Optical Engineering, Vol. 17, #4, pp. 371-384 (1978); note: Commercial products are now available from Hughes.

4 W. E. Cleland, D. E. Kraus, and J. A. Thompson, *Optical Trigger Processor for High Energy Physics*, Nuclear Instruments and Methods, Vol 216, #3, pp. 405-414, New-Holland, Amsterdam (1983).

5 W.H.Steier and R.K.Shori, *Optical Hough Transformation*, Applied Optics, vol. 25, # 16, pp. 2734-38, 1986

6 G.Eichmann and B.Z.Dong, *Coherent Optical Production of the Hough Transformation*, Applied Optics, vol. 22, #6, pp 830-34, 1983

7 Reynolds, Devetis, Pamert, and Thompson, *The New Physical Optics Notebook: Tutorials in Fourier Optics*, pp. 323-325, SPIE Optical Engineering Press, Bellingham, Washington (1989).

8 At least two potential sources of noise from within the modulator must be considered: The thermal noise of the electrode capacitance $\partial Q=(CkT)^{1/2}$ (integrated over all frequencies) and the ferro-electric noise from within the crystal itself. For a discussion of these two sources see D.A. Bell, *Noise and the Solid State*, Wiley (1985) At room temperature the thermal noise appears to dominate.

9 As V_S grows large, the guiding characteristics of the waveguides are altered such that one will become more lossy than the other—this leads to incomplete interference and reduced extinction at large values of V_S.

10 R. A. Becker, *Multigigahertz Lumped-Element Electro-optic Modulators*, IEEE J. Quant. El., QE-21, 8, pp 1144-1146 (1985).

11 See for instance p. 327 Born and Wolf, *Principles of Optics*, Pergamon Press, Oxford (1986) for a discussion of Fabry-Perot interferometers.

12 F. Roeske, Jr., D. R. Jander, G. D. Lancaster, M. E. Lowry, G. McWright, R. T. Peterson, and W. E. Tindall, *Preliminary Radiation Hardness Testing of Lithium Niobate Optical Directional Coupler Modulators Operating at 810 nm*, Proc. SPIE Technical Symposium Southeast on Optics, Electrooptics, and Sensors, Orlando, FL (May 1987).

Technical Information Department · Lawrence Livermore National Laboratory
University of California · Livermore, California 94551

Resistive Plate Chambers for the GEM Detector: A Proposal for Research and Development

Craig R. Wuest, Richard M. Bionta, Elden Ables, and Dan Makowiecki

Lawrence Livermore National Laboratory

submitted to the Superconducting Super Collider Laboratory and the GEM Collaboration

September 5, 1991

Physics Department
High Energy Physics Group
D Division
Chemistry and Materials Science Division

trodes of the proper impedance. Patterns such as x-y or u-v can readily be laid out. Particular attention will be paid to the study of resistive pick-up electrodes that can allow charge division of the signal between the two ends of the electrode with a corresponding position measurement of the z-coordinate of the muon track.

We already have general purpose electronics and gas handling systems available from previous research projects carried out in FY 1991 for our internally funded L* R&D programs in muon chamber design and liquid scintillator hadron calorimetry. This includes high voltage power supplies, amplifiers, discriminators, TDC and ADC modules, and scalers. We also have data acquisition systems utilizing VaxStation 3100's interfaced to CAMAC via SCSI or Macintosh II/FX interfaced to CAMAC via GPIB. Both systems contain powerful data analysis and color graphics display and visualization software.

The program for R&D we propose is the following:

1. Determine the best coating techniques and characterize them for resistivity and surface uniformity.
2. Assemble a small 30 x 30 cm^2 single layer RPC using resistive glass and cermet sputtered resistive electrodes.
3. Characterize this small counter for noise, operating efficiency (plateau), time resolution and spatial resolution. This includes characterizing the size and temporal duration of the localized dead region after an electron avalanche is generated. Spatial resolution along the long pickup strips will also be studied, with particular attention being paid to uniformity and linearity of the position measurement near the edges of the chamber. Also, chamber lifetime and aging effects can be studied with accelerated tests using high rate localized pulsing. Tracks can be generated using tagged cosmic rays, radioactive sources, and UV lasers. In addition the LLNL 140 MeV Electron Linear Accelerator could be utilized as a source.
4. Based on the experience with the small RPC we would next build a larger RPC of about 1 m^2 area. This effort would be carried out keeping in mind the goal of large scale production of RPCs. As such, materials, cost, and manpower would be optimized.

Collaborative work with MIT

We have initiated discussions with Professor Irwin Pless of MIT to form a collaborative effort on RPC R&D.[5] Dr. Pless has indicated that he can bring a phenolic RPC back to MIT from Gran Sasso for study and characterization. We envision a research program at LLNL that is complementary to the effort of the MIT group. Initial work at MIT will focus with designing a test stand for the Italian RPC and carrying out various tests on that RPC.

Independently, LLNL will perform the tasks outlined above with the goal being to provide a suitable GEM prototype RPC that could then be compared to existing RPC technology. A meeting with Dr. Pless to work out these details was scheduled to coincide with the GEM Muon Sub-system meeting to be held in Boston on August 23, 1991. This meeting resulted in an agreement to perform the tasks outlined above with the work to be performed by the two institutions as previously stated.

A Proposal for R&D on Resistive Plate Counters for the GEM Detector

Craig R. Wuest, Richard M. Bionta, Elden Ables, Dan Makowiecki

Lawrence Livermore National Laboratory

Introduction

Resistive Plate Counters, or RPCs have been proposed as part of the prompt trigger and muon detection system for the GEM detector - to be built at the Superconducting Super Collider.[1] RPCs of various types have been built for air shower arrays as well as charged particle detectors at accelerators.[2-4] In its most basic form an RPC consists of a thin (2 mm) gas-filled region sandwiched between resistive plates coated with resistive electrodes (usually made from graphite-based paints). An electric potential is applied to the resistive electrodes to form a field in the gas region of about 4-5 kV/mm. The resistive electrodes typically have surface resistivities of a few 100 kΩ/square. The resistive plates typically have a volume resistivity of 10^{11} Ω-cm and have been made in the past with plasticized PVC[2], bakelite (phenolic)[3], or resistive glass.[4] Timing resolutions are reported to be a few hundred picoseconds to a few nanoseconds.

RPCs also offer the potential of providing z-coordinate information along with the fast trigger pulse identifying the passage of a muon. Z-position information is provided by charge splitting using resistive readout electrodes, or time-differencing of the charge signals at each end of the readout electrode, and has the potential of providing the z-coordinate of the muon with a resolution of about 100-200 microns.

Experimental Program

There are indications that RPCs based on plastics and phenolics suffer from noisy operation and deterioration because of the deposition of hydrocarbons on the inner surfaces of the resistive plates and because of electrical breakdown in the regions where the plates are separated by spacers. To address these issues and to develop an appropriate trigger counter for the GEM detector, we propose to study alternative materials for RPCs utilizing the expertise at LLNL in the areas of Chemistry and Material Science (CMS) and Physics. We have already identified candidate resistive glasses that could be easily coated with various resistive electrodes by sputtering. We are equipped to sputter a number of different materials on large area plates and could, for example, provide cermet thin film coatings (chrome/silicon monoxide) with resistivities controllable from a few tens of kΩ/square to a few MΩ/square. We have extensive experience in sputtering cermet coatings as well as other types of resistive coatings. While many resistive coating technologies should be suitable for RPCs, we would concentrate on the application of cermet thin film coatings because we have experience in producing these coatings for other position sensitive avalanche counters under development at LLNL, and because we feel that the surface resistivity and uniformity of these coatings can be more readily controlled.

Sputtering processes provide fast uniform coatings that can be adapted to large volume production of RPC parts. In addition, complex patterns can be sputtered utilizing masking techniques to provide metallic (copper, aluminum, etc.) or resistive (cermet) pick-up elec-

Cost

We estimate the R&D funding needed to perform this work at about $200 K for FY1992. This amount covers 0.25 FTE of a CMS engineer, 0.5 FTE of technician support, 0.5 FTE of an Electronics Engineer as well as an estimated $20 K for materials and $30 K for travel.

RPC materials (glass, coating targets, spacers, masks, etc.)	$20K
RPC gas system	supplied by LLNL
RPC electronics (computer, data acquisition, muon telescope, etc.)	supplied by LLNL
0.25 FTE Chemistry and Materials Science Engineer	$35K
0.25 FTE Chemistry and Materials Science Technician	$22.5K
0.25 FTE Mechanical Technician	$22.5K
0.50 FTE Electronics Engineer	$70K
Travel (for physicists)	supplied by LLNL
Travel (for engineers and technicians)	$30K
TOTAL	**$200K**

References

1. "An Expression of Interest to Construct a Major SSC Detector," B. Barish, W. Willis, Co-spokespersons, pps. 3-38 - 3-40, July, 1991, unpublished.

2. G. Battistoni, et al., "Plastic Spark Counters with PVC Electrodes," Nucl. Inst. Meth. **A270**, p. 190, 1988.

3. R. Cardarelli, et al., "Progress in Resistive Plate Counters," Nucl. Inst. Meth. **A263**, p. 20, 1988.

4. M. Anelli, et al., "Glass Electrode Spark Counters," Nucl. Inst. Meth. **A300**, p. 572, 1991.

5. I. Pless, "Proposed Request for R&D Funds to Study Resistive Plate Counter," memorandum to S. Ahlen, D. Marlow, and F. Taylor, August 8, 1991.